Rate-Based Modelling of Plate-Packed Heat Integrated Distillation Columns

B.A. Biesheuvel

TechnipFMC

TU Delft

Rate-Based Modelling of Plate-Packed Heat Integrated Distillation Columns

by

B. A. Biesheuvel

to obtain the degree of Master of Science
at the Delft University of Technology,
to be defended publicly on Thursday June 25, 2019 at 13:00.

Student number:	4094565	
Project duration:	February 26, 2018 – June 03, 2019	
Thesis committee:	dr. ir. C. A. Infante Ferreira,	TU Delft, supervisor
	Prof. dr. ir. T.J.H. Vlugt,	TU Delft,
	Ir. T. Woudstra,	TU Delft,
	dr. ir. M. W. M. van Goethem,	TechnipFMC, supervisor

This thesis is confidential and cannot be made public until 25 June 2020.

TechnipFMC

TU Delft

Preface

This thesis was written to conclude the master of mechanical engineering with a specialisation in process and energy technology at the Technical University Delft. The work was performed in Zoetermeer, at the office of major ethylene technology supplier, TechnipFMC.

This document describes the model development of a plate-packed heat integrated distillation column, one of the exciting new improvements in distillation technology. There are many aspects to the successful development of this piece of equipment, and I hope that this work can contribute to that.

Bastiaan Anton Biesheuvel
Zoetermeer, June 2019

Abstract

TechnipFMC is pushing innovations to reduce the emissions of ethylene plants separations. This development is also driven by customer demands. They face increasingly strict legislation on CO_2 emissions. Separation in distillation columns is one of the major energy intensive unit operations in an ethylene plant, and increasing their efficiency directly improves the overall plant efficiency.

This work is commissioned by TechnipFMC, which is part of the HEADLINES consortium for heat integrated distillation column development.

The plate-packed heat-integrated distillation column (pp-HIDiC) is a promising new distillation column design that could replace current ethane/ethylene fractionators (C_2-splitter). A numeric model and calculation tool is needed to aid the design of a pp-HIDiC for the C_2-splitter as proposed in the work by Bruinsma, Krikken, Cot, Sarić, Tromp, Olujić & Stankiewicz [1]. A numeric modelling procedure for this type of column was developed in this work. This modelling procedure was then implemented in Python.

A rate-based modelling methodology was applied to describe the continuous heat- and mass transfer on the internal column structures. The aim of the model is to find column dimensioning and duties, which followed from the model's balance equations. A designer should be able to input the column dimensions and flow rates, and run the model to retrieve mole fractions, heat transfer and temperatures along the column.

Heat- and mass transfer correlations were needed, despite there being no special correlations for the proposed setup. Generic structured packing correlations were used from literature as a modelling approximation. The performance of different available thermodynamic packages for Python was compared. Diffusivity and viscosity correlations were implemented to aid in mass transfer calculations. A Python Newton solver was chosen to solve the model equations, using CoolProp to perform thermodynamic calculations.

Due to the choice of model variables, convergence of the equations remained an issue. In the system of equations, column temperatures cannot follow from the equilibrium relation on the vapour-liquid interface, as they do not depend on each other strongly enough. It is not possible to find condenser and reboiler duties as an output of this model while specifying boil-up and reflux ratios. The model needs to be changed so that these variables are fixed by the user, and the reflux ratios are a model result instead.

A model's thermodynamic calculation packages should be robust. Additionally, a well-documented interface with the used programming language and validated data is needed. This could require the use of commercial thermodynamic software, or validated process simulators. The model designer is then less hindered by programming environment related issues.

A model that is purely based on theory and inapplicable correlations cannot be the only basis of design decisions. The used heat and mass transfer correlations are not made for the studied geometry, so their usage introduces inaccuracies in the model results. Applicable correlations from experiment are recommended to characterise pressure drop, heat transfer between HIDiC compartments, heat transfer coefficients, and vapour and

liquid mass transfer coefficients on the packing surface. Further experiments can also aid in better understanding of the wetting, flooding and liquid distribution of various pp-HIDiC geometries.

Beside characterising one packing geometry, it will be beneficial to experiment on different viable geometries that are specifically suitable for a pp-HIDiC. Too few alternative designs have been tested so far. Investigating more geometries can help to find the most promising designs more quickly. After that, models and experiments can then complement each other to develop the most promising geometries and accelerate the column development.

Contents

Nomenclature

The following list provides an overview of the symbols in this thesis, their meaning and their unit.

Acronyms

CSMP	Corrugated Sheet Metal Packing
DIPPR	Design Institute for Physical Properties
ECN	Energy Centre of the Netherlands
EOS	Equation of state
ETS	Emissions trading system
HETP	Height Equivalent of a Theoretical Plate
HIDiC	Heat Integrated Distillation Column
MERSHQ	Mass, Energy, Rate, Summation, Hydraulic and eQuilibrium equations
MESH	Mass, Equilibrium, Summation and Energy equations
pp-HIDiC	Plate-packed HIDiC
PR	Peng-Robinson
s-HIDIC	Structured HIDiC
SRV	Secondary reflux and vaporisation
STP	Standard pressure and temperature
VC	Vapour Compression
VLE	Vapour-liquid equilibrium
VRC	Vapour ReCompression

Roman

A	Surface area for heat transfer Q	m^2
a_e	Effective interfacial area	m^2/m^3
a_p	Packing surface area	m^2/m^3
a_{wet}	Area of the packing covered in liquid	m^2/m^3

A_s	The cross-sectional area of the packing,	m^2
C	Total number of components (generally 2 in this study)	–
C_e	Correction factor for surface renewal in a packing	–
c_p	Specific heat at constant pressure	$J/(kg \cdot K)$
c_t	Total concentration / Molar density	mol/m^3
D	Characteristic length / Hydraulic diameter	m
E	Energy residual	J/s
e	Total energy flux (on a stage j)	$J/(m^2 \cdot s)$
Ex	Exergy	J/s
f	Feed molar flow rate to a stage	mol/s
F-factor	Troughput factor $F = u_s\sqrt{\rho_V}$	$Pa^{0.5}$
h	Enthalpy	J/mol
h_l	Liquid hold-up	–
H_s	The height of a non-equilibrium stage	m
H_{res}	(Hydraulic) Pressure residual, following convention	Pa
htc	Heat transfer coefficient	$J/(m^2 \cdot s \cdot K)$
h_p	Partial molar enthalpy	J/mol
J	Diffusion flux	$mol/(m^2 \cdot s)$
j	Chilton-Colburn j-factor	–
K	Equilibrium constant (K-value)	–
k	Mass transfer coefficient	m/s or $kg/(m^2 \cdot s)$
L	Liquid phase total molar flow rate	mol/s
M	Mass residual	kg/s
M_{mol}	Molar mass	kg/mol
N	Mass flux	$mol/(m^2 \cdot s)$
N_s	Total number of stages	–
N_{min}	Minimum number of stages	–
p	Pressure	Pa

Pr	Prandtl number, $\frac{\mu c_p}{\lambda}$	
Q	Heat transfer to a stage by a heating element	J/s
q	(Conduction) heat flux towards the interface on a stage	$\mathrm{J/(m^2 \cdot s)}$
Q_{res}	Equilibrium condition residual	–
$\mathbf{R}$	Vector of residuals	–
R	Mass transfer residual	mol/s
r	Draw from a stage	mol/s
R_g	Gas constant	$8.3144\,\mathrm{J/(mol \cdot K)}$
Re	Reynolds number, $\frac{\rho u D}{\mu}$	–
S	Mole fraction residual	–
Sc	Schmidt number,	–
St_h	Stanton number for heat transfer, $\frac{h}{\rho u c_p}$	–
St_m	Stanton number for mass transfer, $\frac{k}{u}$	–
T	Temperature	K
U	HIDiC heat transfer coefficient from rectifier to stripper	$\mathrm{W/(m^2 \cdot K)}$
u_s	superficial vapour velocity	m/s
u	Velocity	m/s
V	Vapour phase total molar flow rate	mol/s
V_s	The volume of a non-equilibrium stage, $A_s \times H_s$	$\mathrm{m^3}$
w	Packing cell width in the pp-HIDiC geometry	m
$\boldsymbol{x}$	variables vector	–
x	Mole fraction in the liquid phase	–
x	mole fraction in the liquid phase	–
y	mole fraction in the vapour phase	–
z	Overall feed mole fraction	–

Greek

α	Separation factor / relative volatility	–
β	Correction factor for dilute liquid diffusivity	–

Δ	Difference between two values of a quantity, $(\ )_2 - (\ )_1$	
ε	Void fraction	–
γ	activity coefficient	–
κ	Specific heat ratio	–
λ	Thermal conductivity	$\mathrm{J/(s \cdot m \cdot K)}$
μ	Dynamic viscosity	$\mathrm{Pa \cdot s}$
φ	Internal corrugation angle	–
ρ	Density	$\mathrm{kg/m^3}$
θ	Bulk flow correction factor / Corrugation angle	–

Other

$\mathcal{D}$	Diffusion coefficient	$\mathrm{m^2/s}$
$\mathcal{E}$	Total energy transfer in a non-equilibrium stage	J/s
$\mathcal{N}$	Total mass transfer in a non-equilibrium stage	mol/s
$\sum_V$	Sum of atomic diffusion volumes of species in a mixture	–

Subscripts

0	Property at standard (atmospheric) consditions
0	Reference state
B	Property of the Bottoms stream
c	Compressor
$cond$	Condenser
D	Property of the distillate stream
dry	Dry (for when packing is not wetted)
e	Effective, e.g. effective interfacial area or flow velocity
f	Property of the feed stream
fs	feed stage number
h	Related to heat transfer
i	Indicates a species, e.g. for a partial molar quantity
j	Stage number

k	Indicates a species, distinguishes between another species i
L	Property or stream of the liquid phase
lam	Laminar
m	Related to mass transfer
R	Rectification section
r	Reduced (e.g. reduced pressure)
reb	Reboiler
S	Stripping section
$strip$	Related to the stripper
T	Total, e.g. total mole flow rate or non-partial quantity
$turb$	Turbulent
u	Utility
V	Property or stream of the vapour phase

Superscripts

$\bullet$	Property that is corrected for a bulk flow contribution
I	Property of the vapour-liquid interface
L	(In MERSHQ equations) Property or stream of the liquid phase
lp	Low pressure
T	Transpose of a vector
V	(In MERSHQ equations) Property or stream of the vapour phase

1
Introduction

This thesis work is commissioned by TechnipFMC, one of world's leading suppliers of ethylene technologies. Although distillation technologies have seen major improvements over the years, including heat integration, new regulatory challenges require further reduction of emissions and energy usage. The societal significance of these developments is illustrated in the following sections, followed by an outline of the document.

1.1. Societal context

The Paris climate agreement from 2015 aims to limit global warming to a maximum of 2°C. The agreement was signed by the European Union, obligating its member states to cooperate with the necessary measures that limit the global average temperature increase. There is a wide support for the conclusion that CO_2 emissions contribute to the measured temperature rise of the earth. The Paris agreement therefore prescribes that countries are to substantially reduce their CO_2 emissions [2]. The EU has agreed to a binding 40% reduction in CO_2 emissions compared to 1990 levels by 2030. Also, a 27% increase of the total share of renewable energy and a 27% of reduction in energy usage have to be realised before 2030. The Paris agreement is legally binding for the signatories.

To gradually implement the reduction, the European Union set itself a goal for 2020 of 20% reduction in emissions compared to 1990 levels. Additionally, the share of renewable energy sources has to increase to at least 20%, and the overall energy efficiency must rise by 20% [3]. EU member states are obliged to reach this reduction. The Dutch government communicates that this is to be imposed via a 'robust and effective legislative framework' [2]. In other words, companies and residential emitters and users are going to be bound by law to reduce emissions and energy usage.

The EU is on track to reach its 2020 emission targets, but pre-2020 emission laws are not enough to also meet the 2030 targets [4]. This is shown in Fig. 1.1. Existing measures by the EU do not lead to a quick enough decline of emissions. On top of this, wealthier countries are required to reduce their emissions more quickly than the average. The Netherlands, for instance, have already reached a nationwide agreement [5] to achieve emission reduction of 49% by 2030. Different sectors are expected to contribute to this percentage based on the estimated potential for reductions in the sector.

Since the Paris agreement is legally binding, the EU is already taking steps to extend its Emissions Trading System (ETS). The following two measures are proposed [6]:

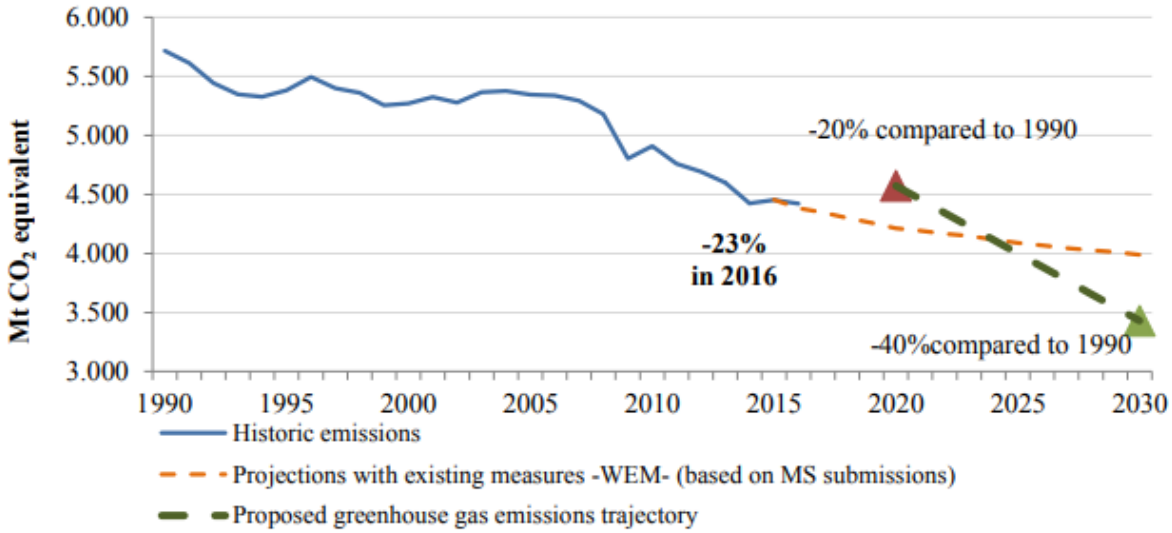

Figure 1.1: Total EU CO_2 emission since 1990. Historical EU CO_2 emission, predicted emission under current legislature and a proposed trajectory to meet 2030 targets. This figure is as published in the November 2017 European Commission progress report [4]. Usage is according to the European Commission reuse policy.

1. Revision of the ETS into a system that is stricter.
2. Non-ETS sectors must reduce emissions by 30%, which is to be enacted by putting in place nationally determined legislation.

The revision of the ETS for the period after 2020 will entail that the number of emission allowances will be reduced. The number of allowances will go down by 2.2%, opposed to an annual decrease of 1.74% before 2020. Consequently, allowances become scarce quicker, which will be reflected in the price that plant operators have to pay to emit greenhouse gases. Aside from ethical reasons, companies thus increasingly face financial reasons to switch to environmentally friendly technologies.

1.1.1. Industrial consequences of the Paris agreement

In 2018, an increase in energy efficiency is accompanied by a reduction of CO_2 emission since the majority of the power is still generated by burning fossil fuels. Targeting energy efficiency of existing applications is therefore a way to work towards two of the main goals of the Paris agreement. Additionally, energy savings directly decrease operational cost of all users because less fuel or electricity is needed for operation.

CO_2 reductions through energy saving, however, cannot indefinitely decrease emission. Some applications inherently require a fixed amount of energy due to the nature of the application - for instance, to melt steel or to operate a steam cracker. Many of these processes have been around for a long time and have been optimised over time. Further emission reduction can then only be achieved by switching to renewable energies, or by an overhaul of the process, the latter of which, if possible at all, requires major investments.

The price of solar and wind energy has been decreasing ever since their introduction, with a continuous price decrease per kWh from about 2010 to 2017 [7]. Yet, burning gas

or coal for heat is still cheaper than using electricity for the same purpose, and this will likely remain so in the nearby future. Hence, in the current situation, there is still little economic incentive for companies and residential users to switch to renewable sources of energy, albeit subsidies and research funding have created a drift toward renewables. In the years toward 2030, this incentive will be created by legislation. Industries have yet to develop technologies to allow them to remain profitable during this period. The 2030 targets are, however, only a part of the total challenge to industry: After 2030, there will be new EU emission targets. EU is aiming for a low-carbon economy, with 60% reduction in 2040 and 80% reduction in 2050 [8].

TechnipFMC is looking onto in energy- and emission reducing technologies, both for financial reasons and ethical reasons [9]. Distillation is cited in literature as one of the most energy-consuming unit operations; it is reported to use over 40% of the total energy required in ethylene plants [10], and about 50% of its operational cost [11]. The heat-integrated distillation column is a technology that brings down the energy use of some of the highest-demand distillation columns significantly.

Given the context that this section illustrates, TechnipFMC is interested to see if heat integrated distillation is a feasible way to achieve energy savings and emissions reduction for distillation in their ethylene plants.

1.1.2. Scientific significance

Prior work on the Heat Integrated Distillation Column (HIDiC) concept was done by several research groups around the world, most of them in academic environments. Research groups at the Northwestern University in Chicago and at several institutes in Japan have done major contributions to HIDiC research before the year 2000. After 2000, contributions at the Technical University of Denmark and Delft University of Technology in the Netherlands have expanded HIDiC knowledge. This thesis draws from all aforementioned work and aims to translate the knowledge to a model that can indicate the size, energy usage and energy consumption of the device. The model can be used as a tool to determine the practical viability of the HIDiC technology for different separations.

The HIDiC technology has been researched since the 1970's. It has so far seen only one successful commercialisation in Japan, which does offer some advantage over conventional column, but not enough to see widespread adoption and commercial success. The 2012 paper by Bruinsma, Krikken, Cot, Sarić, Tromp, Olujić & Stankiewicz [1] showed that a slit-configuration with pieces of packing performed better than the authors expected. The viability of the structured internal heat integrated distillation column (s-HIDIC) with a sheet metal packing and its potential for process intensification needs to be explored further. The separation performance of the sheet packed HIDiC configuration made it one of the most promising candidates for industrial implementation.

More work is needed to definitively tell if a design can be made in such a way that it would be applicable in an ethylene plant. Some of the uncertain factors at the time of writing are both steady and unsteady operation, start-up phenomena, coupling of stripping and rectification sections, liquid holdup, flooding characteristics and determination of the optimal compression ratio and build cost. Most of these ideally need to be answered to determine the viability as a competitor to other column designs.

1.1.3. Introduction to current research

The energy usage of close-boiling distillation columns can be improved by re-using the heat that is available throughout the column. One way to do this, is by applying the principle of operation of a heat pump to a distillation column. A part of the column is compressed, which causes its phase equilibrium to be at an elevated temperature. The higher temperature, higher quality heat that is available in the compressed section, can be used as a heat source for the remaining part of the column. The electrical power for compression is effectively traded for heat recovery, which leads to lower condenser and reboiler duties. The HIDiC thus promises to be an *intensified* process operation that could replace current conventional distillation columns for a column that uses fewer resources and has lower emissions.

In a heat integrated distillation column, the rectification section is compressed and heat is exchanged with the entire stripping section. The required heat exchange surface must be introduced in the column without compromising its separation performance. This thesis focuses on modelling one of the possible device configurations that allow this heat exchange to take place.

The plate-packed HIDiC (pp-HIDiC) configuration as described by Bruinsma, Krikken, Cot, Sarić, Tromp, Olujić & Stankiewicz [1], compared to previous HIDiC designs, has a larger specific surface area for heat transfer from the stripper to rectifier. In designs from before this publication, researchers struggled to implement enough area for heat transfer in conventional columns - with the exception of a finned-plate configuration, which in turn had worse mass transfer characteristics compared to the plate-packed configuration.

Subject of this thesis

This thesis therefore focuses on modelling the pp-HIDiC. A modelling technique is needed to estimate and predict the performance of the pp-HIDiC in more detail. Optimisation of the setup may lead to improvements over the published setup, which could decrease the column size, and improve its efficiency.

This thesis describes modelling work that is done to calculate process variables and size of one of the most promising HIDiC applications - the C_2-splitter, one or the major separations done in an ethylene plant. The goal of this thesis is to contribute to model development that could aid future distillation column designers in choosing dimensions, duties and flow rates to properly design a HIDiC.

1.2. Document outline

The outline of this document is described in this chapter to serve as a reading guide. Appendix A contains basic distillation theory to introduce the reader to some distillation concepts. A brief overview of conventional distillation also serves as a motivation for the use of heat-integrated distillation columns in industry.

Chapter 2 starts with a short summary of distillation equipment. It serves as an introduction of structured packings and the modelling of equipment with that type of packings, which is the subject of this thesis. After this, the rate-based modelling of distillation in this type of equipment is discussed. Rate based models need a mass transfer description, which is discussed next.

After this, different distillation technologies are compared with the Heat Integrated Distillation Column (HIDiC) technology. This comparison shows the separations for

which HIDiC could be a beneficial technology over other existing technologies. The first section of chapter 2 is then completed by a short review of several HIDiC projects around the world and their contributions to the technology.

Chapter 2 also provides the description of the transport phenomena for heat and mass transfer. Corrugated sheet metal packings are introduced, and several aspects that determine their performance are discussed. The heat and mass transport section continues by explaining engineering correlations for heat and mass transfer, and finally, existing correlations and their relevance are discussed.

The model description in Chapter 3 describes the model implementation in Python. It gives a motivation for the choice of Python packages, and gives some more background on the calculation procedure.

Next, the work is discussed in Chapter 4. Finally, conclusions and recommendations are given in Chapter 5.

2

Theory

This chapter provides the theory that is the basis for this study. The discussion starts from the distillation principle and proven technologies. Although the modelling work done in this work focuses on the modelling software development for a plate-packed HIDiC, most of the developed theory in literature for different HIDiC configurations is applicable for the plate-packed HIDiC as well. Also, terminology and knowledge from conventional distillation are applicable, and are useful for reference and for comparison between technologies. Attachment A therefore starts with the basics of the principles of distillation that also apply for conventional columns, building up from first principles.

2.1. Distillation equipment

Conventional distillation columns use trays of varying designs to make the fluids flowing up and down the column come to equilibrium, after which vapour and liquid flow up and down to come into equilibrium on subsequent trays. Often, equilibrium is not established completely, which can be displayed in the McCabe-Thiele diagram in the following way depicted in Fig. 2.1. The mixture does not reach the composition of the separation curve, and is passed to the next tray before it is able to do so. It can be seen that more trays are needed to perform a separation due to this effect.

Another observation from figure 2.1b is that a tray with a very low efficiency will lead to a larger number of stages. A packed bed could be seen as the extended version of this, as the mixture is never in equilibrium. Instead of trays, they have a continuous transfer of mass and heat along the column height. The driving force for mass transfer - concentration difference between the phases - can thus in principle be kept larger than in an equilibrium tray. Additionally, structured packings have a large surface area per cubic metre, making it possible to exchange more mass per unit volume compared to trayed columns.

A description of the heat and mass transfer rate is thus needed to model these columns. In a McCabe-Thiele diagram, this could be represented with a continuously curved McCabe-Thiele line. This will be further explained in section 2.7.1.

2.1.1. Packed columns

Mass transfer from the liquid to the vapour phase happens continuously, until equilibrium is reached. Near equilibrium, mass transfer is slower because its driving force, chemical potential difference, is smaller [12]. The entropy production that accompanies

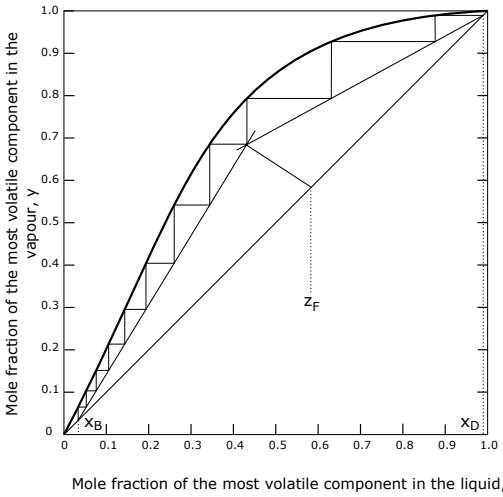

(a) A McCabe-Thiele diagram for trays with 100% tray efficiency

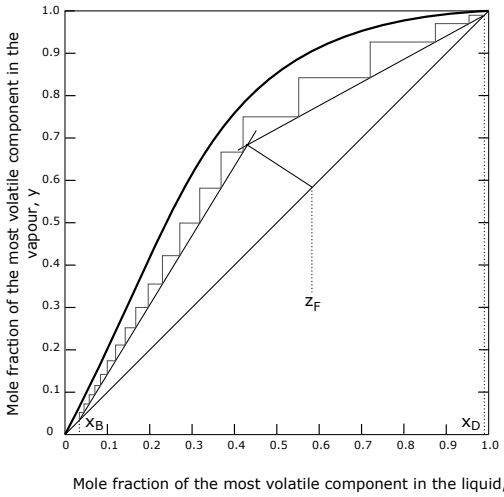

(b) A McCabe-Thiele diagram for trays with less than 100% tray efficiency

Figure 2.1: McCabe-Thiele diagrams

heat and mass transfer is small if their driving forces are small. A gradual increase in concentrations in the liquid and vapour phase will therefore result in a lower entropy production. This is advantageous, because high entropy production is paid for by more energy degradation in the irreversible processes [13].

If driving forces become minimised, sufficient surface area for mass transfer must be available to maintain the desired overall rate of mass transfer. The use of *packed beds* creates both a larger surface area and continuous contacting operation [14–16]. A packed bed is a random or ordered porous geometric structure, made from metal or plastic, that fills the distillation column. Its purpose is to create a large interfacial area, to redistribute liquid and vapour, reducing pressure drop and reducing liquid holdup [14].

The operation of the column differs only slightly, but mole fractions gradually change over the height of the column, rather than step wise in trays. Consequentially, mass transfer takes place along the whole height of the column, and the mixture is never in equilibrium. Equilibrium models can therefore not be used if the physics behind packed bed operation is to be described correctly [17]. Instead, *rate-based* models describe this process. This is why this study considers Rate-based models. Rate-based models are explained in section 2.3.

Because of historical reasons, and to provide a quick height estimation method for packed bed columns, the separation performance of a packed bed is often expressed in terms of how many theoretical trays it is equivalent to. The HETP - Height Equivalent of a Theoretical tray is the packed bed height that is needed to equal the separation effect of one equilibrium stage [17]. This approximation is not accurate, because heat and mass transfer in structured packings both depend on flow regimes, temperature, pressure and mole fractions. HETP should therefore not be used in more detailed designs past initial estimations [18, 19]. Still, HETP is often used in comparisons between packings, and researchers that measure packing performance often do so in terms of HETP. Rate-based models do not make use of HETP, but calculation of HETP from mass transfer coefficients (described in section 2.3) is sometimes required to compare literature results.

(a) Smooth, perforated surface

(b) 3D Grooved, perforated surface

(c) 3D embossed, unperforated surface

Figure 2.2: A close up of a corrugated sheet that packings are made of. Pictures are from the work of Subramanian & Wozny [20].

Also, rate-based models require more details about the heat and mass transfer in a packing, so a quick HETP model can be used for preliminary design studies.

2.1.2. Sheet metal corrugated packings

An overview of all types of packings will not be provided; only the considered packing in this study and its behaviour will be discussed. This study considers Sulzer Mellapak 350Y packing, as existing measurement data were based on using this type of packing [1]. This packing is a type of Corrugated Sheet Metal Packing packing (CSMP). These types of packing are made of a thin corrugated sheet of metal that are folded and surface treated to enhance mass transfer. Figure 2.2 [20] shows common different surface treatments of packings and shows what the sheets look like.

Multiple of these sheets are then placed in a bundle, alternating the angle of the corrugation (see Fig. 2.3). A good description of the structure of CMSP can be found in the paper by Stoter, Olujić & de Graauw [21]. The surface is dented and perforated to increase wetting - the degree to which the surface is covered with liquid. Good wetting ensures that the area to exchange heat and mass between vapour and liquid phases is roughly the same as the packing specific surface area. Dry spots on the surface render part of the available area for heat and mass transfer unused. This causes problems when the column was designed with the assumption of complete wetting, because the decrease in mass transfer efficiency can prevent the column product from reaching its desired specification. All sheet metal corrugated packings are quite similar at a glance, but parameters like their angle and depth of corrugation or surface treatments influence their effectiveness. Different commercial packings therefore differ in performance and price. In literature, many of these packings have been characterised by equations for heat transfer, mass transfer and pressure drop, which will be discussed in section 2.3. The benefit of corrugated sheet packings is that they have a large specific surface area and good lateral mixing. Due to these effects, the packings have fewer dry spots, and possible initial maldistribution of liquid can be compensated by the distribution of flow by the intrinsic flow characteristics belonging to the packing. When implemented correctly, there is a lower chance of mixing of streams of different compositions.

Figure 2.3: Sulzer's Mellapak™ packing is one type of CSMP [22]. It comes in different materials, corrugation angles and specific surface areas.

2.2. Thermodynamic property model

All the calculations done on distillation columns require accurate models of the fluid mixture behaviour. The accurate approximation of real properties is necessary to make models reliable [23]. The C_2-splitter separates light, non-polar hydrocarbons that have negligible other interactions. Seader, Henley & Roper [17] provide a quick selection procedure for different compounds.

The authors write that the Soave-Redlich-Kwong equation of state is not recommended for cryogenic purposes. For all temperatures, as long as the pressure is not near the critical region, the Peng-Robinson equation of state can be used.

The Peng-Robinson (PR) equation of state is a commonly used tool in engineering and does not have a large deviation in comparison with other equations of state [24]. In a review by Valderrama [25], the author argues that the Peng-Robinson equation is usable for light hydrocarbons mixtures. The author also provides recommendations for the use of mixing rules for polar or non-polar mixtures, as well as the choice of the expression for the temperature-dependent term. It is convenient that both molecules are linear, nonpolar molecules, and their critical temperatures and pressures are well known. The equations for the Peng-Robinson equation of state can be found in the work by Peng & Robinson [26].

Along with the Peng-Robinson equation of state, a Helmholtz-free energy approach is used by CoolProp [27], one of the software packages that is used for this work. Chapter 3 discusses this package in more detail.

2.3. Rate-based models

Section 2.1 argued that HETP does not accurately predict the performance of packed beds. Rate-based models are a method of calculating the performance of the bed that more closely resembles the actual physics of mass transfer across a vapour-liquid interface. This section draws heavily from Seader, Henley & Roper [17] and Taylor & Krishna

[28] and their description of the workings of rate-based models.

2.3.1. Rate based model for a non-equilibrium stage

Analogous to the diffusion equation and film models, mass transfer rate in a multi-phase mixture can be expressed by transport rate equations for each present component. For distillation of a two-component mixture, also called *binary distillation*, there are two components and two phases. Because components removed from the vapour phase are added to the liquid phase, only two equations are needed for mass transfer - one for both components. The same applies for heat transfer at the interface. Rate-based models are a set of conservation and equilibrium equations for N_s (incremental) stages and C components. The variables that are required are displayed in the schematic diagram of a nonequilibrium stage in Fig. 2.4. For a further explanation, the reader is referred to the nomenclature of this document.

Following the notation of Taylor & Krishna [28], the total mass transfer of component i in an incremental stage j is the flux $N_{i,j}$ of that component integrated over the incremental packing specific surface area. If the element is sufficiently small however, it will suffice to take the component molar fluxes $N_{i,j}$ and multiplying them with the effective specific surface area of the slice of packing $a_{e,j}$. This is a packing-specific area that describes the area of the packing that is used for mass transfer. Section 2.5.4 contains more information on the effective surface area of packings and its dependence on flow characteristics.

$$\begin{aligned} \mathcal{N}_i^V &\approx N_{ij}^V a_{e,j} V_s \\ \mathcal{N}_i^L &\approx N_{ij}^L a_{e,j} V_s \end{aligned} \tag{2.1}$$

In the limit of a very small incremental stage, the fluxes and interfacial area are considered constant in the stage, and the integral becomes a multiplication. The notation with $\mathcal{N}$ is used to distinguish the total heat and mass transfer in an incremental element and the fluxes per surface area. The total transfer of both components on stage j is given by the sum of the individual component rates (Eq. 2.2).

$$\mathcal{N}_{T,j} = \sum_{i=1}^{C} \mathcal{N}_{i,j} \tag{2.2}$$

The following section is a list of all the equations for an incremental non-equilibrium stage. The equations are written in their *residual form* in Eqs. 2.3 to 2.30. All terms are moved to the right-hand side, and a residual term is introduced on the left-hand side of the equations. The left-hand sides represent the computational residuals that are to be minimised during the solving procedure. These equations have to be solved N_s times for a column part that is partitioned in N_s pieces.

The convention for heat and mass transfer is that they are positive from the vapour to the liquid phase. The notation in Eqs. 2.3 to 2.30 uses the notation from Fig. 2.4. The terms $\mathcal{N}$ and $\mathcal{E}$ describe the total mass and energy transfer across the interface. These require separate equations that are discussed in the next section. Liquid phase component balance

$$M_{i,j}^L \equiv (1 + r_j^L) L_j x_{i,j} - L_{j-1} x_{i,j-1} - f_{i,j}^L - \mathcal{N}_{i,j}^L = 0 \qquad (i = 1, 2, \ldots, C) \tag{2.3}$$

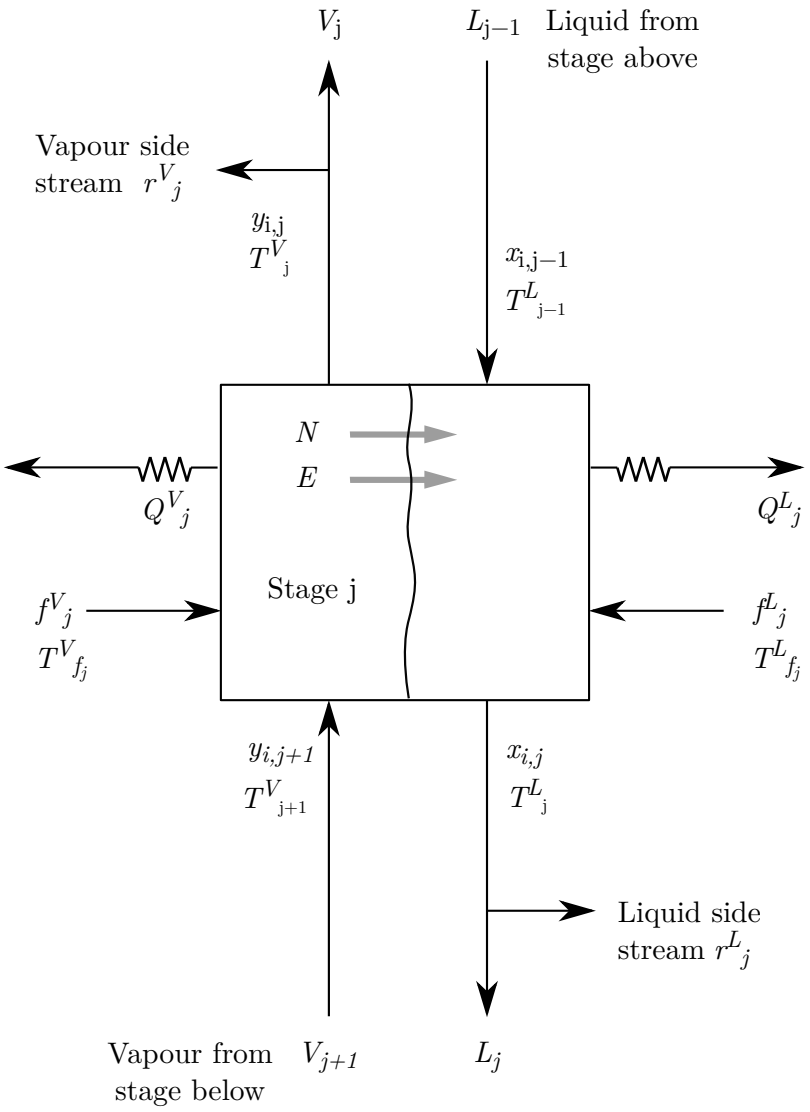

Figure 2.4: An incremental stage j in the non-equilibrium model is a mass and energy balance control volume. The variables that are required to calculate all fluxes are indicated beside the stream. The interface between liquid L and vapour V is the only location at which the two phases are in equilibrium. This figure is adopted from by Taylor & Krishna [28].

Vapour phase component balance

$$M_{i,j}^V \equiv (1 + r_j^V)V_j y_{i,j} - V_{j+1} y_{i,j+1} - f_{i,j}^V + \mathcal{N}_{i,j}^V = 0 \qquad (i = 1, 2, \ldots, C) \quad (2.4)$$

Liquid phase energy balance

$$E_j^L \equiv (1 + r_j^L)L_j h_j^L - L_{j-1} h_{j-1}^L - h_j^{f,L} \sum_{i=1}^{C} f_{i,j}^L + Q_j^L - \mathcal{E}_j^L = 0 \quad (2.5)$$

Vapour phase energy balance

$$E_j^V \equiv (1 + r_j^V)V_j h_j^V - V_{j+1} h_{j+1}^V - h_j^{f,V} \sum_{i=1}^{C} f_{i,j}^V + Q_j^V + \mathcal{E}_j^V = 0 \quad (2.6)$$

Mass transfer rates

$$R_{i,j}^L \equiv N_{i,j} - N_{i,j}^L = 0 \qquad (i = 1, 2, \ldots, C - 1) \quad (2.7)$$

$$R_{i,j}^V \equiv N_{i,j} - N_{i,j}^V = 0 \qquad (i = 1, 2, \ldots, C - 1) \quad (2.8)$$

Summation of mole fractions at the vapour/liquid interface

$$S_j^{LI} \equiv \sum_{n=1}^{C} x_{i,j}^I - 1 = 0 \quad (2.9)$$

$$S_j^{VI} \equiv \sum_{n=1}^{C} y_{i,j}^I - 1 = 0 \quad (2.10)$$

Hydraulic equation

$$H_{res,j} \equiv p_j - p_{j-1} - \Delta p_{j-1} = 0 \qquad (j = 1, 2, \ldots, N_s - 1) \quad (2.11)$$

Equilibrium at the interface

$$Q_{res,i,j}^I \equiv K_{i,j} x_{i,j}^I - y_{i,j}^I \qquad (i = 1, 2, \ldots, C) \quad (2.12)$$

Taylor & Krishna [28] and Seader, Henley & Roper [17] both write that additional equations are needed to solve the system. By using the component mass transfer rate balances, both publications use the total material (mole) balances to obtain a total balance equation, (Eqs. 2.13 and 2.14). The last term in these equation is the total mass transfer rate in the incremental element, given in equation 2.2.

Liquid phase total component balance

$$M_{T,j}^L \equiv (1 + r_j^L)L_j - L_{j-1} - \sum_{i=1}^{C} f_{i,j}^L - \mathcal{N}_{T,j} = 0 \quad (2.13)$$

Vapour phase total component balance

$$M_{T,j}^V \equiv (1 + r_j^V)V_j - V_{j-1} - \sum_{i=1}^{C} f_{i,j}^V + \mathcal{N}_{T,j} = 0 \quad (2.14)$$

Similarly, Taylor & Krishna [28] give the working equation for the energy balance around the interface (Eq. 2.30).

$$E_j^I \equiv e_j^V - e_j^L = 0 \tag{2.15}$$

Taylor & Krishna [28] assume both the vapour and liquid bulk phases to be completely mixed. This is a reasonable approximation of reality, and it is one of the modelling simplifications in rate-based models. Besides this assumption, rate-based models rely on the accuracy of correlations for the rate of heat exchange and mass transfer. Mass and energy transfer across the interface are the distinguishing part of rate-based models. The calculation of these rate equations is discussed in sections 2.4.1 and section 2.4.2.

In equations 2.5 and 2.6, $\mathcal{E}$ represents the heat transferred in a stage on the packing by both heat conduction and the heat transfer that accompanies mass transfer. Q is the heat transfer to a stage from outside of the stage, for example by a heating coil or other heating element. Q is used in this study to represent the heat transfer between the stripper and rectifier.

2.3.2. System solving method

Seader, Henley & Roper [17] write that $5C+5$ equations are needed to solve the system, where C is the number of components in the system. The authors mark the hydraulic equation as optional. Although the effects of the changing pressure may be small in practice, the accuracy of all calculated thermodynamic properties depends on the quality of the pressure estimation. It is easy to see that a good pressure estimation will, to an extent, be of influence on the outcome of the model. Taylor & Krishna [28] do therefore not see the equations for pressure drop as optional, bringing the total number of equations per stage to $5C + 6$.

The number of variables for N stages is $7N_sC + 14N_s + 1$. The number is brought down with thermodynamic relations that specify the feed conditions, with provided sidestream information and stage heating Q^L and Q^V. If a constant pressure drop per stage is specified, the pressure on a specific stage, p_j is easily calculated. If, however, a correlation for the pressure drop is used, the number of independent variables is brought back to 5C+6, which makes the system solvable.

The system of the equilibrium stage that is considered, is solved by minimising a vector containing all the equation residuals on the left hand side of Eqs. 2.3 to 2.30. First, a vector x_j of all variables is made. The equations are then grouped in a vector $\boldsymbol{R_j}$ containing all equations for stage j. The residuals must be minimised to create a set of variables that are closest to the solution of the problem. This transforms the problem into a root finding problem, which can be solved using one of many available root-finding

algorithms such as the Newton-Raphson method.

$$\begin{aligned}\boldsymbol{R}_j^T \equiv \Big[& M_{1,j}^L, M_{2,j}^L, \ldots, M_{C,j}^L, M_{1,j}^V, M_{2,j}^V, \ldots, M_{C,j}^V, M_{T,j}^L, M_{T,j}^V, \\ & E_j^L, E_j^V, E_j^I \\ & R_{1,j}^L, R_{2,j}^L, \ldots, R_{C-1,j}^L, R_{1,j}^V, R_{2,j}^V, \ldots, R_{C-1,j}^V, \\ & S_j^{LI}, S_j^{VI}, \\ & H_{res}, \\ & Q_{res,1,j}^I, Q_{res,2,j}^I, \ldots, Q_{res,C,j}^I, \Big]\end{aligned} \tag{2.16}$$

$$\begin{aligned}\boldsymbol{x}_j^T \equiv \Big[& V_j, y_{1j}, y_{2j}, \ldots, y_{C,j}, T_j^V \\ & y_{1j}^I, y_{2j}^I, \ldots, y_{Cj}^I, x_{1j}^I, x_{2j}^I, \ldots, x_{C,j}^I, T_j^I, \\ & L_j, x_{1j}, x_{2j}, \ldots, x_{C,j}, T_j^L \\ & \mathcal{N}_{1j}, \mathcal{N}_{2j}, \ldots, \mathcal{N}_{C,j}, \\ & p_j \Big]\end{aligned} \tag{2.17}$$

The equations for the whole column are then constructed by putting all vectors j together for all N stages. The condenser and reboiler equations are a separate set of equations. They are added to this vector. They are modelled as equilibrium stages, as described in the next section, 2.3.3.

$$\boldsymbol{R}^T = \Big[\boldsymbol{R}_1, \boldsymbol{R}_2, \ldots, \boldsymbol{R}_n \Big]^T \tag{2.18}$$

$$\boldsymbol{x}^T = \Big[\boldsymbol{x}_1, \boldsymbol{x}_2, \ldots, \boldsymbol{x}_n \Big]^T \tag{2.19}$$

This study does not attempt to write a new solver. The above vectors are implemented in an existing solver.

2.3.3. Condenser and reboiler equations

The vapour and liquid in the condenser at the top of the column and in the reboiler at the bottom of the column are assumed to be in equilibrium. There is an additional set of equilibrium equations that specify the equilibrium condition and the flow rates associated with the condenser and reboiler.

The partial condenser and reboiler are modelled as equilibrium stages, where vapour and liquid are in equilibrium. The equations for these do not include mass and heat transfer but assume equilibrium in the devices. This is realistic, since heat and mass transfer are either fast, or the mixture has enough time to get to equilibrium. An equilibrium model is made by using Fig. 2.4 and removing heat and mass transfer. The liquid and vapour phases are then in equilibrium.

The MESH equations describe the mass and energy balances to compute the variables of the equilibrium stage. The equations are similar to the MERSHQ equations, but heat and mass transfer occur instantly inside the stage. Material and energy balances have to be satisfied. Their outcome is prescribed by the equilibrium condition, constrained by

the summation of mole fractions. In literature, the residuals are named using the letters MESH, but this thesis will use the same names for the residuals for both the MESH and MERSHQ equations. Q_{res} will for example be the equilibrium equation residual in both cases.

Material balance

$$\begin{aligned} M_{i,j} \equiv\ & L_{j-1}x_{i,j-1} + V_{j+1}y_{i,j+1} + f_j z_{i,j} \\ & - \left(L_j + r_j^L\right) x_{i,j} - \left(V_j + r_j^V\right) y_{i,j} = 0 \end{aligned} \tag{2.20}$$

Equilibrium condition

$$Q_{res,i,j} = y_{i,j} - K_{i,j}x_{i,j}, \tag{2.21}$$

Summation requirement for mole fractions

$$S_j^V \equiv \sum_{i=1}^{C} y_{i,j} - 1 = 0 \tag{2.22}$$

$$S_j^L \equiv \sum_{i=1}^{C} x_{i,j} - 1 = 0 \tag{2.23}$$

H: enthalpy/energy balance

$$\begin{aligned} E_j \equiv\ & L_{j-1}h_{j-1}^L + V_{j+1}h_{j+1}^V + f_j h_j^f \\ & - \left(L_j + r_j^L\right) h_j^L - \left(V_j + r_j^V\right) h_j^V - Q_j = 0 \end{aligned} \tag{2.24}$$

The equilibrium equations can be added to the non-equilibrium equations (Eqs. 2.3 2.14). In the model for HIDiC, there is one reboiler and one condenser, at the top stage and bottom stage. This leaves 2C + 3 equations (2.20 - 2.24) for both pieces of equipment that appear at both ends of the system vector.

2.4. Rate equations for heat and mass transfer

The transport of mass $\mathcal{N}$, and heat $\mathcal{E}$, on the packing surface is included in the system of MERSHQ-equations, where the transport appears in the component and energy balances (Eqs. 2.3 to 2.8). The rate of transport varies per packing, flow regime, mixture composition and pressure and temperature. The theory for the use of different correlations is provided in the this section.

All the theory discussed in this section holds for every non-equilibrium stage. Therefore, the index j, that applies for nearly every variable, is omitted in this section.

2.4.1. Mass transfer rate equations

To find the total mass transfer N^L and N^V in a stage, contributions from bulk flow and diffusion are combined. Consider the piece of the vapour-liquid interface in Fig. 2.5. Mass is transported by bulk transport and by diffusion. Only mass transport perpendicular to the interface is considered, allowing the transport to be defined with scalar equations. The overall mass transfer coefficient can depend on the rate of transport

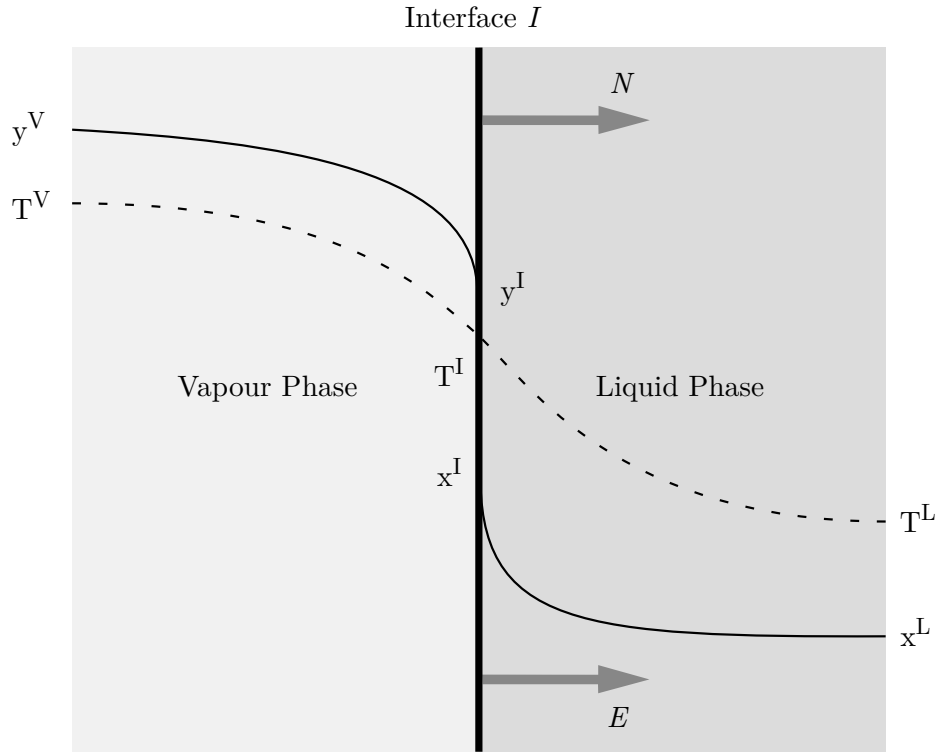

Figure 2.5: The vapour-liquid interface is assumed to be in thermodynamic equilibrium. Bird [29] writes that this assumption is valid as long as the mass transfer resistance of the interface is negligible.

itself. In that case, a *bulk transport* term is added in the equation. These effects are usually small in distillation and therefore neglected, but they will be included here for a complete description of the theory.

The diffusion of species i between the bulk compositions x_i^b or y_i^b, and the composition of the interface, x_i^I and y_i^I, is given by Eq. 2.25 [30]. An interface is present in every non-equilibrium stage, so the index j is omitted from the following discussion to improve readability. Eq. 2.25 is based on c_t, which is the total concentration (or molar density) in mol/m^3. Therefore, the units of k are m/s.

$$\begin{aligned} J_i^V &= c_t k_V^\bullet (y_i^V - y_i^I) \\ J_i^L &= c_t k_L^\bullet (x_i^I - x_i^L) \end{aligned} \tag{2.25}$$

Following notation of Bird [29], a dot ($\bullet$) is used as a superscript for transfer coefficients that include a bulk flow correction. This correction must be implemented as large rates of mass transfer distort the surface of the interface and contribute to the mass transfer coefficient. The bullet notation distinguishes the low-flux and high-flux coefficients.

Equations 2.25 give the diffusion fluxes of all species in both phases, with a mass transfer coefficient that is concentration-based. The mass transfer coefficients in literature can be concentration based or pressure based, the latter of which is usually only the case for vapours. In that case, the partial pressure of the components is used instead.

The total flux, N_i, of component i is its diffusion speed through the bulk, plus the speed at which it is transported by bulk transfer, N_T [17, 28, 30]. This total (bulk) transfer N_T must be included in the transport of all species. For a binary mixture, the bulk flux becomes simply $N_T = N_1 + N_2$. The transfer of a species, N_i is thus defined by the following expression:

$$\begin{aligned} N_i^V &= J_i^V + y_i N_T = c_t k_V^\bullet (y_i^V - y_i^I) + y_i N_T \\ N_i^L &= J_i^L + x_i N_T = c_t k_L^\bullet (x_i^I - x_i^L) + x_i N_T \end{aligned} \tag{2.26}$$

Bulk flow correction will be discussed in section 2.4.3.

Taylor & Krishna [28] write that multicomponent mass transfer can have mass transfer coupling effects, where the flux of one species affects the mass transfer rate of the other species. The multicomponent case requires consideration of the Maxwell-Stefan equation and all relevant mass transfer coupling effects, which will not be done in this study. N_i, which appears in the system of equations in section 2.3, is needed to solve the set of equations.

2.4.2. Heat transfer rate equations

Heat transfer is described similarly to mass transfer, with a low-flux heat transfer coefficient htc that is corrected into $htc^\bullet$. The heat transported towards the interface by conduction per unit area is given by:

$$\begin{aligned} q^V &= htc^{\bullet V}(T^V - T^I), \\ q^L &= htc^{\bullet L}(T^I - T^L), \end{aligned} \tag{2.27}$$

which requires a corrected heat transfer coefficient (discussed in 2.4.3). The heat transfer (per unit area) is found by adding the bulk convection of heat that accompanies mass

transfer. There is mass added to the bulk that comes from the interface. The added enthalpy of that mass must be counted for in the energy balance too. $h_{p,i}$ is the partial molar enthalpy of component i.

$$\begin{aligned} e^V &= q^V + \sum_{i=1}^{C} N_i h_{p,i}^V \\ e^L &= q^L + \sum_{i=1}^{C} N_i h_{p,i}^L \end{aligned} \tag{2.28}$$

Multiplying by the effective interfacial area (which is usually given in m^2/m^3) and by the stage volume gives the total transfer of heat in a stage.

$$\begin{aligned} \mathcal{E}^V &= q^V a_e V_s + \sum_{i=1}^{C} \mathcal{N}_i h_{p,i}^V \\ \mathcal{E}^L &= q^L a_e V_s + \sum_{i=1}^{C} \mathcal{N}_i h_{p,i}^L \end{aligned} \tag{2.29}$$

These equations can be used together with Eq. 2.15 to establish the following final expression for the energy balance around the interface.

$$E_j^I \equiv htc^{\bullet V} a_e V_s \left(T^V - T^I\right) - htc^{\bullet L} a_e V_s \left(T^I - T^L\right) + \sum_{i=1}^{C} \mathcal{N}_i \left(h_i^V - h_i^L\right) \tag{2.30}$$

2.4.3. Film model and bulk flow corrections

The shape and mass transfer properties of the interface determine the mass transfer rate and bulk transport term. This term is not taken into consideration when equimolar counterdiffusion is assumed, which is explained in this section. A number of modelling approaches for the bulk flow correction are known in literature [17]. These approaches include liquid film theory using diffusion, penetration theory using eddy currents, and surface renewal theory using an improved eddy renewal time. Film theory is the most common approach, but other approaches generally require mixture-specific parameters to be specified. Surface renewal models, for instance, require a time constant that describes how fast the surface of the interfaces refreshes by eddy currents. These models cannot be applied without knowledge of these parameters.

The film model is the simplest - yet often used - model to describe the bulk flow influence on the mass transfer. It assumes that two well-mixed bulk regions are separated by an interface that is in thermodynamic equilibrium. On both sides of the interface, mass is transferred towards and away from the interface in a thin film. The two films on either side of the interface are the only resistance to mass transfer [17, 28, 29]. A brief but straightforward derivation of the solution of the film model differential equations can be found in a text by Erickson, Gomezplata & Papar [31]. Taylor & Krishna [28] provide a more detailed discussion, but a similar conclusion can be drawn from their work. The bulk correction term is found by taking the ratio of latent heats for the two components in a mixture. This ratio is almost 1 for ethylene/ethane, since their latent heats are similar.

The bulk flow correction that follows from the film model is implemented as a correction factor on the mass transfer coefficients [28, 29, 31, 32]:

$$k^{\bullet} = \theta_k k, \tag{2.31}$$

where θ_k is the correction factor that is applied on the transport coefficient to compensate for bulk flow.

$$\theta = \frac{\phi}{e^{\phi} - 1}, \tag{2.32}$$

where

$$\phi = \frac{N_1 + N_2}{c_t k}. \tag{2.33}$$

The above expression however relies on N_T itself, since $N_1 + N_2 = N_T$. Since mass transfer in distillation is slow, according to Seader, Henley & Roper [17], it is a good approximation that $N_T = 0$ for distillation purposes, which then gives $\theta = 1$.

There are thus two reasons why the bulk transfer term can be neglected in this study. The corrected transport coefficients are thus equal to the non-corrected ones (Eq. 2.34):

$$k^{\bullet} = k, htc^{\bullet} = htc, \tag{2.34}$$

2.5. Engineering correlations for heat and mass transfer coefficients

The constants k and htc are found using engineering correlations that are made specifically for an application. So different packings have difference equations, or at least different constants to use in the equations. This means that the theoretical modelling of heat and mass transfer with rate-based models always requires one or more experiments to make a suitable correlation. Many authors have come up with expressions that predict coefficients for heat and mass transfer in often-used structured packings in varying ranges of operation [18, 21, 33–39]. Most available mass transfer coefficients are found by fitting measurement data with a function that depends on relevant dimensionless groups. A few of the available models try to combine this with a slightly more theoretical approach to derive the coefficients, such as the model by Olujić, Kamerbeek & de Graauw [37]. This study attempts to use known mass transfer correlations in a rate-based model for HIDiC. In the review of Wang, Yuan & Yu [40], the authors write the following:

"*Because of the lack of understanding of the complex transport phenomena occurring in the packed columns, the present state is that the modelling is mainly based on empirical and semi-empirical correlations, most of which were obtained from experimental data-fits.*"

Even mass transfer models that are based on theory rely on experimentally determined constants and do not fully capture all the physics and flow phenomena in random or structured packings. All available models in literature are for bundles of packing installed in a cylindrical column, much like in Fig. 2.3. The plate-packed HIDiC as described by Bruinsma, Krikken, Cot, Sarić, Tromp, Olujić & Stankiewicz [1], which is the subject of this study, is not a cylindrical configuration. Although some models describe

the behaviour of cylindrical packings quite accurately, the different flow characteristics in other geometries cause the heat and mass transfer behaviour to be fundamentally different. In principle, a different correlation could then be made by making experimental fits with data from the new system, or existing models for cylindrical packings could be adapted to match the changed geometry. These measurement would require time and investment.

This study nevertheless uses mass transfer correlations for cylindrical packings to model the behaviour of plate packed configuration. The aim of the study is also to create an estimation tool for HIDiC design, and assumptions about mass transfer must be made to make a working model. Possible further HIDiC development after this study may then require a higher-precision experimental mass transfer specification. Preferably, these correlations are made for the exact configuration and conditions that are modelled. This includes the type of mixture, flow rates, temperatures, pressure and packing geometry.

Nonetheless, results using the Delft model may be compared with earlier work of Bruinsma, Krikken, Cot, Sarić, Tromp, Olujić & Stankiewicz [1] and also the master thesis work of Krikken [41]. A model can be used as a tool for making preliminary HIDiC designs. The deviation and uncertainties that are introduced by the use of existing models can be substantial, but are considered to be acceptable and necessary at this phase of development.

Different models for packings are given in the following section. Heat transfer coefficients are usually not correlated, but found instead by making use of the so-called Chilton-Colburn analogy. This will be discussed first.

2.5.1. Chilton-Colburn analogy

It is possible to find heat transfer coefficients by making use of an equation that relates them to the mass transfer coefficients and vice-versa. One such analogy is the *Chilton-Colburn analogy*, originating from the work by Chilton & Colburn [42]. The equations governing heat and mass transfer show many similarities, so their dimensionless forms - with corresponding dimensionless numbers - show the same behaviour. This makes it possible to approximate the mass transfer coefficient by providing data on heat transfer coefficients. The correlation is as follows (replace subscript V with L for the liquid side equivalent):

$$j_h \equiv \frac{htc}{\rho u c_p}\mathrm{Pr}^{2/3} = \mathrm{St}_h\mathrm{Pr}^{2/3} \tag{2.35}$$

$$j_m \equiv \frac{k}{u}\mathrm{Sc}^{2/3} \quad = \mathrm{St}_m\mathrm{Sc}^{2/3} \tag{2.36}$$

where:	Sc	Schmidt number: $\frac{\mu}{\rho\mathcal{D}}$	–
	St_h	Stanton number for heat transfer: $\frac{htc}{\rho u c_p}$	–
	St_m	Stanton number for mass transfer: $\frac{k}{u}$	–
	Pr	Prandtl number: $\frac{c_p\mu}{\lambda}$	–
	j	j-factor	–

The Chilton-Colburn analogy dictates that the j-factors for heat and mass transfer

are of comparable magnitude. This allows for the estimation of either of the coefficients from Eqs. 2.35 and 2.36 if the other one is known.

In this work, heat transfer coefficients are found via the Chilton-Colburn analogy after using one of the mass transfer correlations to get the mass transfer coefficients.

2.5.2. Packing-specific mass transfer coefficients

A number of authors have investigated the possibilities of predicting mass transfer coefficients in structured and unstructured packings. Although trayed columns are cheaper, more predictable and have been applied for many years, packed columns offer many benefits, including a better mass transfer efficiency, lower HETP, lower pressure drop and better control characteristics [40]. The available models for the prediction of packing performance are all applicable in their own window of operation. Caution is needed when extrapolating behaviour for different flow regimes, mixtures, and geometries. Hanley & Chen [43], who provided a new model for mass transfer coefficients in 2012, write:

"*In particular, it is generally well known that packing mass-transfer correlations available in the public domain are unreliable when they are applied to chemical systems and column operating conditions outside of those used to develop the correlations in the first place.*"

The results of the HIDiC model can thus give an indication of the system's workings, and further studies and optimisation of the packing type and configuration can be done to improve the model. A couple of mass transfer models will be compared in this study. Most (but not all) of these models were specifically made for sheet metal corrugated packings. In packings, a large number of variables contribute to the overall performance of the packing, such as:

- Pressure drop
- Vapour distribution and contacting characteristics
- Liquid distribution characteristics
- (Effective) interfacial area
- Wetting characteristics
- Liquid holdup
- Maldistribution of vapour and liquid due to the liquid distributor
- Inherent maldistribution

Pressure drop in packed columns is usually lower for a given HETP than for the trayed column counterpart. Also, liquid will stay in the trays if a trayed column is shut down, creating a natural amount of liquid hold-up. This effect also makes the control of trayed columns less responsive than packed columns.

At the top of a column, vapour leaves in an upward direction, while liquid is supposed to drip down evenly across the whole cross-section of the column. A liquid distributor sits at the top of the column and has dripping points that attempt to make the liquid dripping pattern uniform over the column cross-section. A characteristic of the packing

itself is the inherent maldistribution, created by the flow patterns within the packing. This type of maldistribution is hard to predict, and practically unavoidable.

The main goal of the packing is to have a large area for mass and heat transfer. This transfer does not happen on the surface area of the packing, but on the interfacial area between liquid and vapour. It is true that liquid will mostly cover the packing surface, but the liquid may fail to cover the entirety of the packing, decreasing the *effective interfacial area* on which all the transport phenomena take place. At high loading operation, where the vapour throughput is high, the liquid surface may be enlarged due to rippling effects, creating more surface area. The interfacial area a_e is thus coupled to flow characteristics, and mass transfer coefficients depend on these characteristics as well. The interfacial area is always multiplied by the transfer coefficients to obtain the total transferred heat or mass. Some researchers therefore correlate a combined value of these variables, that is, $k_L a_e$ for the liquid case and $k_V a_e$ for the vapour phase. Others find coefficients $k_{L,V}$ and a separate value of a_e.

In either case, fluid properties and packing geometry information are used to calculate both variables, but the transfer coefficients and interfacial area are always functions of the flow conditions too, making it so that the coefficients and interfacial area need to be recalculated for each point at the column when the flow rates change.

The following subsections discuss the available models in literature and comment on their usage and range of applicability. Only the final expressions for the mass transfer coefficients are given in the following discussions. An elaborate description can be found in the original publications by the model authors. The authors of each model in literature often indicate how to calculate length scales and corresponding dimensionless numbers, which is important for correct usage of their correlation.

The SRP model

In 1982, Bravo & Fair [34] made a model while working for the Separations Research Program at the university of Texas. This model is often called the SPR-model for this reason, or BRF-model after its authors. The authors published an improved model in a split publication that was published in 1993 and 1996 [44, 45].

According to the authors, the model basis does not account for surface effects due to proprietary surface modifications on the packing, and these effects are being factored in by some empirical, packing-specific constants. C_e is a correction factor for surface renewal in a packing. These constants are listed in the publication for Mellapak, which has been around since the time of the publication, but they need to be determined for any new type of packing. The constant could change if Mellapak is used in a different configuration like the one this study uses. Therefore, the SRP model could need adjusting of the packing-specific constant.

The authors of the SRP model used the side length of a corrugation as a hydraulic diameter. The latest revision of the liquid transfer coefficient for the SRP model is given by:

$$k_L = 2\left(\frac{\mathcal{D}_L C_e u_{L,e}}{0.9\pi D}\right)^{1/2}, \tag{2.37}$$

which is similar to the 1982 liquid side coefficient. The vapour phase coefficient is

correlated by a Sherwood number relation:

$$k_V = 0.054 \left(\frac{(u_{V,e} + u_{L,e})\rho_V D}{\mu_V} \right)^{0.8} \left(\frac{\mu_V}{\mathcal{D}_V \rho_V} \right)^{0.33} \frac{\mathcal{D}_V}{D}, \tag{2.38}$$

which can be identified as a relation in terms of the following non-dimensional numbers:

$$\mathrm{Sh}_V = 0.054 \mathrm{Re}_V^{0.8} \mathrm{Sc}_V^{0.33}. \tag{2.39}$$

The complete model equations and description of the SRP model can be found in the work by Rocha, Bravo & Fair [45] or in the summary by Fair, Seibert, Behrens, Saraber & Olujic [35]. In these correlations, the effective liquid and vapour velocities $u_{V,e}$ and $u_{L,e}$, as well as expressions for all other model variables, are specified in detail in the original paper by Rocha, Bravo & Fair [44] and Rocha, Bravo & Fair [45].

The SRP model is based on falling film considerations, and its expressions include variables such as the packing angles, corrugation depths and surface treatment parameters. Liquid film thickness prediction is based on the assumption that liquid flows as a film on the surface of the packed bed [44]. Rocha, Bravo & Fair [44] use the interfacial area correlation of Shi & Mersmann [46].

One difference in the SRP model, compared to other models, is that a_e can become larger than the metal surface area, under certain flow conditions. The authors comment that this is realistic, since surface disturbances at a high vapour flow rate can create ripples and unevenness in the liquid surface, enlarging the surface area beyond the specific surface area of the packing, a_p.

The equations for the effective velocities that appear in Eqs. 2.37 and 2.38 require correlations for the liquid hold-up. Liquid holdup is a parameter that determines the amount of liquid that is present in the packing at a given time. The liquid film is assumed to be equal in thickness on the packing surface, so the liquid holdup can directly be linked to the film thickness. The liquid holdup is therefore an important parameter that is used to find effective phase velocities, which are used directly to calculate the transfer coefficients of both phases as shown in Eqs. 2.37 and 2.38.

The SRP model interfacial area was tested on a water system, and the static holdup correlation includes the surface tension as a variable. The surface tension of ethane/ethylene is much smaller, which means that the small contribution of static holdup is expected to become negligible. Indeed, Rocha, Bravo & Fair [44] found that this simplification made a fit that was just as good as the fit that used the full expression. This does however not mean that the full expression with the varying hold-up is valid for the ethane/ethylene system.

Measurements by Bruinsma, Krikken, Cot, Sarić, Tromp, Olujić & Stankiewicz [1] were unable to reach the liquid hold-up in their experimental setup. The hold-up in the new geometry of the pp-HIDiC is therefore not known precisely enough. Additionally, C_e is known for an air-water system, but not given for any other mixture, albeit that the authors write that the factor has a value close to 1 in the air-water system. The SRP model is not used because of this missing information.

The Delft model

The Delft model, developed at the Delft University of Technology [37, 47, 48], was developed by making use of conservation principles of the pockets that are created when

two corrugated sheets are alternately placed in 90° angles. The model assumes that the liquid flows on the packing surface in a laminar fashion, making use of a falling film model for an expression for the film thickness.

Several versions of the Delft model were published by its author, progressively making changes to increase the match with experiments. The review by Fair, Seibert, Behrens, Saraber & Olujic [35] compares the Delft model as of 2000, and a last revision of the model was done in 2001 [47], where the correlation by Onda, Takeuchi & Okumoto [18] was adopted as a measure of the effective interfacial area.

The Delft model makes use of the liquid transfer coefficient of the SRP model, Eq. 2.37. The vapour phase coefficient is given by the sum of contributions of individual laminar and turbulent mass transfer coefficients:

$$k_V = \sqrt{k_{V,turb}^2 + k_{V,lam}^2} \tag{2.40}$$

$$k_{V,turb} = \frac{\mathrm{Sh}_{turb}^V \mathcal{D}^V}{D} \qquad k_{V,lam} = \frac{\mathrm{Sh}_{V,lam} \mathcal{D}^V}{D} \tag{2.41}$$

The required Sherwood numbers and diffusion coefficients D_V are calculated using correlations from other literature, which is explained in 2.5.3. The original publications by Olujic, Behrens, Colli & Paglianti [48] make use of the recommendations from the VDI Heat Atlas [49] for some expressions. The full set of equations for the Delft model and their derivation can be found in the work by Olujić, Kamerbeek & de Graauw [37] and Olujic, Jansen, Kaibel, Rietfort & Zich [47].

Although the considerations behind the Delft model are presented by their authors as fundamentally sound, the model does sometimes fail to correctly predict the influence of vapour load on HETP, such as shown in the measurements by Krikken [41] and the PhD thesis by Erasmus [50].

Hanley and Chen

Hanley & Chen [43] made a new correlation for mass transfer for multiple packing types, found by varying relevant dimensionless groups in experiments. The model uses a least-squares fit for the relevant groups: Reynolds, Weber and Froude numbers for the interfacial area and the Reynolds and Schmidt number for the mass transfer coefficients.

For corrugated sheet metal packings, the correlations are as follows:

$$k_L = 0.33 \mathrm{Re}_L^1 \mathrm{Sc}_L^{1/3} \frac{c_t^L \mathcal{D}_L}{D} \tag{2.42}$$

$$k_V = 0.0084 \mathrm{Re}_V^1 \mathrm{Sc}_V^{1/3} \left(\frac{c_t^V \mathcal{D}_V}{D} \right) \left(\frac{\cos\theta}{\cos\left(\theta/4\right)} \right)^{-7.15} \tag{2.43}$$

The Billet and Schultes model

The model by Billet & Schultes [51] and its updated version [52] assume that the open areas for flow in corrugated sheet metal packings can be modelled as vertical channels. The liquid is assumed to be in counter-current flow with the vapour.

The Billet and Schultes model is an experimental fit using extensive measurements at the Ruhr-Universität Bochum. The model applies different expressions depending on which phase is the most dominant contributor to the mass transfer resistance. Both

Rocha, Bravo & Fair [45] and Hanley & Chen [43] write that the liquid resistance is small in distillation operations, so the vapour-controlled mass transfer equations can be used.

The mass transfer coefficients are given as the product of interfacial area and the coefficient[1]: [52]

$$k_L a_e = C_L 12^{1/6} u_L^{1/2} a_p \left(\frac{\mathcal{D}_L}{D}\right) \left(\frac{a_e}{a_p}\right), \tag{2.44}$$

$$k_V a_e = C_V \frac{1}{(\varepsilon - h_l)^{1/2}} \frac{a_p^{3/2}}{D^{1/2}} \mathcal{D}_V \left(\frac{u_V \rho_V}{a_p \mu_V}\right)^{3/4} \left(\frac{\mu_V}{\mathcal{D}_V \rho_V}\right)^{1/3} \left(\frac{a_e}{a_p}\right), \tag{2.45}$$

The constants C_V and C_L vary for different packing types. Some values of these constants are given by Billet & Schultes [52], for both random packings and a selection of structured packings. This correlation is one of the better-known mass transfer correlations, but it is less useful in this study since the liquid hold-up is unknown.

Onda's correlation

One of the earliest correlations that predict packing performance was the correlation by Onda, Takeuchi & Okumoto [18]. The correlation is often cited and used for different types of packings, but the correlations were originally made for random, dumped packings like Raschig rings and Berl saddles. Some units, such as those of viscosity and the gravitational constant, are based in hours instead of seconds.

The coefficients are found as follows:

$$k_L = 0.0051 \left(\frac{\rho_L}{\mu_L g}\right)^{-1/3} \left(\frac{u_{s,L}}{a_{wet} \mu_L}\right)^{2/3} \left(\frac{\mu_L}{\rho_L \mathcal{D}_L}\right)^{-1/2} (a_e D_p)^{0.4} \tag{2.46}$$

$$k_V = 5.23 \left(\frac{a_t \mathcal{D}_V}{RT}\right) \left(\frac{u_{s,V}}{a_t \mu_V}\right)^{0.7} \left(\frac{\mu_V}{\rho_V D \mathcal{D}_V}\right)^{1/3} (a_e D_p)^{-2.0} \tag{2.47}$$

Onda's correlation is known to be inaccurate. Its dependence on the nominal diameter D_p causes the equations itself to become ambiguous when the packing is not installed in a cylindrical bundle. This correlation could be used for comparison, but even then its validity is questionable.

Model choice for HIDiC modelling

Onda's correlation is not very suitable for the HIDiC model, since the intended geometry is very different. The model choice between the Delft model, Billet and Schultes or SRP model is arbitrary, since none of the models are made specifically for the application and all of them are in principle applicable to structured packings.

All the models have their own uncertainties and deviations between measurement and their predictions for mass transfer. Fair, Seibert, Behrens, Saraber & Olujic [53] compare the SRP model with the Delft model in a paper co-written by the authors of both models. The work by Bruinsma, Krikken, Cot, Sarić, Tromp, Olujić & Stankiewicz [1] uses the Delft model for assessment of their measurement results. This is the reason that the Delft model is chosen as the working model for the present work.

[1]The equations given in the 1993 publication by Billet & Schultes are provided in a more convenient form than their later 1995 publication [52]). The 1993 form is used for this reason.

There is no optimal model for the proposed HIDiC configuration as described in the work by Bruinsma, Krikken, Cot, Sarić, Tromp, Olujić & Stankiewicz [1]. Other models could be used in future work by comparison. A new correlation could improve accuracy and trust in model outcome if developments for the pp-HIDiC continue.

2.5.3. Molecular diffusivities

The rate equations for mass transfer have non-dimensional terms like the Reynolds and Schmidt numbers to include the effects of the flow regime and the characteristic lengths for mass diffusion. They do also depend on the type of species in the mixture, which diffuse into each other throughout the column, in both phases. The diffusion constants, $\mathcal{D}$, also known as diffusivities, can be calculated using correlations that are described in this section.

Literature distinguishes between many recommended correlations different solutions and substances. Logically, correlations are chosen that apply for pressurised hydrocarbons without polar compounds and no electrolytes for this study. Changing the diffusion correlations could be necessary if the model is run for different solutions. The following section elaborates on the usage restrictions of these diffusion constant correlations to justify their usage in the model.

Liquid diffusivities

Most expressions for the diffusivities of liquids at higher concentrations are correlated with the infinite dilution diffusion coefficients. In practice, this means that diffusion coefficients are calculated for a solute that is very dilute in the solvent. Two coefficients, $\mathcal{D}_{AB}$ and $\mathcal{D}_{BA}$ are calculated using one of the binary solution's components as either the solute or solvent. Using these infinite dilution coefficients, an empirical expression is used to calculate the diffusion coefficients at any concentration between the two infinite dilution values.

Seader, Henley & Roper [17] recommend the empirical Hayduk-Minhas correlation to find infinite dilution values. Poling, Prausnitz & O'Connell [54] compare several diffusion models, and conclude that the Hayduk-Minhas predictions have an average deviation of 3.4% for solvents and solutes from C_5 to some larger chain compounds. The Matthews-Akgerman correlations, according to Perry, Green & Maloney [55], provide 5% accuracy for hydrocarbon mixtures. Because of the higher reported accuracy and applicability to hydrocarbons[2], the Hayduk-Minhas correlation is used. The Hayduk-Minhas correlation is as follows, with molar volume $v_{m,A}$ in cm^3/mol, viscosity μ_L in centiPoise (cP), and the calculated diffusivity in cm^2/s.

$$\mathcal{D}^*_{AB} = 13.3 \times 10^{-8} T^{1.47} \mu_B^{\left(\frac{10.2}{v_{m,A}} - 0.791\right)} v_{m,A}^{-0.71} \tag{2.48}$$

The diluted liquid diffusivities are now used to calculate the diffusivities at higher concentrations. Perry, Green & Maloney [55] write that a "thermodynamic correction factor" is used to account for non-idealities that influence diffusivities at varying concentrations. The correction factor for component A, β_A is used in all the models and

[2]Poling, Prausnitz & O'Connell [54] write that some restrictions apply to usage of the correlation, but these restrictions apply to aqueous solution, viscous solvents, organic acids and to the solution of non-polar compounds in monohydroxy-alcohols.

is given by the following relation. For the other correction factor β_B, the subscripted variables should change accordingly.

$$\beta_A = 1 + \frac{\partial \ln \gamma_A}{\partial \ln x_A}, \tag{2.49}$$

An estimate for the derivative in Eq. 2.49 at a given concentration could be made by evaluating some activity coefficients with perturbed concentrations. An accurate enough approximation for ethane-ethylene can be made by equating β to 1, since it exhibits little non-ideality. If the model would later be extended to other mixtures, the derivative term needs to be evaluated at every point in the column to find a more accurate value for the diffusion coefficients.

An overview of the different correlations for combining both infinite dilution constants into an overall, pressure-dependent constant is given by Perry, Green & Maloney [55]. For light hydrocarbons that show no cluster formation and do not deviate much from Raoult's law, the Caldwell-Babb equation applies.[3] Caldwell-Babb is one of the simpler relations, but it is reported to work well for compounds that do not show nonidealities. The Caldwell-Babb equation is simply a change of diffusivities weighted by the liquid mole fractions of components A and B:

$$\mathcal{D}_{AB} = \left(x_A D^*_{BA} + x_B D^*_{AB}\right) \beta_A \tag{2.50}$$

Vapour diffusivities

Diffusion in vapours is generally much quicker than in liquids, so diffusivities in the vapour phase are generally higher. Vapour diffusivities are different from liquid diffusivities because of their greater pressure dependence. The standard way to estimate these diffusivities is to calculate a low pressure diffusivity, and then correct it for the higher pressure.

For low-pressure diffusivities for hydrocarbons, Seader, Henley & Roper [17], Perry, Green & Maloney [55] and Poling, Prausnitz & O'Connell [54] all recommend Fuller-Schettler-Giddings correlation:

$$\mathcal{D}^{lp}_{BA} = \mathcal{D}^{lp}_{AB} = \frac{0.001 T^{1.75} \left(1/M_A + 1/M_B\right)^{1/2}}{p\left[\left(\sum_V\right)_A^{1/3} + \left(\sum_V\right)_B^{1/3}\right]^2} \tag{2.51}$$

$\mathcal{D}^{lp}_{AB}$ has units cm^2/s, molar mass of one of the components should be given in g/mol and pressure should be in atm.[4]

All atoms in a compound have an atomic diffusion volume as tabulated by Fuller, Schettler & Giddings [56]. The atomic diffusion volume for carbon is 15.9, and its value for hydrogen is 2.31. For ethylene, the atomic diffusion volume is C_2H_4, $\sum_V = 2 \times 15.9 + 4 \times 2.31 =$ 4
For ethane, the value becomes 45.66. According to this correlation, species have an equal diffusivity into each other, so $D_{AB} = D_{BA}$.

[3] The Rathbun-Babb correlation, that gives a better estimation for some binary pairs, has β elevated to some power n, reduces to the Caldwell-Babb equation when $n = 1$.

[4] The unit of pressure is atmosphere, as taken from the original 1966 paper by Fuller, Schettler & Giddings [56]. The books by Poling, Prausnitz & O'Connell [54] and Perry, Green & Maloney [55] give a different unit, which is at odds with the original publication.

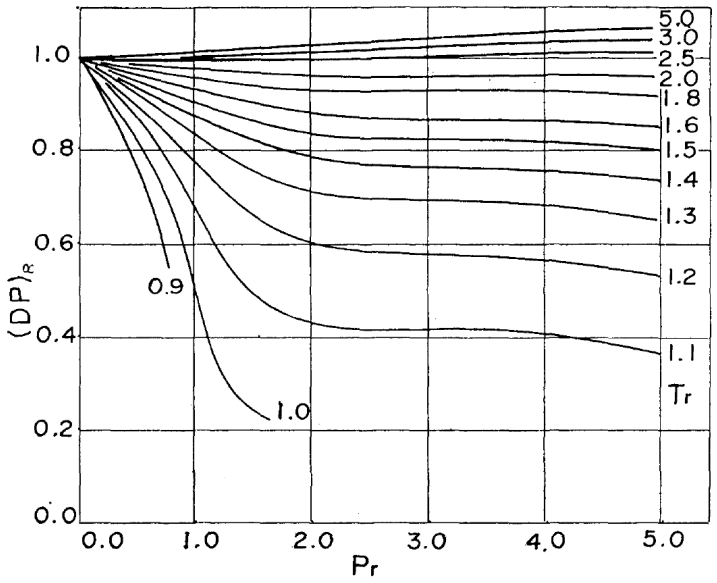

Figure 2.6: Takahashi correction on the low pressure diffusivity. Plot taken from Takahashi [57]. The lines are at different reduced temperatures T_r. The y-axis gives the function f in Eq. 2.52, so $f(T_r, p_r) = (DP)_r$

Poling, Prausnitz & O'Connell [54] propose to use the Takahashi correction to get the diffusivity at high pressure p as follows:

$$\frac{p\mathcal{D}_{AB}}{p_0\mathcal{D}_{AB}^{lp}} = f(T_r, p_r) \tag{2.52}$$

where T_r and p_r are the reduced temperature and pressure. The function f needs to be specified, but it is (rather unfortunately) a figure from which the value is to be read, as shown in Fig. 2.6. The ethane-ethylene separation will occur at pressures no greater than 30 bar, while the critical pressures are around 50 bar. The separation temperature will be just below the critical temperature. So $T_r \approx 1$ and $p_r \approx 0.66$. Fig. 2.6 shows that the non-ambient conditions make it so that $\mathcal{D}_{AB}$ is much lower than at temperatures near the critical temperature. This means that the mass transfer is limited if temperatures approach the critical temperature. At 30 bar, around $p_r \approx 0.66$ and 280 K, around $T_c \approx 1$, the combination of T_r and p_r can decrease the mass transfer rate by around 40%. This is however a necessary design criterion, since a lower pressure would increase the size of the column, and would push the dew and bubble points to lower values as well. Mass transfer would be faster, but a much more demanding refrigeration system would be needed.

Figure 2.6 is not very convenient for repeated calculations, which are needed in a numerical model. Seader, Henley & Roper [17] do not propose any other methods. Poling, Prausnitz & O'Connell [54] write that, albeit less accurate, the Riazi-Whitson correlation could be used. Perry, Green & Maloney [55] write that the Riazi-Whitson correlation (Eq. 2.53) has a deviation from measurements of about 8%, which seems large, but Takahashi [57] note that experimental values of diffusivities can vary wildly

as well, as much as 18% around the average measured values around the critical point.

$$\frac{\rho \mathcal{D}_{AB}}{\rho_0 \mathcal{D}_{AB}^{lp}} = 1.07 \left(\frac{\mu}{\mu^0} \right)^{b+c \cdot p_r} \tag{2.53}$$

Again, the vapour diffusivity is in cm^2/s. The acentric factor for a mixture is found by taking a mole-fraction average $\omega_{mix} = y_1\omega_1 + y_2\omega_2$. For the reduced pressure p_r, the mixture critical pressure is needed, which is found in the same manner as ω_{mix}. The terms b and c are given by:

$$\begin{aligned} b = &\quad -0.27 - 0.38\omega \\ c = &\quad -0.05 + 0.1\omega \end{aligned}$$

Ideally, diffusivities are measured for the desired compounds at different compositions and conditions.

In absence of measurements, the Riazi-Whitson equation is used to obtain an estimate for the diffusivity coefficient. This way, the diffusion coefficient will be a possible source of errors in the model. At this point in the studies, where the feasibility of the design concept is still in question, the accuracy will be enough. For more detailed studies, it is required to have a better estimate of the diffusion coefficient. A couple of hundredths difference in the diffusion coefficient can lead to a considerable change in the required packed column dimensions that are needed to transport all of the molecules involved.

2.5.4. Effective interfacial area of the packing

Mass and heat are not transferred everywhere on the packing's surface. Places where the packing surface is not covered with liquid do not participate in the separation process. On the other hand, extra contact surface can be created by droplets formation or by rivulets on the packing surface. The mass transfer coefficient is multiplied with the area that does contribute to the overall mass transfer, called the *effective interfacial area*, a_e. The total transport of mass is obtained by multiplying the local transport rate by the effective interfacial area.

The interfacial area a_e generally depends on dimensionless quantities such as the Reynolds, Froude and Weber numbers. This is a logical way to account for the multiple effects of flow regime and fluid properties that can influence the mass transfer area.

Different authors of previously discussed mass transfer correlations have their own preferred method of estimating the effective interfacial area. Some authors use their own correlation. Others use interfacial area models from literature to make the estimation. This work uses the interfacial area correlation from the Delft model, which can be found in the work by Fair, Seibert, Behrens, Saraber & Olujic [53].

2.5.5. Improved distillation technologies

In Appendix A, it is discussed that heat is added in a distillation column at the bottom, and heat is removed at the top. The useful result of the operation is the separation of a mixture. A theoretical thermodynamic minimum amount of work is needed to do the separation, but this work is typically only a fraction of the actual amount of energy spent in distillation columns. The cooling and heating at the top and bottom cause a large degree of heat degradation [58]. This heat degradation makes the energy usage much

higher than the theoretical minimum, and consequently, the thermodynamic efficiency can be lower than 10%.

Several technologies are available to achieve a higher thermodynamic efficiency. Some of these technologies that are relevant to HIDiC are discussed in this section. A brief introduction to several distillation techniques such as multiple effect distillation, compression/resorption heat pumps and thermo-acoustic heat pumps is provided in the 2011 publication by Kiss, Flores Landaeta & Infante Ferreira [11].

2.5.6. Diabatic distillation columns

A way to reduce the energy degradation of distillation columns is to distribute the energy demand of the column over the height of the column[59]. The energy can then be added slightly above the local column temperature, along the height of the column. This type of column with side heating is called a *diabatic distillation column*, opposed to an adiabatic column that exchanges no heat. In a diabatic column, heat is supplied at different temperatures on each tray separately. This does complicate the design by introducing heating coils into the column. Designs often use fewer heating coils than the total number of stages to reduce the number of punctures of the column shell for inserting the heating elements. Due to these complications, diabatic distillation column are not widespread.

2.5.7. Pressure dependency of boiling points

The following sections discuss energy conserving columns that conserve energy by applying the heat pump principle. At higher mixture pressures, the vapour-liquid equilibrium will shift to higher temperatures. A hot stream can receive heat input from a cold stream, if the cold stream is first compressed to higher pressures and temperatures.

2.5.8. Vapour (re)compression

Binary, close-boiling distillation operations often have a high energy demand due to the high reflux and boilup ratios that are required to reach a desired degree of separation. Additionally, many trays are required for these operations, creating large structures that are costly and hard to install: the C_2-splitter is usually the tallest structure in an ethylene plant.

The operating principle of a heat pump can be applied to reduce the reboiler and condenser duties. The heat available at the top of the column can be upgraded by compression. If a large enough pressure difference is used, the temperature of the top stream section becomes higher than the bottom of the column, making it possible to heat the bottom reboiler with the heat that has become available through compression. [60, 61]

While this heat pump principle works in any distillation column, it is potentially more useful for the separation of close-boiling mixtures. The temperature difference between the top and bottom of the column is small in those separations. The pressure does not have to be increased a lot to get a higher temperature in the rectifier than in the stripper. If the boiling point difference is larger, the pressure must be increased further, so the compression work becomes higher.

The compression can be a classical heat pump setup that works with an external working fluid, which requires heat exchange to a secondary circuit. Just like a regular

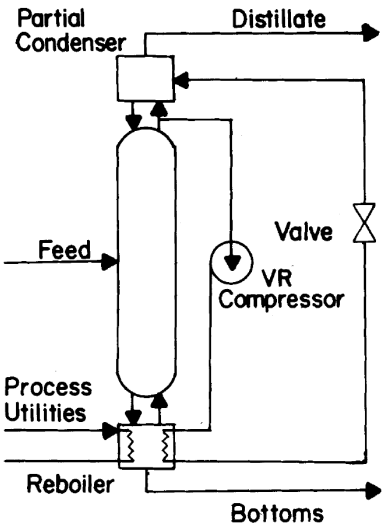

(a)
VRC basic flow sheet

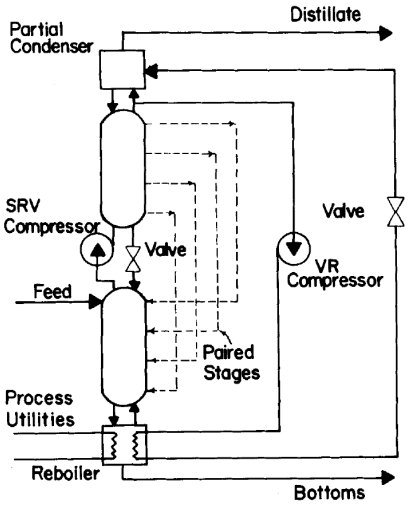

(b) Early SRV basic flow sheet, combining a HIDiC and an additional VR compressor for heat pumping of the top vapour.

Figure 2.7: The Vapour ReCompression (VRC) system and Heat Integrated Distillation column (HIDiC), images by Fitzmorris & Mah [59].

mechanical heat pump, a compressor and two heat exchangers are needed, one at the top and one at the bottom of the column. The pressure is increased to overcome the temperature difference across the column, plus the required ΔT in the heat exchangers. A throttling valve is used to reduce the pressure [11]. This type of operation is called Vapour Compression Distillation (VC) in older distillation literature, although *heat pumped column* is in use as well.

A second way of introducing the heat pump into the distillation column is to compress the process fluid itself, instead of a secondary working fluid. Vapour coming out of the top of the column is compressed and used as a heating medium for the reboiler at the bottom of the column. The pressure is then reduced, the fluid cools down and enters the condenser. This technique is called Vapour Recompression, or VRC (Fig. 2.7a by Fitzmorris & Mah [59]). Since the process fluid is both heated and cooled in the condenser, the heat duty of the system is much lower than the duty of a conventional distillation column. A major advantage of the VRC system is that it can be added to existing technology, while changing nothing in the column itself. The acceptance of this technology in the rather conservative process industry was therefore relatively quick. A vapour recompression system can even be retrofitted onto existing column by adding a compressor, a throttling valve and a heat exchanger.

2.5.9. VRC drawbacks

The limitation of VRC distillation is that the required pressure increase can become significant, because the temperature difference across the whole height of the column must be bridged by increasing the pressure. To get around this, Mah, Nicholas & Wodnik [58] were one of the first to describe a system that they called Secondary Reflux and Vapourisation (SRV) Column[5], part of which is presently known as a Heat Integrated

[5]The term 'secondary reflux and vapourisation' got out of use, and some authors write that the technology is equal to HIDiC. This is not strictly true because the "secondary reflux" refers to the additional,

Distillation column (Fig. 2.7b). The authors proposed first to compress the rectification section itself, rather than the top outlet stream. The rectification section is now hotter than the stripping section, and heat can be transferred from the rectification tot he stripping section. The HIDiC is discussed in detail in the next section.

2.5.10. Energy efficiency of distillation alternatives

To compare these technologies, it is useful to look at their total energy demand, but also to compare their theoretical efficiencies. The next section compares aforementioned distillation alternatives and HIDiC from an energy perspective. Electric energy and energy from boilers and coolers are not distinguished. While using electricity is more expensive at the time of writing, there is a societal trend that favours the use of electricity. It is expected that this trend will continue in the future, where the availability of renewable electricity is likely to increase, and the operational cost of combustion boilers will increase.

Appendix C contains more details about comparing different distillation column alternatives. These comparisons are not made in this study, but a column designer could opt for one of the described comparison methods.

2.6. Heat Integrated Distillation Column

In the heat-integrated distillation column, the cooling and heating is done between the column sections instead of in the condenser and reboiler. The required external duties are thus decreased and the equipment size can go down considerably. If the column heat integration allows for it, it can be possible to bring down either the cooling or heating duties entirely. In that case, the condenser or reboiler can be removed entirely. Some authors [63] proposed the term *ideal* HIDiC, that allows for the removal of both the condenser and reboiler, the column is then driven by compressor shaft work only. Just like any other ideal (reversible) processes, this ideal HIDiC cannot be made in practice.

In HIDiC columns, heat is supplied and withdrawn along the height of both column sections. The sections have a temperature glide, which is different from conventional heating at a fixed utility temperature at the top and bottom of the column. This means that the heat that is available in the column is used by matching temperatures and exchanging heat between those. Appendix C contains a more in-depth description of the thermodynamic advantage of HIDiC over conventional distillation columns.

The main advantages of HIDiC over VRC distillation are thus: smaller auxiliary equipment size and cost, a much lower compression ratio and the heat exchange with a temperature glide, which lowers exergy loss. The main drawbacks for HIDiC and its introduction are: the need for a new column design to allow heat transfer, the cost of developing this column and the possibly high manufacturing cost.

Temperature profiles in many distillation columns are not linear, and the stripper is generally not the same size as the rectifier due to an uneven feed composition (The case of multiple feed locations is not discussed in this study). Since heat is exchanged from stage to stage, stripper and rectifier stages are paired by a heat exchange mechanism.

secondary VR compression heat pumping that is applied on the vapour stream that leaves the rectifier. In other words, a SRV system is equal to a HIDiC combined with a vapour recompression system. Bisgaard [62] therefore proposes to refer to the system in Fig. 2.7b as SRV, and to the scheme in 2.8 as HIDiC.

This heat exchange mechanism must be inserted into the column. This insertion is cumbersome in many designs that have been studied since the 1980's.

Some publications, like the one by Fitzmorris & Mah [59], do not attempt to design the HIDiC, and approach HIDiC development theoretically. However, since few of these devices have been built, most writers give a more practical approach as well. Since the rectifier is maintained at a higher pressure, both sections have to be physically separated, and researchers have over the years done measurements or simulations on different setups. All groups indicate a positive effect on the overall energy usage of the different setups. These setups can be by using secondary heat transfer loops that connect stages of the column, as the design study by Wakabayashi & Hasebe [64] suggests. Other design suggestions include:

- the plate-fin configuration suggested by Tung, Davis & Mah [65] and further researched by Hugill & Van Dorst [66],
- the concentric column by Glenchur & Govind [67], who also patented the concentric trayed column concept [68],
- a test facility at the Technische Universiteit Delft for a concentric column with heat panels [63] was made, and patented by de Graauw, Steenbakker, Rijke, Olujic & Jansens [69],
- a multitubular design, which was researched and built commercially in Japan [70, 71], patented by Nakaiwa, Wakabayashi & Tamakoshi [72],
- a plate heat exchanger-like configuration with extra packing (subject of this study) as first researched by Bruinsma, Krikken, Cot, Sarić, Tromp, Olujić & Stankiewicz [1].

2.6.1. Flow sheet discussion

A simplified flow sheet for HIDiC is shown in Fig. 2.8. The stripping and rectification sections are separated and exchange heat along their height. The feed enters at the top of the stripping section in liquid phase. If the feed contained a vapour fraction, this vapour is immediately sent to the rectifier via the compressor (which can also be done using an external flash drum). The rectification section operates at a higher pressure. The rectification section bottom liquid is expanded using an expansion valve, after which it is fed back into the stripping section along with the liquid part of the feed. The height of reboiler and condenser utilities depend on the degree of heat integration and the position of the heat integration along both columns. Gadalla, Olujic, Sun, De Rijke & Jansens [74] developed a method based on traditional pinch analysis to work out the ideal coupling between stages. Heat integration in a plate-packed HIDiC is continuous, but concentric designs need heat panels that exchange heat at certain positions along both columns. Both configurations can be thought of as a series of heat exchanging streams. Analogous to heat exchanger networks, the rectification section and stripper temperatures along both columns can be plotted against the duties, as shown by Gadalla, Olujic, Sun, De Rijke & Jansens [74] (Fig. 2.9). Transferring heat across the pinch, as is the case in heat exchanger networks, should not be done, as it increases the overall required duties. Gadalla, Olujic, Sun, De Rijke & Jansens [74] performed this analysis

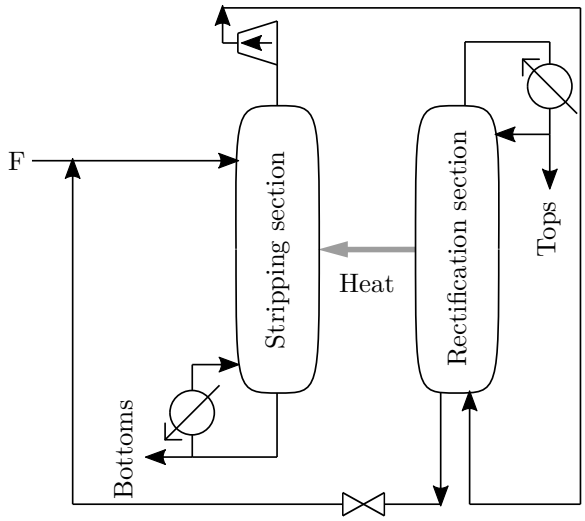

Figure 2.8: A simplified HIDiC process flow diagram. This figure is adapted from Olujić, Sun, de Rijke & Jansens [73]. Heat is transferred along the length of the whole column.

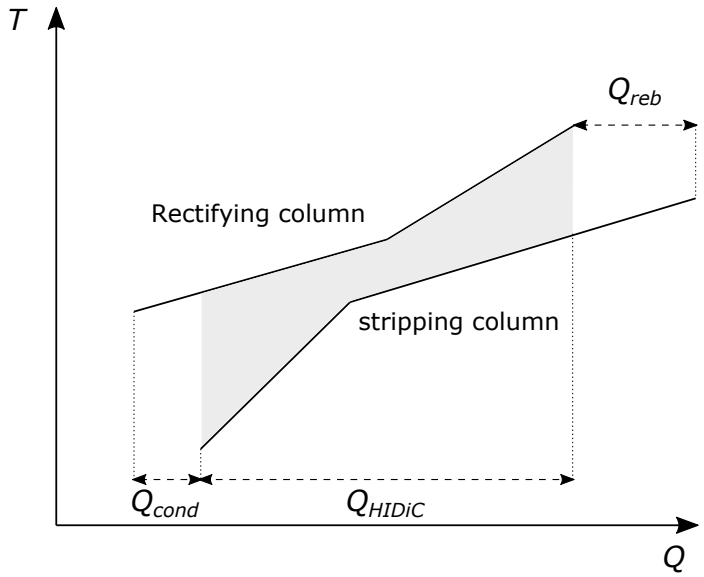

Figure 2.9: A pinch can be identified when plotting both column sections' composite curves. The top curve of the rectification section is hotter than the bottom stripping section curve, and the heat that is exchanged between the column sections has to be supplemented with the heat at the reboiler and the condenser. This figure serves as an example and is not based on a particular mixture. Image based on work of Gadalla, Olujic, Sun, De Rijke & Jansens [74]

.

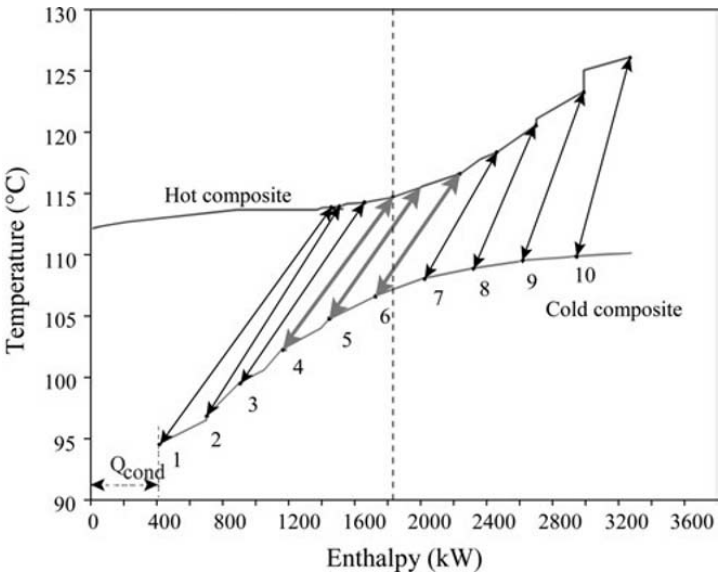

Figure 2.10: An example of heat exchange matching of trays on a trayed HIDiC column. The 10 stripper stages are matched to certain rectifier stages. The three links across the pinch should not be made. That is, there is a different combination of heat integration possible where the duties are lower. Image is as published by Gadalla, Olujic, Sun, De Rijke & Jansens [74]

on one the promising applications for HIDiC, the propane-propylene splitter (Fig. 2.10).

The stripping column could for example be split into two series of packing, each connected for heat transfer to a different height along the rectification section. This enlarges the number of possible configurations greatly. The basic approach would be to identify the pinch, and then match stages above and below the pinch.

Since ethane/ethylene in the C_2-splitter are almost an ideal binary mixture, temperature profiles along the column are expected to vary roughly linearly. This is the reason that the pinching method is not currently applied in the model, and the coupling of stripper and rectifier is simply done at the lower stages of the rectifier. This is a point of improvement for future studies.

2.6.2. Comparison of HIDiC concepts in literature

The plate-fin HIDiC, first suggested by Tung, Davis & Mah [65] and later researched by Hugill & Van Dorst [66], was suffering from maldistribution, which was confirmed in later studies, such as Bruinsma, Krikken, Cot, Sarić, Tromp, Olujić & Stankiewicz [1]. This created the incentive for the study of the plate-packed HIDiC. Although it gave an improvement on the conventional column, the plate-fin HIDiC HETP was shown to be higher than the HETP of the plate-packed HIDiC. A potential advantage that the plate-fin HIDiC could give, is that it's construction is much like the plate-fin heat exchangers that it is based on. The reuse of existing design could make the development and construction less involved and cheaper. Its development was halted after the plate-packed HIDiC seemed to be more favourable and the plate-fin HIDiC showed the effects of maldistribution much more severely, having a much higher HETP in measurements[1].

The concentric column did not suffer from the maldistribution that the plate-packed HIDiC suffered from, and its design is more alike a conventional column with trays. The separation performance of the existing trays was well-known, and, according to some of the researchers of these columns [63], the heat has nowhere else to go than to the rectification section. While this is partly true, the heat can also just go up or down the column along with the vapour or liquid if not enough area is provided, without being transferred anywhere. The limited rate of heat transfer between stripper and rectifier was found to be a major shortcoming of the concentric HIDiC configuration.

For the HIDiC to function properly, enough heat transfer area must be introduced. For concentric trayed columns, the heat is transferred on the outside of the rectifier, into the stripper. This means that the outside of the rectifier must be adjusted to accommodate area for heat transfer. A possible option for this adjustment is shown in Fig. 2.11a [63]. It is a trayed column with additional heat panels. The heat panels do increase the available surface area, but are still the limiting factor in these designs.

Researchers in Japan [75] found another setup that could accommodate extra heat transfer area, which is displayed in Fig. 2.11b. The inside of the column is fitted with structured packing. This is however not the setup that was developed in Japan, which indicates that this setup was ultimately not viable, for reasons not provided in literature. On their website [76], the Toyo Engineering Company shows their SUPERHIDIC® design, which is a regular trayed column with an external working fluid that exchanges heat between trays. To this end, a wall puncture is made and some stages are paired. The displayed number of paired stages is low, which indicates that the product has fewer heat integrated stages than theoretically possible. The diminished advantage due to the lower degree of heat integration could lead to a similar performance as the VRC distillation, which is easier to implement and cheaper. As of the time of writing, the SUPERHIDIC® has not seen market adoption, from which one can conclude that the advantage of implementation of this particular design is not large enough to compete with alternatives. The plate-packed HIDiC is an attempt to approach the HIDiC design. The approach creates a much larger area for heat exchange between the stripper and rectifier. The configuration is similar to a plate heat exchanger, but packing material is added between the plates to serve as a means to increase vapour-liquid contacting, since the separation function is added to the original heat exchanger setup. The setup is much different from both traditional trayed and packed columns, which means that the separation performance of the plate-packed HIDiC is an uncertain factor. The work by Krikken [41] and the publication by Bruinsma, Krikken, Cot, Sarić, Tromp, Olujić & Stankiewicz [1] are the only available literature on this setup.

The manufacturer of Mellapak 350Y, Sulzer Chemtech, write in their folder of structured packings [77] that the HETP of MELLAPAK 350Y lies between 0.2 and 0.4 per metre, increasing with higher vapour flow rate. The measurements of Bruinsma, Krikken, Cot, Sarić, Tromp, Olujić & Stankiewicz [1] show an entirely different trend than the manufacturer's specifications, but the measured HETP lays in the same range. Although the setup is much different from the original structured packing bundles, this could indicate that the usage of structured packing in the pp-HIDiC configuration does not lead to a much worse packing performance. Flow phenonena are so different in the pp-HIDiC that it is not possible to draw this conclusion.

Beside the simulation results of this study, more experiments with, for example,

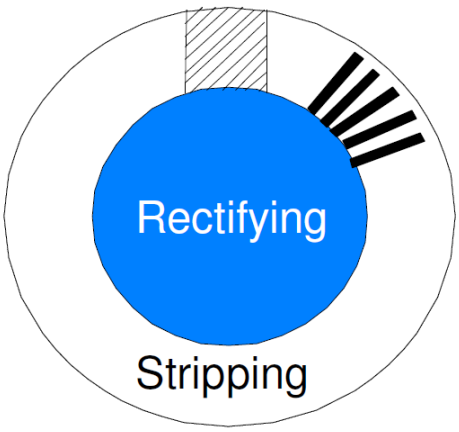

(a) De Rijke [63] proposes different setups to exchange heat in concentric columns. One of such proposals is displayed schematically. The compressed (and thus smaller diameter) rectifier is placed inside the stripping section, with heat panels extending into the stripper. Figure by De Rijke [63].

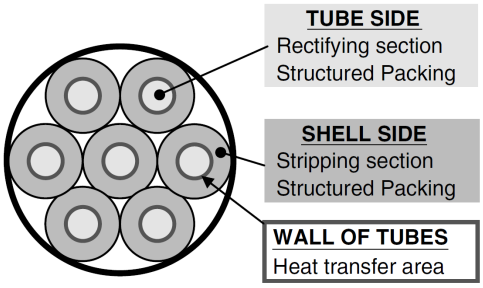

(b) The setup in Japan that was placed on the market makes use of a multitubular setup that naturally has a larger inter-section area than the single-tube design. Figure by Iwakabe, Nakaiwa, Huang, Matsuda, Nakanishi, Ohmori, Endo & Yamamoto [75]

Figure 2.11: Two possible configurations of concentric columns from literature.

different packing configurations or dimensions could help to further improve the understanding and the ability to predict the performance of the pp-HIDiC.

2.7. Rate based modelling of a plate-packed HIDiC

The modelling differences between a conventional packed column and a structured HIDiC are an elevated pressure in the rectifier, and heat transfer between the both sections. The rate-based equations from section 2.3 are valid for this system as well. The hydraulic equation should incorporate the higher pressure in the rectifier. If this pressure is fixed, all state variables and transport properties in the rectifier are calculated accordingly.

The second adjustment is the energy transfer Q, which is the energy that is taken from the rectifier and transferred into the stripper. The rectifier is most often not the same size as the stripper. If the cross-sectional width of the stripper and rectifier compartments is the same, they can not be the same height. It must be determined which parts of the differently sized sections are into contact with each other.

The heat Q is an unknown variable in the model, so another equation is needed to couple the heat flow in both compartments. The heat flow through the coupled stages can then be approximated by an extra equation.

2.7.1. Heat transfer between stripper and rectifier

This section describes the heat transfer from the rectifier to the stripper. The wetting conditions of the perpendicular plate are not known. An approximation must be made by assuming that the surface is completely wetted. The paper by Bruinsma, Krikken, Cot, Sarić, Tromp, Olujić & Stankiewicz [1] has a couple of measured U_{HIDiC} values (Table 2.1) for the overall heat transfer coefficient for their model configuration, which is the setup that this study tries to model. There are three reported U-values, given for different F-factors. The F-factor is a 'vapour load term' of a column, given by F-factor $= u_s\sqrt{\rho_V}$. Kister [15] describes it as the root of the kinetic energy of the vapour. The

Table 2.1: The U_{total} as calculated from the measurements and work by Bruinsma, Krikken, Cot, Sarić, Tromp, Olujić & Stankiewicz [1].

F-factor $[Pa^{0.5}]$	U_{HIDiC} $[\mathrm{W/(m^2 \cdot K)}]$
0.80	373
1.60	473
2.20	550

F-factor is often used to correlate HETP values at different flow rates.

Bruinsma, Krikken, Cot, Sarić, Tromp, Olujić & Stankiewicz [1] used n-heptane/cyclohexane in their test-setup, which has a density of roughly 3.5 kg/m^3, so the used vapour velocities in Table 2.1 were around 0.4, 0.85 and 1.2 m/s. The test setup had a perpendicular surface area per unit height of $2 \times 100 \times 20$ cm/m, so 0.08 m^2/m. This area per unit volume is 22.2 m^2/m^3, which is high for a distillation column. The large surface area between stripper and rectifier is the reason why this geometry could be advantageous, and the reason why Bruinsma, Krikken, Cot, Sarić, Tromp, Olujić & Stankiewicz [1] compared it to the plate-fin HIDiC, which is another high-transfer area geometry.

The total heat transfer through the HIDiC wall is found using:

$$\dot{Q}_{HIDiC} = UA\Delta T_{SR} \tag{2.54}$$

The calculated HIDiC U-values were as displayed in Table 2.1. The rate-based calculations can make use of these values in combination with Eq. 2.54 and the calculated stage temperatures to obtain a value for Q_j in equation 2.24.

McCabe-Thiele and HIDiC

The McCabe-Thiele diagram (Fig. A.1 in Appendix A) can be used for a HIDiC as well. The separation factor curve is then not a single curve, but is split into two separate curves that represent the separation factor at the low pressure and high pressure column parts. The K-values K_i, and therefore also the separation factor α, depend on the pressure and temperature. Since ethylene and ethane are quite similar molecules, the separation factor does not change as much at higher pressures.

The operating lines' slopes represent the ratio of vapour and liquid flow rates, but the HIDiC heat transfer and mass transfer cause continuous condensation and evaporation along the column. The liquid and vapour flow rates thus vary along the column, and so do the slopes of the operating lines.

An indicator for the strength of driving forces for mass transfer is the distance of the α-curve from the operating lines. Generally, slow driving forces cause a smaller entropy production and thus a larger efficiency, at the cost of a slower process and larger equipment. De Rijke [63] writes that an ideal packed HIDiC could get very close to the separation factor curve, decreasing entropy production, but requiring a very large surface area. An infinite number of theoretical trays would be required if the separation factor curve would coincide with the operating lines. A larger HIDiC will allow for more surface area and a higher efficiency, which is a trade-off against the cost of a larger column.

A rate-based model of the HIDiC can yield mole fractions along the HIDiC column, which can be used to plot the operating lines. This operating line can then be compared

with the separation factor curve for the calculated temperatures and pressures along the column.

3

Model Description

This section describes the implementation of the discussed theory. The Python programming language [78] was used for modelling. The SciPy [79] module delivers the main numerical procedures for solving the system of MERSHQ equations. The NumPy module [80] is the fundamental package for scientific computing with Python and provides the structures to contain and process data.

The core of the model is an iterative solving procedure to solve the MERSHQ and MESH equations. This procedure is in Appendix B. Thermodynamic properties are found using the CoolProp Python package [27] and the Thermo Python package, [81].

This chapter describes most of the aspects of model development. The calculation must be started with initial conditions, which is described first. After this, the geometric configuration of the pp-HIDiC is discussed. The rest of the chapter discusses the calculation of all remaining properties that are required in the model.

3.1. Total system of model variables and their initial guess

The variables in the rate-based model are contained in the vector $\boldsymbol{x_j^T}$ from section 2.3.2. The column is partitioned in N_s stages. The top and bottom stage are equilibrium stages, and the middle stages are non-equilibrium stages. An initial guess must be supplied for all the variables in the equations that describe the process in those stages. The following tables list the variables, their initial guess, and the total number of variables. The non-equilibrium model variables are as shown in Table 3.1. The equilibrium and non-equilibrium variables are tabulated separately in the next section.

Table 3.1: Non-equilibrium variables with their units and total count. The way of generating the initial guess is indicated. These variables are used in solving the equations described in section 2.3.

Variable	Initial guess	Unit	No. of rate variables
$x_{i,j}$	Linear profile between bottom, feed and desired top liquid composition	–	N_sC
$y_{i,j}$	Linear profile between bottom, feed and desired top vapour composition	–	N_sC
$x^I_{i,j}$	Average of stage liquid and vapour mole fractions	–	N_sC
$y^I_{i,j}$	Average of stage liquid and vapour mole fractions	–	N_sC
$N_{i,j}$	A small value, e.g. 0.001	mol/s	N_sC
$T^L_{i,j}$	Bubble point temperatures per stage at $x_{i,j}$, minus a few degrees	K	N_s
$T^V_{i,j}$	Dew point temperatures per stage at $x_{i,j}$, plus a few degrees	K	N_s
$T^I_{i,j}$	The middle point between bubble and dew point temperatures	K	N_s
Q_j	$U_{HIDIC}A\left(T^R_j - T^S_j\right)$	J/s	N_s
L_j	Linear profile between the feed and desired top/bottom liquid flow rates	mol/s	N_s
V_j	Linear profile between the feed and desired top/bottom vapour flow rates	mol/s	N_s
		Total:	$N_s(5C+6)$

There are two equilibrium stages (condenser and reboiler) so the total number of equilibrium equations is equal to twice the number of equations per stage, as shown in Table 3.2. The total liquid and vapour flow rates from the top and bottom of the column follow from a mass and component balance over the whole column. The feed composition and flow rate are known, and the top and bottom specifications can be fixed according to the desired specification.

Table 3.2: Equilibrium variables with their initial guess, units and total number

Variable	Initial guess	Unit	No. of equilibrium variables
$x_{i,j}$	Desired top or bottom liquid composition	mol/mol	$2C$
$y_{i,j}$	Desired top or bottom vapour composition	mol/mol	$2C$
$T_{i,j}$	Bubble point calculation at the condenser, or a dew point calculation at the reboiler	K	2
L_j, V_j	Overall column mass balance using the desired product mole fractions	mol/s	2
Q_j	An engineering estimation (e.g. ± 5 MW)	J/s	2
		Total:	$2(2C+3)$

The grand total of variables and equations of the system is thus $N_s(5C+6)+2(2C+3)$.

Notably, the stage pressure p_j is missing from these variables. It is decided to keep a constant pressure in the stripper and the rectifier as a modelling assumption. Pressure drop in structured packings is generally small, and a small pressure change would have minimal influence on the column conditions. Adding a pressure gradient would additionally require a specialised correlation for the pressure drop in the packing. The Delft model pressure drop equations could be used for this, but it was decided that adding the pressure drop is a detail that should not be included in this phase of the study.

3.2. Geometry and physical dimensioning of the column

The top and bottom stages are a classic reboiler and a condenser. The model assumes that only vapour enters the condenser, and only liquid enters the reboiler. After a flash distillation step, either liquid or vapour is put back into the column at the first or last HIDiC non-equilibrium stage. The separation in these stages is heavily influenced by the geometry of the packing, which is explained in this section.

3.2.1. Packing details

The packing geometry and surface need to be specified to get the correct interfacial area that mass transfer acts on. The geometry from the pp-HIDiC from Bruinsma, Krikken, Cot, Sarić, Tromp, Olujić & Stankiewicz [1] is used in this study. The packing sheets in the study were Mellapak 350Y, but the model is built such that the packing parameters can be changed if other packing types are preferred.

The side-dimensions of the corrugation are input parameters for the mass transfer coefficient models. They are displayed in Fig. 3.1a. For Mellapak 350Y, $b = 18$ mm, $S = 12.7$ mm and $\theta = 90°$. Packings are made of sheets, such as the one displayed schematically in Fig. 3.1b. The sheets are bundled in a criss-cross pattern (Fig. 3.1c), bundled, and placed in a column upright.

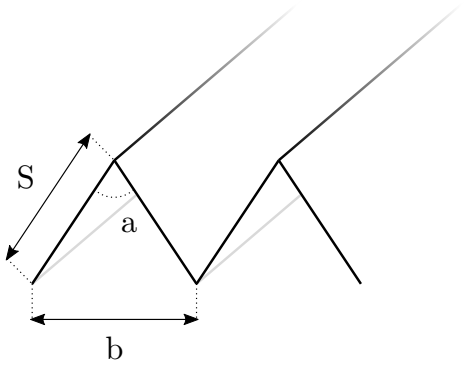

(a) Some dimensions of the packing corrugations.

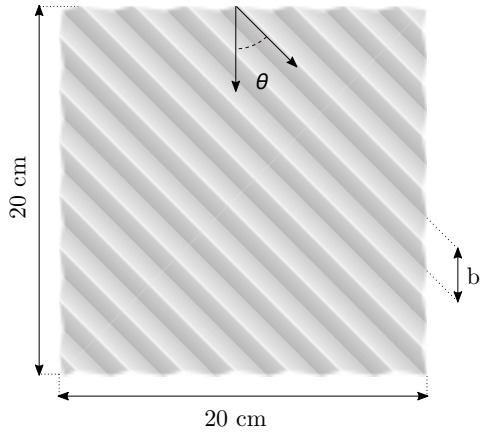

(b) Sheet size of the sheets used in the work of Bruinsma, Krikken, Cot, Sarić, Tromp, Olujić & Stankiewicz [1], and b, which is around 2 cm. Picture is not to scale and only used as a sketch, so the number of corrugations may vary. The corrugation inclination angle θ is 45deg for Mellapak packings with letter Y, and 60deg for Mellapak packings with names ending with X.

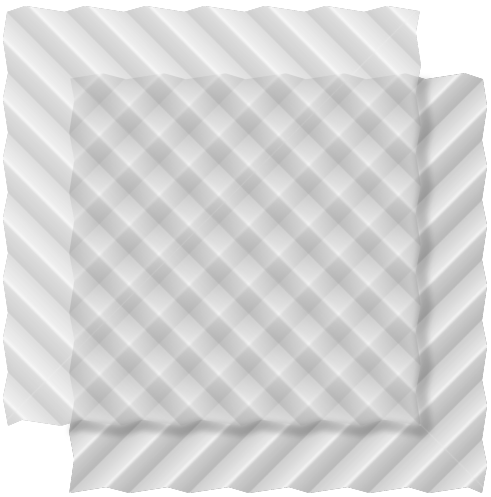

(c) Sheets overlap and create a grid pattern inside of the packing.

Figure 3.1: The structure of sheet metal packing Modern packing types do not have straight corrugation, but a curved one, creating a better distribution of fluids.

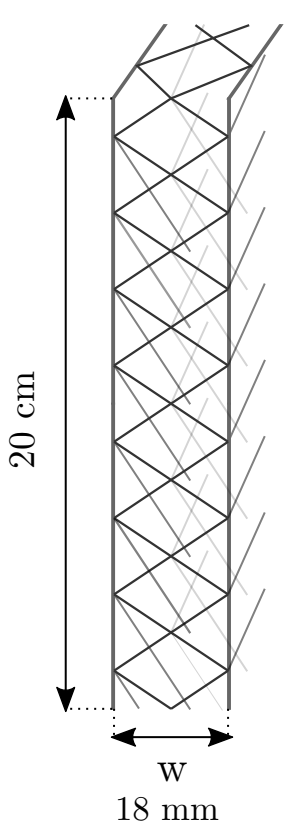

(a) A zoomed-in cell of the plate-packed HIDiC as proposed by Bruinsma, Krikken, Cot, Sarić, Tromp, Olujić & Stankiewicz [1]. Two corrugated sheets are placed together between two straight metal sheets.

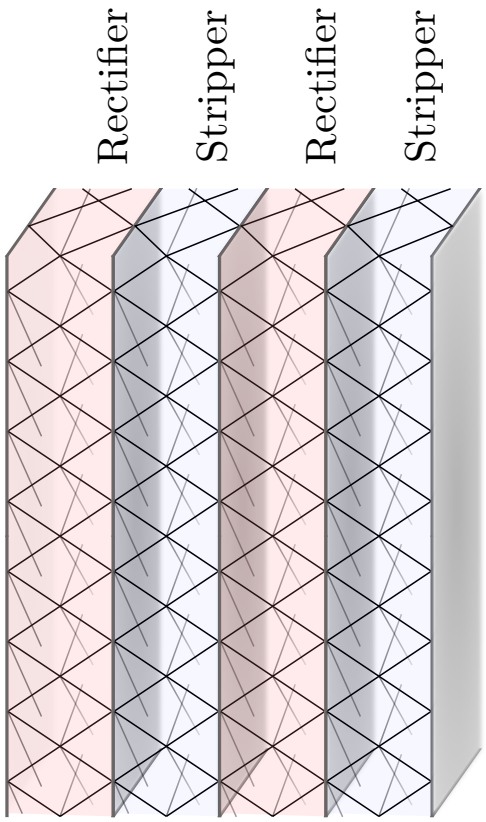

(b) Schematic drawing of the packing cells of the stripper (colder, blue) and the rectifier (hotter, red) alternate each other, where the wall between them both serves as a separation between high and low pressure, and a close contact for heat transfer.

Figure 3.2: Build-up of the pp-HIDiC cell element.

3.2.2. An entire HIDiC non-equilibrium stage

Bruinsma, Krikken, Cot, Sarić, Tromp, Olujić & Stankiewicz [1] made a packing by sandwiching two sheets between two steel plates, as displayed in Fig. 3.2a. To build a pp-HIDiC, the resulting cells are stacked together as shown in Fig. 3.2b. It is not said that this is an optimal configuration. It was the only configuration that was tried out, so other geometries or packing orders could prove to work better.

The walls on the outside of packings allow heat to transfer from the rectifier to the stripper. The wall heat transfer coefficient found by Bruinsma, Krikken, Cot, Sarić, Tromp, Olujić & Stankiewicz [1] is dependent on the vapour load, but a value of $U_{HIDiC} = 450\ \mathrm{W/(m^2 \cdot K)}$ is used during the modelling. This is about the average value that was found by the authors. More research is needed to find a good correlation of this heat transfer coefficient. This would give a more precise estimate for U_{HIDiC}. U_{HIDiC} is simply multiplied by the area of a stage to get the HIDiC heat input for that stage.

The setup from Fig. 3.2b is the setup that this modelled in this study.

3.3. Properties from the CoolProp and Thermo packages

The CoolProp python package is used to obtain properties and calculations in this work. Its flash calculations are faster, more accurate, and computationally more reliable than the thermo package's flash routines. An alternative to CoolProp for property calculations would be to use proprietary software such as RefProp, provided that there is a (fast enough) interface with the programming language that is used for the model. This section motivates the decision between different python packages and shows their strengths and shortcomings.

3.3.1. Transport properties

CoolProp package does not include viscosity and thermal conductivity data for ethane and ethylene [27]. Viscosity properties are calculated by the Python thermo package. The pressure- and temperature-dependent viscosity correlation that is used by thermo for the ethylene/ethane mixture is the recommended viscosity correlation as described in the *VDI heat atlas* [49]. The thermal conductivities for ethylene and ethane are calculated from tabulated data from the DIPPR database [82], after which mixing rules from Poling, Prausnitz & O'Connell [54] are applied.

3.3.2. Bubble- and dew point calculations

The thermo package only comes with few built-in functions for dew point calculations. The only elementary calculation it does is choosing a suitable correlation for the dew or bubble point pressures and evaluate it. The reverse calculation, to find a dew or bubble point temperature at a given pressure, is done by using an iterative solver on the bubble point pressure correlation to find the matching temperature. In the programming work for this study, only dew or bubble point temperatures are needed, since the pressure in the packing is neglected. Every dew or bubble point temperature then needs to be solved iteratively, which is slow and inaccurate.

Additionally, the thermo package has trouble finding the dew and bubble points if their temperature difference is small. This occurs if mole fractions are close to 0 or 1, or if the boiling points of the components in the mixture are very similar. The iterative calculation will then take longer and often fails to converge at all. This makes the thermo package slow and inaccurate in terms of dew and bubble point calculations.

Lastly, the thermo package does not natively contain a function for the dew point temperature as a function of the pressure. This function, dew_at_P(p, x), must be added manually.

CoolProp, compared to thermo, has fast and reliable dew and bubble point calculations at pressures up to 30 bar for an ethylene/ethane mixture. They become unreliable above 30 bar, where the calculations unexpectedly do not return a numerical result in some ranges of pressure. This is shown in Fig. 3.3. The figure shows that the results for the bubble and dew curves vary considerably. After checking using Aspen, the CoolProp calculations turned out to be better.

Above 30 bar, thermo does not do successful dew point calculations at all. CoolProp stutters around 30 bar, but then succeeds again above it. Some calculations might thus give good results, but this is not enough if reliable calculations are needed.

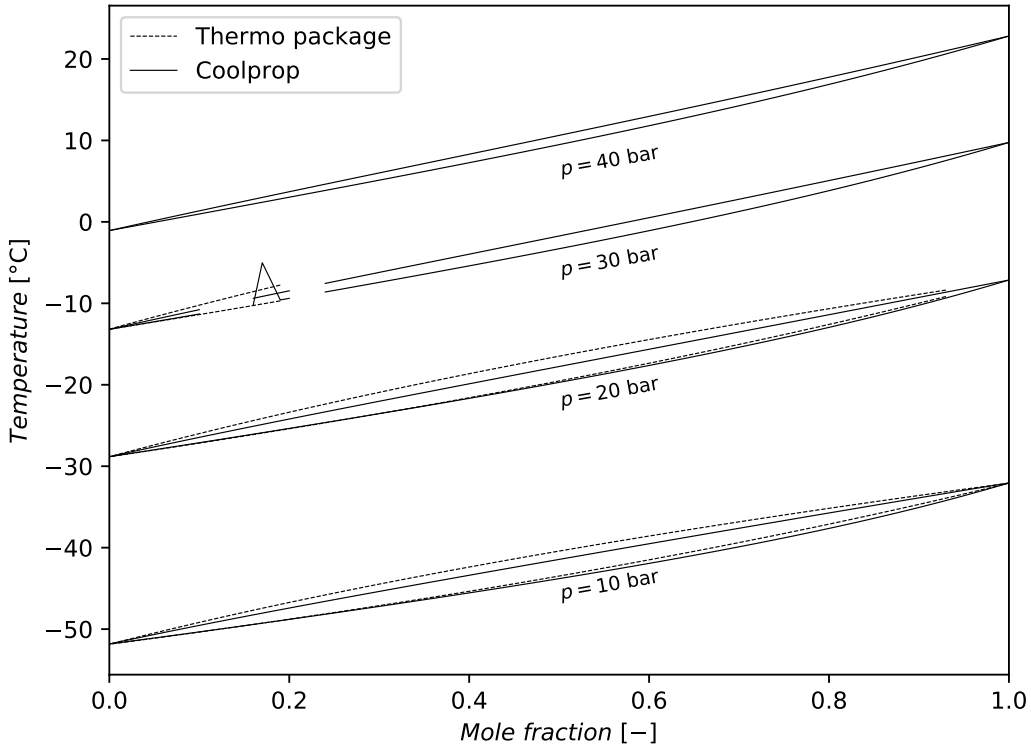

Figure 3.3: Bubble and dew points calculated by Thermo and CoolProp. If a line is missing, discontinuous or interrupted, the respective package failed to calculate the corresponding data points.

3.3.3. Cost of package calculations

The thermo package is computationally inefficient when it comes to repeated calculations with different mole fractions, which happens continuously in distillation. Thermo creates a mixture object with preset mole fractions, and draws lots of extra information from databases, such as component flammability, toxicity, and international chemical identification numbers. Calculations as function of temperature and pressure can then be done with this object and its class methods.

The model in this work does use repeated calculations for different mole fractions. The thermo package then needs to generate a new instance of the mixture class, which then repeats all the previously done database lookups for flammability and so on. This makes thermo incredibly slow for repeated calculations.

The CoolProp package has a much faster approach, where a mixture object is generated first. CoolProp will first create an AbstractState instance to do calculations with. This is a one-time initialisation. The user can then respecify mole fractions if they change, and calculate the state properties as function of two variables that fix the state of the system. After this, the mole fractions of the same instance of AbstractState can be reused.

3.3.4. Comparision of state quantities and accuracy of calculations

The CoolProp package has several equations of state built-in, amongst others the Peng-Robinson (PR) and Soave-Redlich-Kwong equations of state. CoolProp's most powerful calculations for mixtures use excess Helmholtz energy terms [83]. Since the Helmholtz

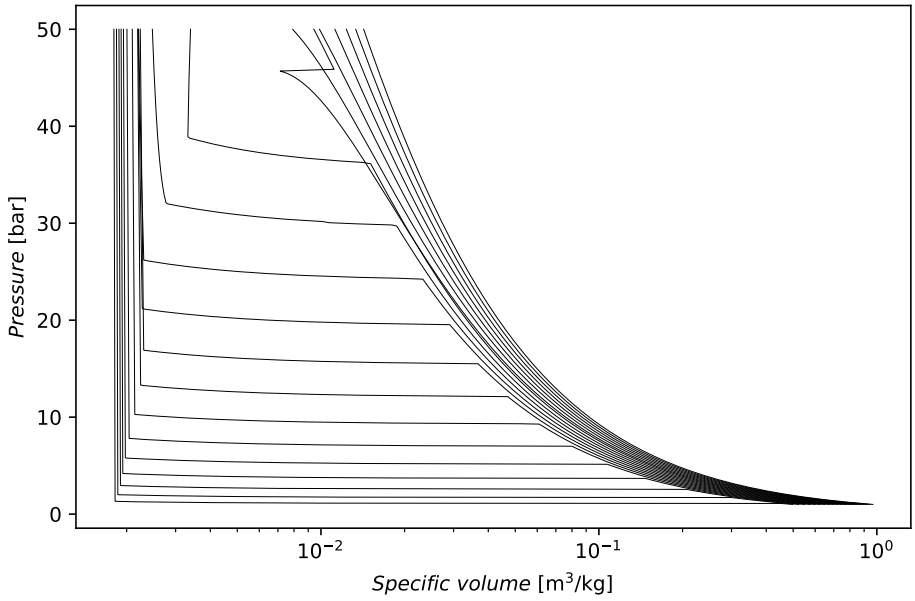

Figure 3.4: A p-v diagram including made using the thermo package. Black lines are isotherms of 50/50 mol% ethylene/ethane between 180 K and 340 K. No phase envelope is plotted, as the bubble and dew calculations from the thermo package are too unreliable to plot a line that is remotely close to the real position of the bubble and dew point locations in the plot. The thermo package shows overlapping liquid isotherms, and has unpredictable behaviour at elevated pressures, and returns nonsense close to the critical point.

energy formulation routines are much more faster and accurate than the EOS methods, the Helmholtz formulation approach is chosen for this model.

A plot showing isotherms made with both the available packages is displayed in Figs. 3.4 and 3.5. While equations of state are known to be harder to solve near the critical point, CoolProp has a full convergence domain even beyond higher pressures with its excess-Helmholtz terms compared to the Peng-Robinson EOS approach. Hence, the Helmholtz approach is favoured over the Peng-Robinson EOS in both the CoolProp and thermo packages.

The thermo package uses the Python fsolve to find the roots of cubic equations of state, which often fails to converge to the proper root of the equation, especially at elevated pressures, as can be seen in Fig. 3.4. This can cause large discontinuities in thermodynamic functions, such as enthalpies and densities, which will then lead to to jumps in transport properties.

Fig. 3.5 contains the bubble and dew curves of the mixture (as a red line) in addition to the isotherms. The isotherms from the CoolProp package are continuous and work in every pressure range. CoolProp does sometime fail at finding values for the bubble and dew points, which makes it unreliable to incorporate bubble and dew points in scripts that require repeated accurate calculations of those points.

Fig. 3.6a shows the low-pressure liquid phase isotherm overlap of the thermo package solver. Fig. 3.6b shows the critical region isotherms when (attempted to be) calculated by the thermo package. It can be seen that the results from the thermo package are inaccurate.

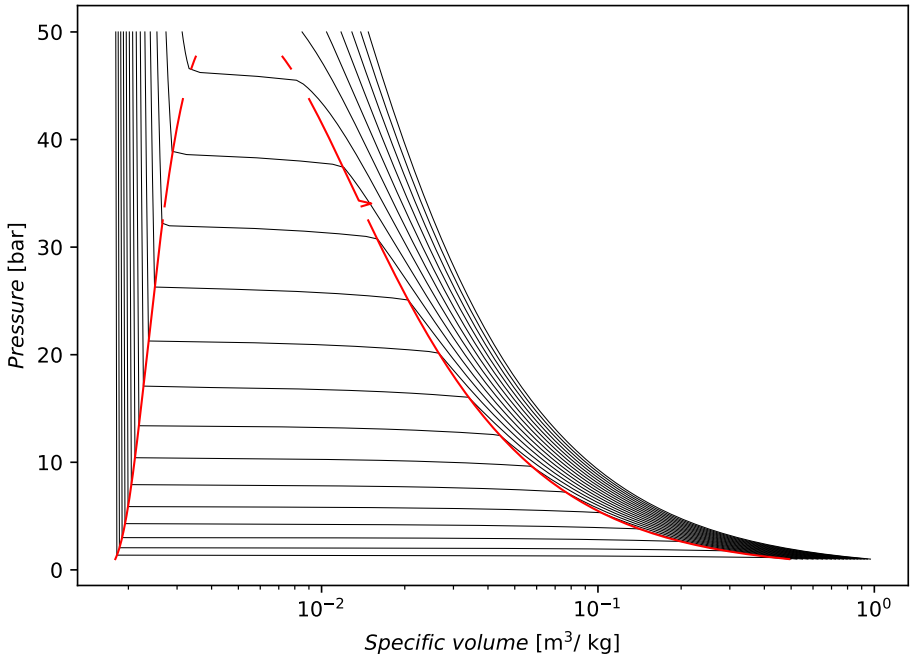

Figure 3.5: A p-v diagram including bubble and dew curves that was made using the CoolProp package. Black lines are isotherms of 50/50 mol% ethylene/ethane between 180 K and 340 K. The state evaluation results in smooth isotherms, even surrounding the critical point. The two-phase region is enveloped by a red line, which is created by performing bubble and dew point calculations in CoolProp. These lines are discontinuous above about 30 bar, where CoolProp sometimes fails to calculate the bubble or dew points.

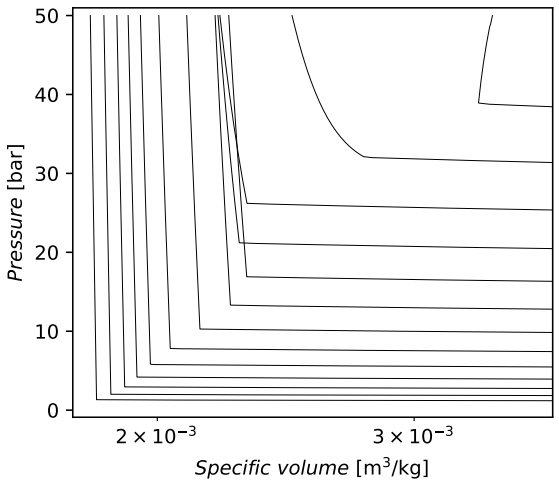

(a) 50/50 mol% ethylene/ethane overlapping isotherms in the liquid phase, calculated using the thermo package.

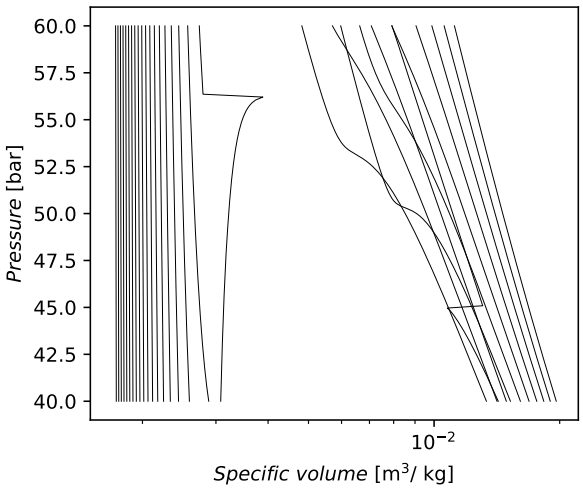

(b) 50/50 mol% ethylene/ethane critical region isotherms, calculated using the thermo package.

Figure 3.6: Two regions where the thermo package fails to return correct values.

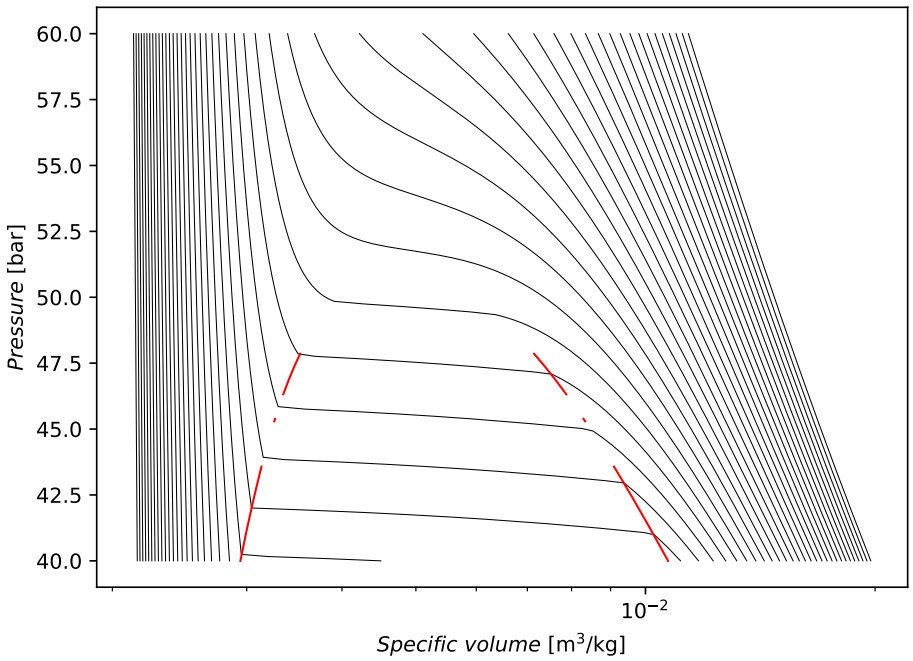

Figure 3.7: Isotherms of 50/50 mol% ethylene/ethane between 180 K and 340 K at high pressure. The state evaluation results in smooth isotherms, even surrounding the critical point. CoolProp easily calculates state points right below or above the critical point. Bubble and dew points are only calculated at some p, T values.

Similar plots around the critical point that are made using CoolProp look much smoother, as shown in Fig. 3.7. The bubble and dew point calculations fail, but the isotherms show that state calculations succeed without exception.

Bubble and dew point calculations

It was seen in section 3.3.4 that the bubble and dew calculations of both the thermo and CoolProp packages have shortcomings. Neither of the packages successfully performs these calculations in the critical region, and thermo lacks one of the needed functions all-together. Fig. 3.8 shows the difference between the two packages at lower pressures.

Dew- and bubble point calculations in thermo are unstable because of their iterative calculation. The vapour pressure that the calculation requires, is not defined for every temperature. This can cause an error while iterating over dew point temperatures. CoolProp does not have any limitations in this regard. The only trade-off for CoolProp is the limited adaptability for the user.

Conclusion

Summarising the preceding section, CoolProp performs better in nearly all aspects and is thus the best of the free python modules. CoolProp has limitations, primarily in unreliably calculating bubble- and dew points.

3.3.5. Diffusivity

Neither the CoolProp or thermo packages include models for inter-species diffusivity. The models discussed in section 2.5.3 were therefore implemented in Python. As de-

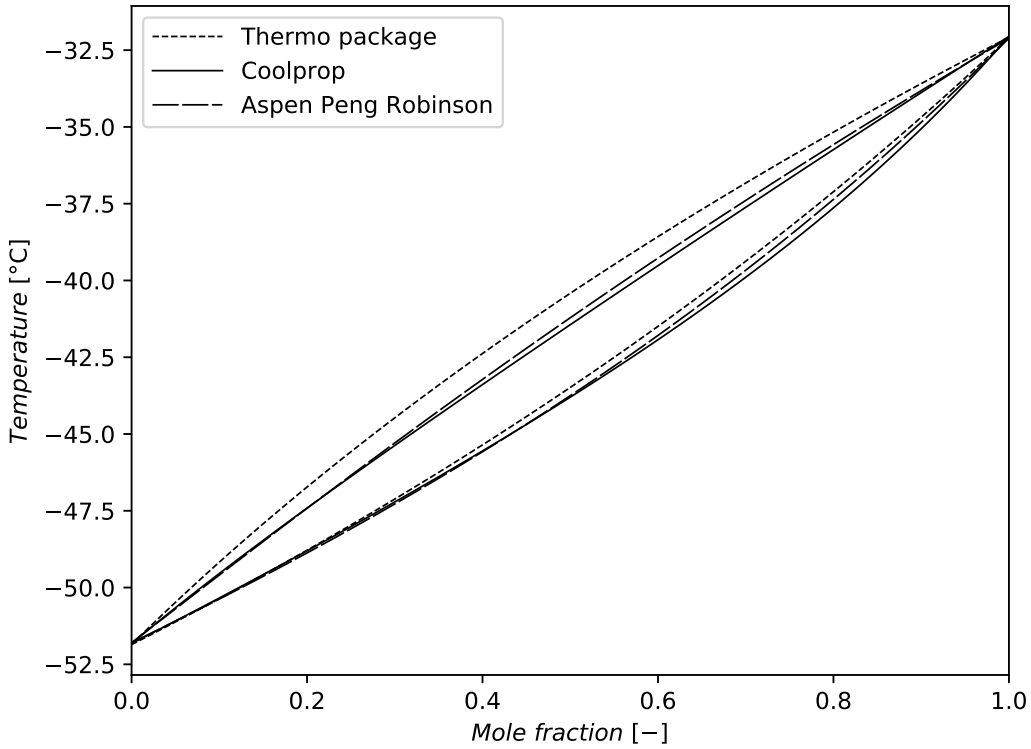

Figure 3.8: Bubble and dew curves for a ethylene/ethane mixture at $p = 10$ bar. Three sets of curves are plotted, generated by the thermo package, by CoolProp and by Aspen. It was shown before that both thermo and CoolProp fail at doing the calculations above certain pressures. This figure is meant to distinguish their quantitative results for the dew point calculations compared to Aspen. The difference between the temperatures between the packages can be ascribed to inaccurate activity coefficient and inaccurate vapour pressure equations in thermo. Aspen and CoolProp give similar results, while thermo's curves deviate slightly more from Aspen.

scribed, the vapour diffusivities are calculated by first evaluating a diffusivity at low pressure, which is then adjusted for a possibly elevated pressure.

Liquid diffusivity is mainly a function of temperature. Typical liquid diffusivities are plotted for different temperatures in Fig. 3.9a. The liquid diffusivities are calculated by first finding the infinite-dilution diffusivity, and then applying the described correction factor for higher concentrations.

Vapour diffusivity is mainly a function of pressure, which is demonstrated by Figs. 3.9b and 3.9c.

3.4. Model variables

The following section contains a clarification of the complete model arrays and boundary conditions. These arrays were implemented in python to do the described calculations. Fig. 3.10 is a shrunk down graphical representation of the whole model. The different streams and other model variables are discussed in the next sections.

In Python, numbering of array indices starts at 0. In this thesis, numbering starts at 0 as well for that reason. This makes it possible to do a direct translation from the thesis to the model, preventing possible confusion. Note that stage number 1 represents the second stage. Thus, in Fig. 3.10, streams labelled 0 are coming from the condenser at stage 0. Streams with subscript 1 exit from the second stage, below the condenser.

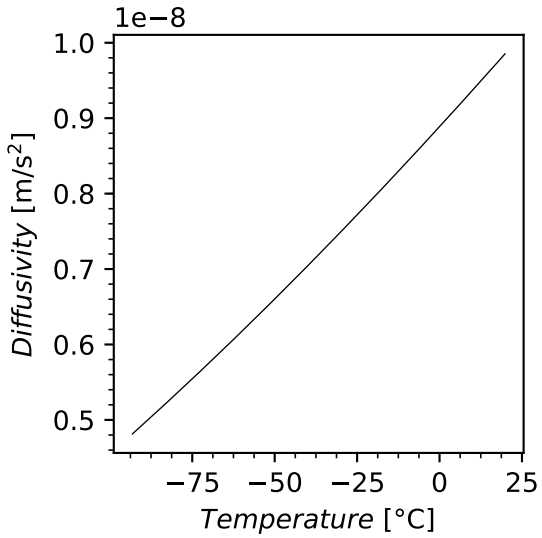

(a) Liquid diffusivity for different temperatures. Diffusivity is not exactly a linear function of temperature. The only other factors affecting liquid diffusivity are the viscosity of either species.

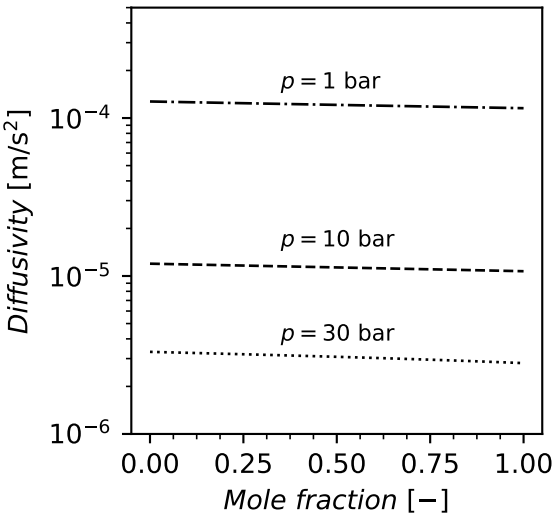

(b) Vapour diffusivity for different pressures and $T = 300$ K, as a function of the ethylene fraction. From top to bottom, the three lines represent diffusivities at 1 bar, 10 bar and 30 bar. The equations for vapour diffusivity are not linear, but the logarithmic scale makes it seem like they are. It is clear from this plot that the pressure has a large effect on the vapour diffusivity. This effect is plotted separately in Fig. 3.9b

.

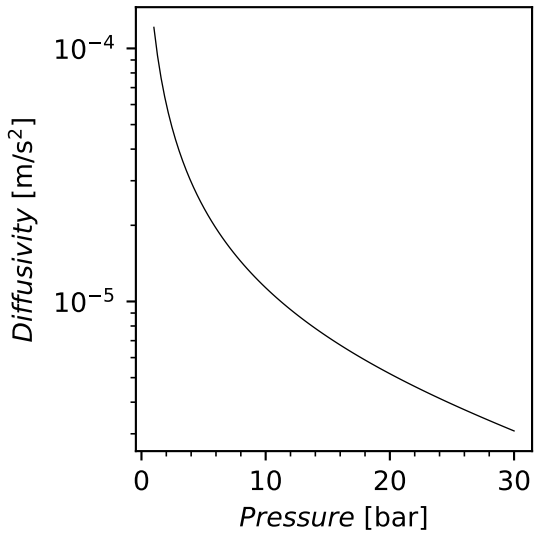

(c) Vapour diffusivity at 280 K, as a function of pressure. It can be seen that diffusion in the vapour phase is over an order of magnitude slower at between 1 and 10 bar, and another order of magnitude between 10 and 30 bar. This will lead to smaller rates of mass transfer at higher pressures. The diffusivity relies on viscosity data, which come from the thermo model. This model was not verified in this work, so this could very possibly lead to inaccuracies in diffusivity calculations.

Figure 3.9: Diffusivity for an ethylene/ethane mixture in two phases and in different conditions.

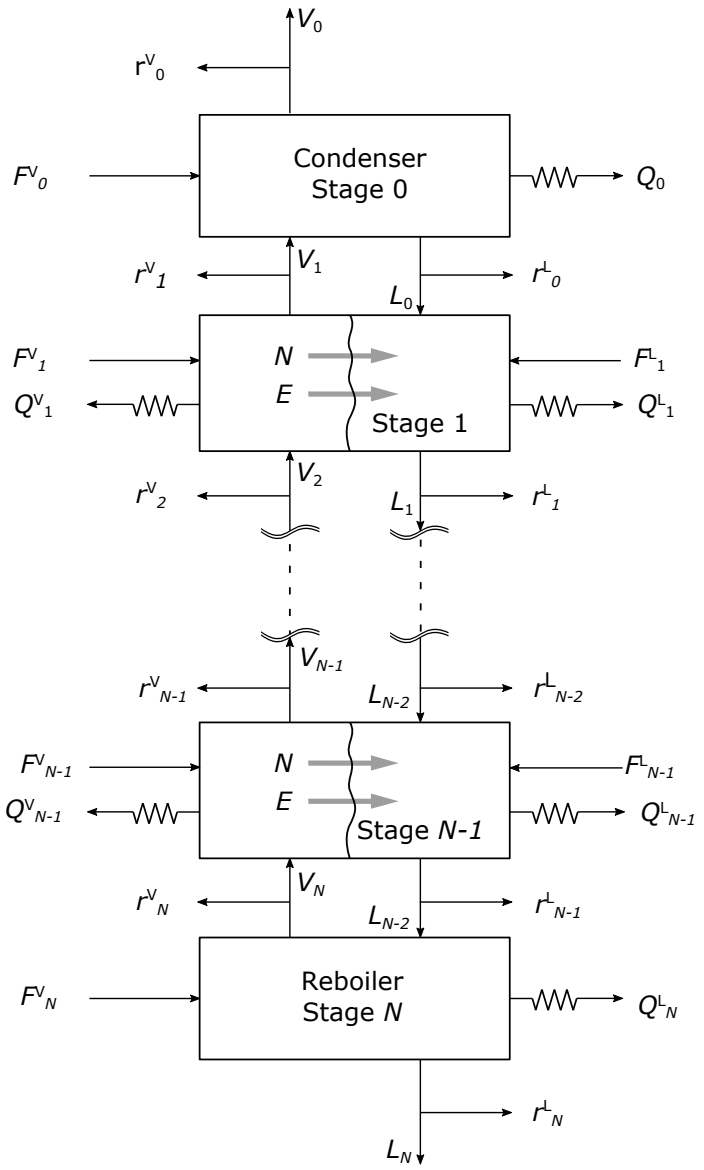

Figure 3.10: An example of the full model and all relevant streams. The dotted lines indicate that a large amount of stages can be inserted.

If there are N_s stages, there are also N_s vapour and liquid steams, with corresponding mole fractions and temperatures. Side streams r are not considered in this study, so their value is set to 0 mol/s. The mole fractions x and y are put into matrices where the rows represent the height in the column, and the columns are the different components. The subscript names are corresponding: the liquid mole fractions on stage j are x_{ji}, where the j is the row in the matrix, and i is the column. The model is made for a binary system, so all components are indicated with numbers 0 and 1.

The length of the vector of heat transfer to the different stages Q is equal to N_s. The first and last elements of the vector Q represent the condenser and reboiler duties, and all the middle stages represent the part of the HIDiC that is filled with packing. The packing-filled part of the column consists of a stripper and rectifier compartment. Likewise, the top part below the condenser of every array, including Q, represents the

rectifier heat transfer, and the bottom part above the reboiler represents the stripper heat transfer.

The unique feature of the pp-HIDiC is that the stripper and rectifier exchange heat continuously along their height. Certain stages in the rectifier are thus linked to the stripper stages in he HIDiC, depending on at what height they are installed next to each other. Naturally, the rectifier could be taller (it will be larger in practice, because the feed usually contains more ethylene than ethane), so the rectifier can not be linked to the stripper along the whole height. The part of Q that is not coupled, simply has no heat transferred from it, so its value is zero:

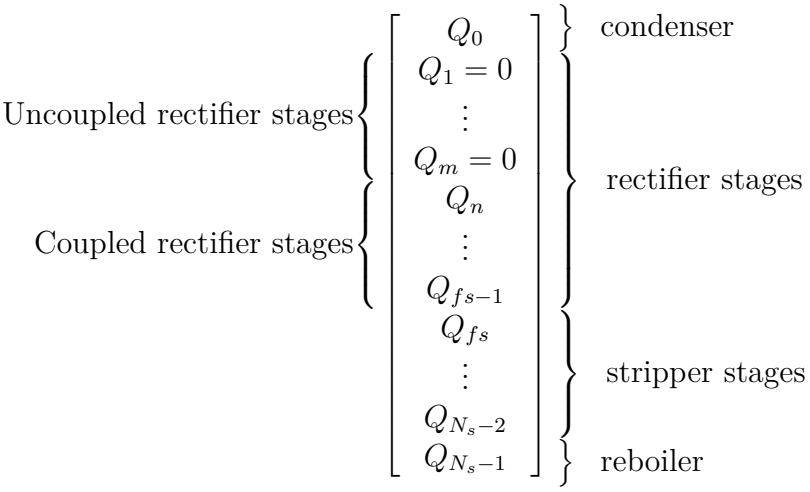

Figure 3.11: Positions in the column of the entries in the heat transfer vector Q.

Assume that the stripper has N_s stages. The rectifier is then heat-coupled with at most that number of stages, since the rectifier has more stages overall. The bottom rectifier stages are linked with all the stripper stages in the developed python model. The top stages of the rectifier should have a higher temperature, so coupling the stripper with the top stages would require more compression work to overcome that extra temperature step.

3.4.1. Model vectors

A brief summary of an iteration can be as follows:

1. Use vectors of initial values to re-evaluate stage properties.
2. Evaluate the system of equations and return an output vector.
3. Repeat.

All variables are stored in vectors, and so are their derived properties and parameters. They are more elaborately displayed in Appendix D.

Notably, the first element liquid flow rate array L_j, and the last element of the vapour flow rate array, V_{N_s}, are not included in the iteration because they follow from the reflux and boilup ratios. These ratios link these flow rates to the bottom liquid and top vapour flow rates respectively, making them dependent. This is a modelling

decision recommended by Seader, Henley & Roper [17], to which they refer as *standard distillation boundary conditions*.

The fixed variables are now replaced by the condenser and reboiler duty, Q_{cond} and Q_{reb}, so the total number of system equations and variables remains equal.

Property calculation

Derived properties are first calculated for each stage after an iteration (or at initialisation). Two calculations are done only once:

1. Partial molar enthalpies are estimated for the stripper pressure and rectifier pressure. They are interpolated from tabulated partial enthalpy data that was generated using CoolProp. Since the pressures are kept constant, these partial enthalpies do not change, and they only have to be calculated once.
2. Molecular weights of the specified components are gathered from the thermo package.

The following calculations are done each iteration:

1. Liquid and vapour molar weights per stage are calculated using the liquid and vapour mole fractions and the molar weights of pure components.
2. The following properties are calculated using CoolProp for both vapour and liquid. Molar properties are found by multiplying by the molar mass.
   (a) Calculate enthalpy $h(T, p, x)$ (CoolProp).
   (b) Calculate specific heat $c_p(T, p, x)$ (CoolProp).
   (c) Calculate density heat $\rho(T, p, x)$ (CoolProp).
   (d) Calculate viscosity $\mu(T, p, x)$ (thermo).
   (e) Calculate thermal conductivity $\lambda(T, p, x)$ (thermo).

   with additionally, only for the vapour phase:

   (f) $\rho_{STP}(x)$ at standard pressure conditions, calculated via interpolation from thermo data, required for vapour diffusivity.

   (g) Viscosity at standard pressure, $\mu_{STP}(x)$, calculated via interpolation from thermo data, required for the vapour diffusivity pressure correction.
3. Vapour and liquid diffusivities, $\mathcal{D}_{a,b}$ for each component.
4. Calculate mass transfer coefficients $k_i(T, p, x)$ and effective interfacial area a_e. Mass transfer greatly depends on the packing geometry input values, interfacial area depends on many fluid parameters, as well as packing geometry.
5. Find superficial velocities in the packing as a function of molar flow rates, $u(L, \rho)$ and $u(V, \rho)$.
6. Calculate heat transfer coefficients *htc* via the Chilton-Colburn analogy.
7. Find overall the total mass transferred per stage, per component $N_{j,i}(x_I, x, y, a_e, k)$.
8. Find the K-values on the interface.

All required information to evaluate the system of equations is known after these calculations, and the model equations are evaluated by the solver.

3.5. Model output

The converged values of the model variables are the outcome of the model. These are the non-blue vectors in Appendix D. Their usefulness and meaning is discussed in the following section.

Values of the model vectors can be visualised by plotting their values on the x-axis against the height of the column on te y-axis. The pressures, geometry or feed flow rates can be changed if the results contain values that are unwanted of unrealistic operating conditions.

Vapour and liquid molar flow rates

Vapour and liquid flow rates should have physically realistic values for a fluid that flows in a packing. When dripping through a packing, liquid flow velocities should not be much higher than 10 cm/s. Vapour velocities should not be much greater than 1 m/s in a packing. Resulting flow rates higher than that should aid the designer in applying a lower feed flow rate, lower reflux rates, or make the column flow area larger. Flow rates directly follow from the provided feed flow rate and column internal geometry. These values can be tweaked to correct the flow rates to values within realistic limits.

Mole fractions and interface composition

The mole fractions of the column at a certain height can be used to determine the necessary height of the column to achieve the desired degree of separation. If the column is small, but needs a high reflux, it might be good to make the column taller and decrease the reflux to save some energy. Conversely, the column may be shortened if the mole fractions do not change considerably above a certain height of the column.

If the column's mole fractions are all right, but its liquid load is too high, the reflux rate might be lowered, and the column could be lengthened to maintain the quality of separation, but also decrease the liquid load.

Separating a mixture is the primary goal of the distillation column, so mole fractions are a model result that a designer tries to get up to specification. The mole fractions are created by the interplay between all the other variables, and the mole fractions can be used to make design decisions about the geometry and reflux rates.

For example, it is in principle possible that the interface composition is way different from the bulk compositions. The interface composition only depends on the pressure, temperature and corresponding K-values. For mixtures that are not showing non-ideality, K-values are such that the interface composition lies between the liquid and vapour compositions.

Temperatures
Column vapour and liquid temperatures are especially important, since they determine the rate of heat transfer along the column on the packing surface, and also determine how much heat is transferred from the stripper to the rectifier at varying heights in the column. Temperatures should:

- not cross each other between the stripper and rectifier. This would lead to a reversed heat flux and lead to higher loads in the condenser and reboiler.
- not lead to too large temperature differences between vapour and liquid. If this happens, driving forces for heat transfer become larger than they need to be, causing more heat degradation and higher duties than absolutely necessary.
- not be too high or low overall. Since the model currently assumes a constant predetermined pressure in the stripper and rectifier, this pressure might lead to high or low temperatures in the model because of the boiling point shift. Since the C_2-splitter is to be integrated in a plant, with peripheral equipment, and will likely be interconnected in a cooling system, setting the right operating temperatures is important in process design. The optimal process temperatures might then directly constrain the column design temperatures to be within a specific range. Convenient temperature outputs are therefore a major design consideration for HIDiC.
- be physically allowable. The interface temperature must be between the dew and bubble point temperatures of the mixture, which should be higher than the liquid phase temperature and lower than the vapour phase temperature.

Heat Transfer
The heat transfer rates in the Q-vector can be examined to determine condenser duties, and to find the heat that is being transferred in the coupled stages of the HIDiC. If negligible heat is exchanged in the coupled stages, their temperature difference might be too small, surface area might be too small, or the column might be too short. The designer can make adjustments accordingly.

Mass transfer
The mass transfer of both species should ideally be one way. If there is a mass transfer reversal, there might be a temperature cross-over as well. Mass transfer is the only way in which species can travel between the phases, and it is the only mechanism that changes the composition along the column. If mass transfer is too low, there are only limited options for the designer. Changing geometry, pressure, flow rates and temperatures will influence the rate of mass transfer, but an important part of it depends on the interfacial area of the packing. If mass transfer is a limiting factor, more area must be provided or flow rates must be decreased to give the streams the time to exchange heat and mass.

3.6. Model Validation

The rate-based model should be compared to experiments to establish confidence in its results. The only measurements on a comparable set-up are described in the work by Bruinsma, Krikken, Cot, Sarić, Tromp, Olujić & Stankiewicz [1]. The authors describe it as a *proof of principle*.

The measurement results can be used for comparison, but Krikken [41] performed measurements with a perforated plate between the packing, causing liquid accumulation and maldistribution. These are the same measurements as the ones used for the paper by Bruinsma, Krikken, Cot, Sarić, Tromp, Olujić & Stankiewicz [1]. Measurements were done with a heating oil instead of a bundled stripper/rectifier system, and the used components were other substances than ethane and ethylene.

There are many different factors between this study and the work of Bruinsma, Krikken, Cot, Sarić, Tromp, Olujić & Stankiewicz [1], which makes it hard to compare the the reported experiments and the model, for a direct validation of an ethylene splitter model. That work's measurements can thus only give a rough qualitative estimate about the model accuracy, since so many of its operating conditions are different.

New accurate measurements, with the correct geometry and flow regimes, could help to establish much needed confidence in model results. Continued development on the HIDiC would need this confidence in the model to justify spending resources on for example a pilot plant.

Additionally, better suitable heat and mass transfer correlations could be developed by doing measurements targeted at a specific application. More accurate measurements of the heat and mass transfer coefficients in the desired packing configuration are needed to properly dimension a column. Especially a C_2-splitter, which is usually the tallest column in a plant, would benefit from an accurate height calculation. An increase of its height by a small factor would make it much less infeasible, and a decrease will make an alternative much more attractive.

The packing geometry, vapour-liquid contacting, and liquid loading should be similar when performing heat transfer measurements. Usually, correlations are made using dimensionless groups, which could cover a large range of fluids. When developing the mass transfer coefficient correlations, it would be best to use conditions that are similar to the eventual column conditions in practice. Developing an entirely new correlation could however require a lot of time and many measurements, which requires investment as well. Other existing models, such as the Delft model could, albeit less ideal, be used to make a first comparison, which is what this study attempts.

4

Discussion

This chapter describes the outcome of the modelling that was carried out. All the described functions and property calculations were executed, but the model would not converge properly yet. There are a couple of primary causes for this, and also some smaller factors that inhibit the model's performance, which is discussed in this chapter. Possible other points of improvement are discussed as well. This chapter is concluded by a general discussion on the literature and the pp-HIDiC development.

4.1. One equation, one variable

A full Python distillation column model was developed. The program allows the user to input a device geometry, flow rates, feed compositions, pressures and flow rates and the type of mixture. This information was processed to generate an initial guess, which is used to generate data structures for the Newton solver. The convergence of the model equations remained cumbersome.

The primary reason for a failing convergence of the model is discussed in this section. The equations in the set have an equal number of variables. Every equation can be thought of as determining or 'fixing' one variable. For example, assume that the liquid phase mole fraction of one component is found at a specific point in the column by solving the mass transfer equation. Then, the other component's mole fraction is fixed by the summation criterion. Likewise, for every model variable, there is one equation that fixes this variable. Of course, the equation does need to depend directly on this variable to be known. An example of this is the interface temperature.

A problem arises when fixing the interface temperature in the non-equilibrium elements. The interface temperature T_j^I only appears explicitly in the energy balance, but so does the heat transfer across the packing per element, $\mathcal{E}_j$. The heat transfer per element only appears in the energy balance, so the energy balance must determine the heat transfer per element. They form a small sub-system of two entries on the Jacobian matrix of the equation solver, which the convergence of the whole model relies on. Thus, the temperature in these two elements can then only be determined by the equilibrium equations.

The condenser and reboiler equilibrium condition partly shows the same problem. The condenser and reboiler temperatures appear in the energy equation enthalpies, and in the equilibrium equations. The system thus depends on the described temperature dependence in these equilibrium elements too.

Since the only place where temperature is of influence is in the K-values and the energy balance, and the temperature-dependency of the K-values is not strong, the convergence of the system is not guaranteed. The temperature and K-values are not uniquely dependent: there can be a similar K-value at different temperatures, at varying mole fractions. Additionally, the dependency is implicit via CoolProp as a data source for this parameter, which makes directly controlling the K-values impossible, unless CoolProp is circumvented altogether.

Possible solution
Since K-values are not unique to a certain temperature. They are only unique to a certain temperature for constant mole fractions and pressures. These are variables in this model, so the K-values are not uniquely defined and they cannot be used to fix the temperature.

The problem could be solved in the reboiler and the condenser, by fixing their duties. They then become an input parameter of the model. This frees up the energy equation, so it can, instead of determining the duties, determine the condenser and reboiler temperatures.[1] This goes against the advice of Seader, Henley & Roper [17], but the designer's task goes from fixing a duty to fixing a reflux ratio. This should be studied further. The energy equation would then directly determine the temperature. The equilibrium equation is freed so it can determine x_{ji} and y_{ji}, which frees up the mass balance. The extra variables that are created are the L_0 and V_{N_s}, which can now be solved by the mass balance.

4.2. Property difficulties in current model

Several thermodynamic properties and transport properties are used in the model. The model is dependent on their precision, but also on how they are evaluated in their respective packages. Their precision is important because their accuracy is needed to get physically feasible and representative values when they are evaluated at many possible different combinations of the model variables. The robustness and computational efficiency of packages can become a limiting factor in quick evaluation of the model, especially if the number of stages increases.

4.2.1. K-value discussion

K-values can destabilise the system of equations by not being uniquely defined, and having no explicit temperature dependence. The K-values are used in the equilibrium equations for the condenser and reboiler, and they fix the mole fractions together with the summation criterion. By manually setting K-values, it was found that, if one of the K-values is greater than 1, the other must be smaller than 1. If both K-values are equal, the system has no solution, since the matrix describing the two equations becomes singular.

K-values have another problem: they are undefined out of the two phase region. Due to a mismatch between equations, the interface temperatures could be iterated to a temperature below or above the dew point temperature of a mixture. This can happen

[1] This temperature lies between the dew point and the bubble points at the specified pressures, so one would say that these temperatures are fixed. However, the temperatures depend on K-values and the mole fractions, which are variables.

quicker in the C_2-splitter, since the bubble- and dew point of the mixture lay only about 2 Kelvin apart. If the interface temperature falls outside this range, the K-values are undefined, and CoolProp will return nonsense K-values, usually a floating point number in the range $0 \leq K \leq 5$. However, the interface temperature cannot physically fall outside of the range of the bubble and dew curves.

Beside returning nonsense values outside of the two-phase region, these nonsense values also create a discontinuity in the K-values outside of this 2 Kelvin temperature range. Optimisation problems and root finders should preferably work outside of the range where functions have discontinuities. Possibly, a clever software solution could be adapted to find a solution to this problem in future work.

4.2.2. Transfer coefficients

Mass transfer coefficients using the Delft model were found to have values in the right order of magnitude. Their inevitable inaccuracy for this application has been discussed before. The value of the mass transfer per stage, $\mathcal{N}$, did become very small, but no conclusion could be drawn from that, since the solution has not converged yet.

The heat transfer coefficients were found using the Chilton-Colburn analogy. This correlation is strictly only theoretically valid in some specific cases. The analogy is used a lot in distillation modelling studies, but they do not suffice for more elaborate modelling attempts. The heat transfer on the packing is therefore a large factor of uncertainty in this work.

4.2.3. Transport models and thermodynamic properties

The thermo package is inconvenient to work with since it is very slow. For future development, it would be best to use viscosity and thermal conductivity correlations from *The properties of gases and liquids* [54] or *Perry's chemical engineers' handbook* [55]. These are described as being reasonably accurate, and their explicit calculation makes them several orders of magnitude more efficient in terms of computational time. Beside that, thermo was shown to be inaccurate in evaluation of the equations of state, and also deviated in comparison with CoolProp and Aspen in flash calculations.

The state evaluation of the thermo package is not used in the calculations, but the state is nevertheless evaluated on every stage on every iteration. This is needed because of the way thermo calculates the mixture mole fractions and then uses those to evaluate the fluid properties. This creates extra overhead calculations and would better be prevented.

4.2.4. State evaluation

CoolProp's state evaluation is fast, but it can return exceptions if the state solver estimates the wrong phase. These exceptions can be caught easily, and the solver can be instructed to search the two-phase region or the other phase for the proper solution. This does come at the cost of some extra calculations per incremental element. Furthermore, as shown in Fig. 3.7, bubble and dew point calculations can become unpredictable at higher pressures. This could be a good enough reason to spend some money on a trusted commercial package such as RefProp or a process simulator that has a proper interface with python.

RefProp and its Python interface is known to be a little bit slower than a single

CoolProp flash calculation. It is however acceptable to sacrifice some computational efficiency if the RefProp calculation is much more reliable. CoolProps quick calculation time effectively increases if it fails to find a solution. The calculation then has to be repeated after specifying the phase that the mixture has.

4.3. Programming-related limitations

The built model could use a couple of possible improvements. Major efficiency steps could be made to make the calculation procedure run quicker. Three different areas of improvement are:

1. Program structure improvements
2. Reduced calculation time for repeated calculations
3. Jacobian specification to calculate it without perturbation

Proper handling of variables and functions could remove redundant calculations and reduce the chance of errors. This study only looks into distillation modelling, so the programming structure improvements are not further discussed. A good program structure would make it easier to do adaptations on the code, and also to make expansions or other adaptations on the model itself.

Flash calculations are expensive, and their speed directly dictates the total run time of the model. In CoolProp, a workaround code was made to properly handle all the CoolProp exceptions. This bit of code can be seen in Appendix E. This function was written so that most CoolProp exceptions and errors are filtered out. Still, it might lead to a general exception in some cases, for example at very high or very low temperatures or pressures. The state will not be evaluated if one of the bubble or dew points fails to be calculated.

There are multiple state.update calculations, which are all separate evaluations of the same state point, which is needed because some of the calculations might return errors. This increases the calculation time per stage considerably. A different property package may be able to perform state calculations a bit more slowly, but it might still be shorter if it would not need such a workaround to prevent errors.

A short calculation time is convenient in usage and debugging of the model. If a designer wants to design a column and runs the model, it might take a few runs of the model to get to a satisfactory design.

If calculation time can become a limiting factor, especially when the number of equations increases. If a column of 80 m is divided into partitions of 5 cm, there are 1600 stages. From section 3.1, there would be over 25000 equations, and the Jacobian evaluation using a perturbation method would find the derivative to these equations one by one per iteration, each requiring at least 1600 stage evaluations. State evaluations quickly become the time limiting factor.

Jacobian calculation

During the model development, it became apparent that the number of function evaluations was very high, and would cause a very long model run time if there would be a large number of stages. Some programming tricks, such as multi-threading the stage calculations and interpolating properties from data tables were tried out. Multi-threading

was unsuccessful, and the table-lookup method was not much faster than the direct function evaluation. The problem was the number of calculations that had to be done, not the time that those calculations took. There is a possible workaround for this.

The system's Jacobian matrix is not calculated, but perturbed instead. Every element of the Jacobian is calculated by taking one input variable, perturbing it, and evaluating the function with that single changed variable. The repeated flash calculations in the function evaluations quickly become very expensive.

The number of function evaluations can be cut considerably if the Jacobian would be calculated algebraically. All variable-derived properties would only have to be calculated once. This would include partial derivatives of enthalpy, temperature and other quantities. All elements of the Jacobian can be calculated directly. These two steps will take much less time for large systems than the perturbation method. A disadvantage is that the Jacobian needs to be worked out analytically.

The first step is to find all the derivatives of the system of equations. The second step is to create a Python function that builds a matrix which size depends on the number of stages. This is an elaborate exercise, where every matrix entry changes position for different system sizes. This is not done in this study and is recommended for later work.

4.3.1. Feasibility and improvements of the pp-HIDiC

It is unlikely that the current proposed geometry is the best geometry, and more configurations have to be tried out to see which configuration works best. For example, the pp-HIDiC's has straight, plain sheet metal walls for each compartment, which might have bad wetting properties, and also might adversely affect liquid distribution. Even the use of existing structured packing elements might not be the best option. Albeit readily commercially available, the existing packings are fine-tuned, modelled and made especially for the use in cylindrical, 3-dimensional bulk columns, which the pp-HIDiC is not. The use of CSMP material is a smart choice for quick testing, but other, tailor-made materials might even work better. However, it is too early to do this kind of optimising at this stage of development.

An important property of the pp-HIDiC is its ability to exchange enough heat through the side walls, from the rectifier to the stripper. For this, the surface-to-volume ratio should be large, so there is a large contact area per unit volume, and the current pp-HIDiC does achieve this. It is still up for debate if the wall surface area is enough, too small or maybe too large. A too large surface area will decrease the ΔT between the stripper and the rectifier. This could make the column larger than the efficiency improvement can justify. There is an optimum in this trade-off, which is probably not the current configuration.

The current configuration has an equally wide packing element width w for both the stripper and the rectifier (see Fig. 3.2a). The feed composition of a column varies, and the reflux and boilup ratios may be very different. The flow rates in both parts of the column may be very different, so the dimensions of the compartments might need to change accordingly. If one of either section becomes much larger than the other, there may be need for a stripper or rectifier width w that are not the same. This was not tested in this work. The feed composition, vapour fraction changes along the column at different loads, and varying boilup- and reflux ratios may make the column very dependent on steady state operating conditions. This decreases its operating window with regards to

the feed composition. That could be a reason for chemical plant operators to opt for a column choice that can handle a larger spread in feed compositions, thereby accepting a lower efficiency.

Additional requirements for a rate-based model

It could be contested that the use of a rate-based model is justified for the development of a HIDiC. The models are more complex, take longer to develop, and demand a larger number of detailed correlations for transport properties and pressure drop. Additionally, HETP is historically used and easy to work with. Although this is all true, the use of pre-existing HETP measurements for cylindrical packings cannot be accurate for modelling the pp-HIDiC. As mentioned in chapter 2, Seader, Henley & Roper [17] and other authors mention specifically that packed columns have continuous heat- and mass transfer, and that these can only be modelled by an incremental model for those phenomena. This is supported by additional hydraulic measurements at the Energy Centre of the Netherlands (ECN), which is part of the consortium that works on the pp-HIDiC development. A rate-based model tries to capture all the physics in packings, and is thus the only way in which the pp-HIDiC can be modelled without introducing major inaccurate simplifications.

Rate-based models demand accurate heat and mass transfer correlations. This study only had access to a mass transfer correlation that was found by the Delft model by Olujić, Kamerbeek & de Graauw [37]. This correlation is made for an entirely different configuration, which makes it unfit for this model. It was a necessary decision, as described in the Theory section, to use the Delft model for this work. The results of the overall calculations can be limited by a poor quality or inapplicability of the mass transfer model. Thus, an applicable, accurate mass transfer model should ideally be made for a promising geometry before any extensive modelling is done. This also holds for the heat transfer correlations.

The Chilton-Colburn analogy is unfit for any detailed modelling. While it is mentioned in literature that it is often used, its derivation from a film model shows that is strictly only really applicable in some specific theoretical cases. Therefore, the rate-based model would need a tailor-made heat transfer correlation as well.

Comparison to existing technologies

In comparison with a regular heat-pumped VRC column, the HIDiC promises some exergy and energy efficiency advantages. Since the model was not successfully run, these advantages cannot be quantified yet. A black-box exergy usage comparison of just the columns without their peripheral installations would be the best tool to evaluate them. Realistically, these columns are built into plants that are heavily much heat-integrated. The current impact of a HIDiC and its exergy use may be of little impact depending on its actual impact on the surrounding processes in the plant. The energy availability from upstream processes might become lower in the future, as upstream processes are improved. If that is the case, the HIDiC column should be compared economically and feasibility-wise with its most direct competitor, the VRC column. If only the columns themselves are considered, an exergy comparison is most suitable.

5

Conclusions and recommendations

This chapter concludes the prior discussion, and does recommendations for future modelling and HIDiC development.

5.1. Conclusions on modelling

Modelling conclusions are discussed first. These are the conclusions that are not related to programming-specific topics.

5.1.1. Choice of variables

From distillation theory, it was clear that a rate based approach is required to accurately model the pp-HIDiC. A rate-based model was chosen to describe the heat and mass transfer phenomena incrementally in the packing-filled HIDiC elements. Literature convincingly recommends these type of models for packed beds and any other device that has a continuous transfer of heat and mass. Literature also advises against the use of HETP and other conventional tray-based calculation methods. Rate-based models are the only models available in distillation literature that try to capture most phenomena in continuous distillation operation, and therefore the only way in which continuous columns can be modelled.

A full distillation column model was made in Python. It became apparent that the choice of model variables is critical in the model's ability to converge. The reflux and boilup ratios should be a variable, and the heat input of the condenser and reboiler should be an input parameter. It is then prevented that a temperature is attempted to be found with an equation that does not depend on that temperature strongly enough. This conclusion was based upon a modelling attempt with an unsuccessful outcome.

Another conclusion from the modelling work, is that it is worth it to build a Jacobian matrix from the system of equations. Built-in Python functions work well, and have the option to specify a Jacobian matrix. The in-house solver from TechnipFMC does have a different convergence routine. Both solvers work well.

5.1.2. Conclusions on properties

The free property packages used for modelling are not ideal. The thermo package had many shortcomings and was not chosen, and the CoolProp package did not always properly return bubble and dew points. CoolProp required workarounds but did return accurate data results.

An attempt was made to avoid the issues with the thermo and CoolProp packages. It was concluded that this should be a project on its own, and its programming and validation requires substantial additional effort. This was stretching the scope boundaries. The shortcomings of the free packages justify the consideration to switch to a commercial property package with validated output data. The use of a commercial, accurate package is thus recommended, as long as the interface between Python (or any other preferred language) is fast enough and well-documented.

5.1.3. Conclusions on transport properties

A rate-based model might work well with any heat and mass transfer correlations, but the results are only reliable and applicable if there is confidence in the validity of these correlations on the physical configuration. The correlations depend on fluid properties, model element geometry, packing surface treatment, and temperature and pressure. For traditional systems, all of these were experimentally determined and validated, but it is unknown if these correlations can be extrapolated to be applicable for the proposed HIDiC configuration.

Tailor-made heat and mass transfer correlations are thus needed to model new geometries properly. Thus, the fact if a model is made for structured packings, does not mean that it is also valid for this particular setup that contains sub-structures of packing. This was further confirmed by additional hydraulic experiments performed by the Energy Centre of the Netherlands.

Heat transfer coefficients should not be found using the Chilton-Colburn analogy. The use of the Chilton-Colburn analogy is strictly only valid in some limited flow profiles, and any other use of the analogy would be an unvalidated extrapolation, so no conclusions can be drawn from its usage. Further experiments are needed to find a good correlation for heat transfer on the packing surface.

Heat transfer from the stripper to the rectifier is simply calculated with a UA-value in this study. It is assumed that the measured heat transfer coefficient from Bruinsma, Krikken, Cot, Sarić, Tromp, Olujić & Stankiewicz [1] is valid for this system. This constant heat transfer coefficient value is a simplification. In reality, this coefficient will change on the vapour fraction of the mixture, which changes along the column. Besides this, different compartment separation plates might have a different surface structure, and wetting properties. The liquid coverage of the surface will affect the heat transfer through it. This needs to be looked into to give a better approximation of the heat transfer between the stripper and rectifier. This would directly improve the model accuracy.

At this point, nothing can be said about diffusivity and viscosity data accuracy. If these properties would heavily affect the model outcome, better correlations need to be found. This study used correlations from Poling, Prausnitz & O'Connell [54] and Perry, Green & Maloney [55]. If improvements would be needed, they could instead also be obtained from direct measurement or via a commercial property package. The best available viscosity information is currently used in this work.

5.2. Conclusion experiment necessity

Experiments are necessary for model validation and tuning. The lack of experimental data hampers the model development. Experiments can also aid in transport phenomena correlation development. The experiment then supports the model development and vice versa, complementing each other positively.

5.3. Model programming conclusions

Evaluating the Jacobian, as described in Chapter 4, would result in a major calculation time improvement. This makes tabular interpolations or parallel computing unnecessary. It could be implemented in future model development. Since implementing the Jacobian decreases the number of state-calculation and transport property function calls, it makes it acceptable to have a slower but more accurate thermodynamics package.

CoolProp works fine for modelling if it is acceptable to do a couple of the same calculation attempts in a row, in case the package fails one of the earlier calculations. However, an external dedicated (commercial) program can increase reliability and accuracy of the thermodynamic state evaluations, which almost makes it necessary. Depending on its user-friendliness, it can also save time during the model implementation.

5.4. Other conclusions

Finally, this modelling work focused on a steady-state model of the pp-HIDiC. The rate-based modelling of this type of HIDiC is not straightforward, and its convergence partly depends on the input variables that the model is given. Even if convergence is achieved in further modelling work, the dynamic behaviour of the column is yet unknown. Additional model development or pilot plant testing are then needed to study its dynamic behaviour. This means that this model is only one of the steps that are needed to design an operational (pilot) HIDiC.

5.5. Recommendations

The recommendations from this work are split into two different categories. Modelling-related recommendations are discussed first, followed by some general HIDiC-related recommendations.

5.5.1. Modelling recommendations

A first recommendation for further model development is to use existing measurements or commercial software where available, and where possible. Every thermodynamic property, and all chemical-dependent transport properties could be obtained from these packages, so no attention has to be given to correctly implementing property models. Then, the model designer would only need to consider the model equations themselves, and the most important correlations for heat- and mass transfer. The number of potential sources of error is decreased, and the model development time is decreased as well.

Secondly, and the most important recommendation for model building, is the development of heat- and mass transfer correlations especially made for the geometry and mixture. Heat transfer correlations, scarcely available in literature, are not applicable

without introducing significant uncertainties. Some available mass transfer correlations can be used, as was done in this study, but these will fail to establish trust in the model results.

Thirdly, directly specifying the system's Jacobian matrix will decrease the required number of function evaluations drastically. If a finer partition of the column is needed, with more incremental elements, this is a necessity.

The fourth modelling recommendation is the development of a better equation for the transfer of heat from the rectifier to the stripper. The simple equation that was implemented in this work does not capture all the phenomena related to this heat transfer. An equation should be developed, preferably with ethane and ethylene, with varying vapour fractions and varying flow regimes. An accurate heat transfer equation could help in a more optimal design and could prevent the column from having more or less contact area than necessary.

Lastly, effort should be made to extend the model's capability for predicting dynamic behaviour and operability.

5.5.2. pp-HIDiC development recommendations

Experiments can help during the modelling phase by providing more accurate correlations, but they can also be used to rule out less optimal HIDiC configurations. It is very likely possible to come up with better packing element geometries, and further research should focus on finding those first. This can be done qualitatively by creating a geometry and observing if the wetting and distribution of the flow is good in different regimes. It can be done quantitatively using the approach as Bruinsma, Krikken, Cot, Sarić, Tromp, Olujić & Stankiewicz [1] used in their work.

Creating tailor-made correlations requires many experiments for every candidate geometry. If an experimental installation is available, it can be used to test different geometries and packing configurations prior to focusing on a particular one. Some of them will have better separation characteristics than others. There is no literature that compares any pp-HIDiC setups, and different imaginable setups have not been tested so far. Before spending many resources on the proposed setup by Bruinsma, Krikken, Cot, Sarić, Tromp, Olujić & Stankiewicz [1], different packing internals could to be considered.

A rough, qualitative approach could result in a selection of packing configurations that look promising. These can then be subject to more elaborate quantitative testing. The development process can be sped up by doing these qualitative experiments first, preventing unnecessary measurements on packings that might end up being less promising.

A few possible options for the packing internals and the packing structure are:

- Varying wall structure and surface treatment
- Varying packing material, for instance by using different types of sheet metal packings, or using random dumped packings
- Varying the packing compartment width w

Finally, a bench-scale or pilot experiment can be used to test additional phenomena that cannot be modelled with a steady-state model as described in this work. Before

large expenses are made on these larger setups, more small scale experiments, literature study, and simultaneous model development on dynamic column behaviour could help in designing these next steps in pp-HIDiC development.

Acknowledgement

The project proved to be quite the challenge. It was a deep dive into the world of process modelling, where I combined newly learned programming skills and the theory of separation systems.

I owe my gratitude to TechnipFMC, who allowed me to work with them on this project, giving me a lot of freedom in its execution, and providing me with a positive working environment.

Special thanks go to my supervisors from TechnipFMC and the TU Delft. Marco van Goethem, whose understanding of process modelling helped in overseeing various challenges. A visit to Marco's office always resulted in a positive way to go forward in the project.

This project would not have been brought to an end without the supervision of Carlos Infante Ferreira. His proofreading and suggestions to approach the project were a big help.

Lastly, I thank my parents, Kees and Adri-Anne Biesheuvel for their love and continuous support throughout all my years.

Appendices

A. The distillation principle

Distillation is separation of a mixture on the basis of a difference between the components' affinity to being in one of the phases that is present. Often, these phases are one vapour phase and a liquid phase, but sometimes more phases are introduced to get around the limits of azeotropes. Azeotropes are not discussed in this work and do not appear in HIDiC literature.

This work focuses on the case study of a C_2-splitter. It separates ethylene and ethane, which have no azeotropes. Both molecules are very similar in terms of mass, polarity and many other physical properties. Equilibrium and mass transfer between the two phases will be described in the following sections.

Since the C_2-splitter fractionates a two-component (*binary*) mixture by good approximation, multi-component separations will not be discussed in this thesis. A real C_2-splitter does contain some other components, but these are neglected in this work. Multi-component HIDiC operation is a complicated topic outside of the scope of this work, which requires additional study.

A.1. Vapour-Liquid equilibrium

If a mixture is dispersed into a vapour and a liquid phase, and mixture is then left to stabilise long enough, its components will distribute themselves between the phases depending on their equilibrium constants, which are a result of the species' intermolecular interactions. How much of each component resides in a phase depends on those constants, most often referred to as K-value. The K-value for the i^{th} component, K_i, is defined by the amount of component i residing in the vapour phase versus the amount in the liquid phase [84]:

$$K_i \equiv \frac{y_i}{x_i} \tag{1}$$

The K-values are in principle determined by the chemical potential of both phases, which must be equal at equilibrium, where the total Gibbs energy must be at a minimum. Direct calculation of the minimisation of chemical potential is done by using an equation of state that suits the components and the purpose [84]. A property model is used in this work, so direct calculation of the free energy is not needed. Equilibrium constants will be used in this thesis to evaluate the driving forces for mass transfer.

A.2. Separation factor

Separation of two components between the liquid and vapour phase happens if one component is more abundant in one of the phases, and, consequently, the second component is more abundant in the other phase. This happens when their *separation factor*, or *relative volatility* is any other number than one. This factor is defined as the ratio of the K-values of both components. At equilibrium, it dictates how much more of component

1 is in the vapour phase compared to the amount of component 2 [17].

$$\alpha_{ij} \equiv \frac{K_i}{K_k} \tag{2}$$

The separation of the mixture can be done by letting the mixture come to equilibrium, taking the top vapour, partly condensing it, and letting it come to equilibrium again. The same can be done with the liquid, and the process can be done multiple times in a row. If $\alpha_i > 1$, the vapour contains increasingly more of component 1 than component 2, and vice versa for the liquid. If the separation factor is much larger than 1, the difference in equilibrium composition between the liquid and the vapour phase is large. It then takes fewer equilibrium steps to reach a desired liquid and vapour composition.

In distillation technology, these sequential operations are called *equilibrium stages*. In a conventional trayed distillation column, the stages are placed on top of each other. Vapour and liquid flow countercurrently, up and down the column respectively. Vapour and liquid meet in each subsequent tray, where they come into equilibrium until they are passed to the next tray.

Purity of the top and bottom product can be increased by condensing the top vapour and putting it back into the column at the top, and by boiling the bottom liquid and putting it back as a vapour at the bottom. The already purified streams at the top and bottom are then again used in the equilibrium stages, making the end result at the top and bottom have an even higher purity.

The liquid returning stream at the top of the column is named the *reflux*, and its ratio to the total top column stream is called *reflux ratio*. The liquid is created by supplying cold to the top stream in a heat exchanger, the *condenser*. Similarly, the vapour stream that is put back into the column at the bottom is called *boilup*, and the *boilup ratio* is the fraction of the bottom liquid that goes back into the column after it is evaporated. A bottom heat exchanger, the *reboiler*, adds heat to the bottom liquid to (partly) evaporate it.

If higher reflux and boilup flows are used, purities will be higher. A column at *total reflux* will have all of its components recycled back into the column, creating the highest purity, but no product at all. The drawback of high reflux and boilups ratios is that the evaporation and condensation duties at the top and bottom become considerably larger for higher ratios.

The minimum number of stages needed to achieve a desired degree of separation can be calculated using the Fenske equation, where α is the average relative volatility [17, 85].

$$N_{min} = \frac{\log\left(\left(\frac{x_{i=1,N+1}}{x_{i=1,1}}\right)\left(\frac{x_{i=2,1}}{x_{i=2,N+1}}\right)\right)}{\log \alpha_{i,j}} \tag{3}$$

$\alpha_{i,j}$ is a function of pressure. At high pressures, it can be as low as 1.12 for the ethylene/ethane mixture. Assuming this value, with a product purity of 99.9% at the top and bottom are required, $N_{min} = 64$. Since ethylene often requires a high purity as a product, setting a top purity of 99.99% gives a minimum theoretical number of stages of 76. There are always more stages needed than the theoretical minimum, resulting in C_2-splitter towers with more than a hundred stages. The splitters are often very tall and unwieldy for this reason.

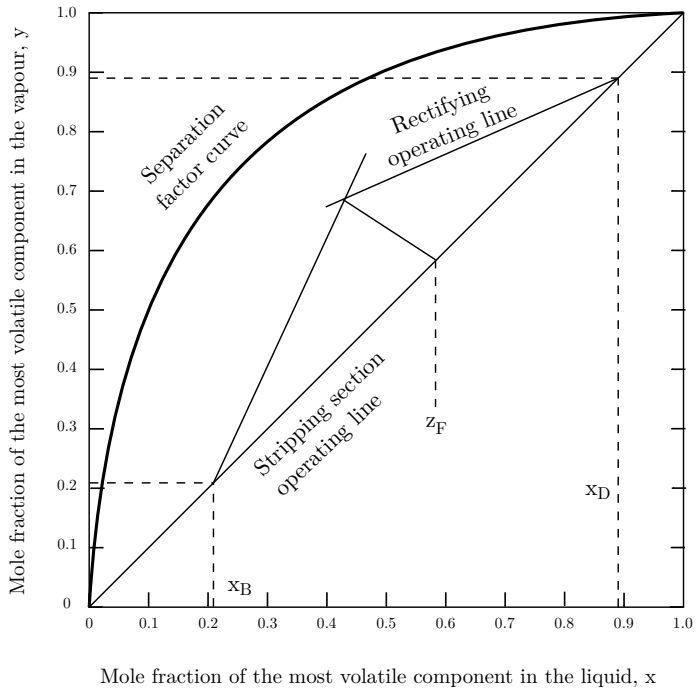

Figure A.1: A McCabe Thiele diagram with operating lines, feed position, adapted from Seader, Henley & Roper [17].

A.3. Theoretical trays and reflux ratio

Another way of creating a higher purity, is to have more trays in the column. The term *theoretical trays* is used to indicate the number of equilibrium stages that is, in theory, required at a certain reflux and boilup ratio to achieve the desired degree of separation. As the ratios decrease, more trays are needed. There exists a *minimum reflux* and *minimum boilup* below which the desired specifications cannot be met, even with an infinite number of trays.

The McCabe-Thiele diagram (Fig. A.1) plots the separation factor curve (also called equilibrium curve), and the *operating lines* along which the separation takes place. Operating lines contain the compositions that are passed on from tray to tray. Their slopes are equal to the ratio between the vapour and liquid molar flow rates. Simpler models often assume that these flow rates are constant along the column. Inside a tray, the mixture then attains the composition as dictated by the separation factor curve. An operating line can be drawn that describes the composition change along the column. At minimum reflux, the operating lines barely touch each other at the separation factor line. Reflux and boilup ratios determine how much of the top and bottom product has to be recycled back into the column. These streams need to be either cooled to condense, or heated to evaporate, so large reflux operation requires more energy for these phase changes.

A.4. MESH equations for equilibrium models

The assumption of trays being in equilibrium can be used to calculate all component flow rates and duties. Four types of equations are needed; the so-called MESH equations, being a Mass balance, equilibrium conditions, component balances (Summation) and the energy (or enthalpy, h) balance. These balances can be made around every tray, for

the vapour and liquid flows, plus the energy added through reboiling and condensing, creating a linear system of equations that can be solved using numerical solvers [17].

B. Iterative solving with SciPy's root finding methods

Equations 2.3 to 2.15 give values for the residuals on the left-hand side when the right-hand side of the equation is computed. Energy and mole (or mass) balances and mole fraction summations must be satisfied in order to describe a physical column. Additionally, the values of all properties must be within the domain of physically permissible values - mole fractions between 0 and 1, realistic temperatures for an ethylene-ethane mixture, and so on. The MERSHQ residuals approach 0 if when the model converges.

If the calculation is successful, the residuals will become minimised close to the column operating conditions that match according the the set of equations. There is a native degree of uncertainty in the model, as the fundamental principles of mass and energy conservation are coupled to empirical models that describe transport phenomena.

An initial guess for the system is a set of values for all the model variables that are required to solve the equations. An initial guess x_0 must be supplied to the set of equations, and passed as a vector of values to a root finding function from the *optimise* module. A selection of methods from the SciPy *optimise* module (scipy.optimise.root [86]) is suitable for solving these kind of functions.

It could be useful to constrain variables in the solver between two limiting values. This can prevent that the solver steps the variables step into physically 'impossible' values. For instance, stepping into negative temperatures will not only make no physical sense, but also the equations for transport properties depend on the temperature to be in the range where the correlation is made for. Constraining the temperature will, for instance, prevent numeric errors in the mass transfer coefficients, which would yield unexpected results or even errors that prohibit continuation of the numerical program.

Yet, constraining variables can also impede the solving procedure, possibly causing the solver to run indefinitely. An in-house numerical solver written at TechnipFMC does have the option to constrain variables. The in-house solver was used alongside the native SciPy solvers during the model development.

Another solving method would be to use a minimisation method from the scipy.optimize.minimize [87] function. Minimisation functions demand an objective function that outputs a scalar, which is then minimised iteratively. If the MERSHQ residuals are squared and added, the minimisation function would look for values of the model variables that minimise the combined MERSHQ residuals. This work does not make use of a minimisation method.

The model residuals are the output of the MERSHQ equations, which are then included in a separate Python function. The solver calculates the function output with an initial guess for all variables into the MERSHQ equations, which return a vector of residuals. The root finder will then approximate the Jacobian of the system by evaluating the model equations at a small deviation from the initial guess. The Jacobian is used to find a good next guess. There are several methods to generate this guess, and the discussion of these is beyond the scope of this study. The new guess is expected to result in smaller residuals, since the Jacobian derivative matrix pushes the solution in that direction. In practice, residuals might go up instead because of to non-linearity. This procedure is repeated until there is no more improvement of the solution after a couple of iterations, or if the residuals fall within the desired limits.

B.1. About numerical solvers in Python

All solvers have some common input arguments and important options, which are discussed briefly. It is beyond the scope of this thesis to discuss numerical solvers in detail. Only some relevant important usage aspects of solvers are discussed in the next section. A solver in python could have the following inputs and outputs:

```
1 scipy.optimize.root(     function,
2 x0,
3 args,
4 method,
5 jac,
6 tol,
7 bounds)
8
9 Returns:          x1
```

These function arguments are explained briefly:

- *function* is a function in Python that takes vector x_0 as an argument. In this work, this function contains the combined MERSHQ and MESH equations. This x_0 will thus be the exact same x_T as discussed in section 2.3.2. It is a concatenation of all the required model variables. The function does some calculations, and gives another vector x_1 as output. The to-be-solved function in this study is the set of MERSHQ equations. Since the number of variables is equal to the number of equations, the output vector is of the same length as the input vector.

- x_0 is the concatenated set of initial guesses for the model *variables*. *variables* are varied in iteration and a result of the solving procedure, while *parameters* are constants that happen to appear in one of the function terms. For all SciPy solvers (and the TechnipFMC solver), this input is a Numpy N-dimensional array (ndarray).

- *args* are function arguments that are needed to evaluate the function, but that are not an unknown model variable. From here onwards, these arguments are referred to as *parameters*. They remain constant and are not involved in the iteration procedure, other than to evaluate the function. Feed flow rates and column height are examples of parameters in this work.

- *method* is the type of solver that is used. Some SciPy functions allow the use of various numerical schemes to calculate the next guess vector for the iteration. It is out of the scope of this study to go into details about these solvers.

- *jac* The Jacobian is the full derivative matrix of the function. It can be provided manually if it is available analytically. If the Jacobian is not provided, solvers will attempt to guess the Jacobian in each iteration step by using a perturbation method on te function around the values of and can be recovered from the function if this input is set to true. This is not used for this study, and the Jacobian is calculated by perturbation.

- *tol* is the tolerance of the solver: the minimum relative change x_0/x_1 at which it will continue calculations. If the iteration results in new guesses that change too little, the procedure is either at its solution, or the procedure is stuck at a local minimum where it will not get out of. The *xtol* value can thus be set to prevent the solver from running indefinitely.

- *bounds* are an upper and a lower value for every model variable. If bounds are specified, the solver will not let the model variables exceed these minimum or maximum values.

The output of solvers has at least the following important variables:

- $x1$: the solution of the optimisation. This vector gives the combination of the variables for which the equations are satisfied according to the current state of the solving procedure.

C. Column efficiency

The energy demand of distillation is an import aspect in the decision process between different technologies. HIDiC and VRC utilise more electric power instead of heating from fuels. The use of entropy production - or exergy loss - would be a way to compare these technologies from a thermodynamic viewpoint. The highest thermodynamic efficiency choice is not the best economic choice in every situation, as the cost of electricity varies, and will vary increasingly in the future as more renewable electric capacity is installed. Nevertheless, the thermodynamic efficiency remains a useful tool to compare performances of different technologies.

C.1. Minimum work and energy efficiency

The minimum work to do a separation of a binary ideal mixture is given by [63]:

$$W_{min} = FRT_F \sum_{i=1}^{C} x_i \ln x_i, \tag{4}$$

where:	F	Feed molar flow rate	mol/s
	R_g	Gas constant	$8.3144\,\mathrm{J/(mol \cdot K)}$
	T_F	Feed temperature	K
	C	Total number of components	–
	x_i	Mole fraction of the i-th component	mol/mol

The compressor duty to compress the top vapour from the stripper[1] is found by Eq. 5 [88].

$$W_c = V_c M_w R_g T_{in} \frac{\kappa}{\kappa - 1} \left[\left(\frac{p_{out}}{p_{in}} \right)^{\kappa/(\kappa-1)} - 1 \right] \tag{5}$$

where:	V_c	vapour molar flow rate at the compressor inlet	mol/s
	M_w	Molar weight	$8.3144\,\mathrm{kg/mol}$
	R_g	Gas constant	$8.3144\,\mathrm{J/(mol \cdot K)}$
	T_{in}	inlet temperature	K
	κ	Specific heat ratio	–
	p	pressure	Pa

The efficiency, assuming that the feed is at the bubble point so only vapour enters the compressor, is shown in Eq. 6 [63]. The energy efficiency η is calculated as follows: the desired separation work (Eq. 4) is divided by the total energy input of the device. The energy input is the sum of compressor work, reboiler duty Q_{reb} and condenser duty Q_{cond}.

$$\eta = \frac{FT \sum_{i=1}^{C} x_i \ln x_i}{V_c T_{in} \frac{\kappa}{\kappa - 1} \left[\left(\frac{P_{out}}{P_{in}} \right)^{\kappa/(\kappa-1)} - 1 \right] + Q_{cond} + Q_{reb}} \tag{6}$$

[1] The vapour flow from the top of the stripper is composed of the vapour generated throughout the stripper, plus the vapour that (possibly) comes along with the feed.

If the compressor is driven electrically, its energy usage is roughly equal to its exergy usage. If the terms for reboiler duty Q_{reb} and condenser duty Q_{cond} are replaced by their respective exergy demand, this equation can also be used to calculate the exergy efficiency of the column.

C.2. Column composite curves

The paper by Dhole & Linnhoff [89] shows a way to analyse distillation columns by making use of a column regular composite curves and its grand composite curve, in which the heat flow into the column is plotted against the temperature, as shown in Fig. C.2a. A regular composite curve of a column consists of a curve for both the vapour and the liquid phases, but the grand composite curve has one of these curves pushed into the T-axis compared to the regular composite curve. Electrical compressor power input does not fit into this representation, which makes it less useful for HIDiC and VRC. The plot would seem unfairly in favour of HIDiC because it does not include the work spent for compression, and HIDiC is the most thermally optimised technology. Still, the benefit of HIDiC can be demonstrated by making use of these plots.

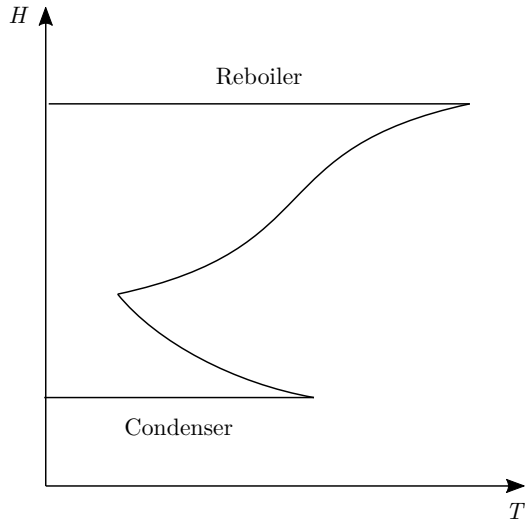

(a) An example of a grand composite curve of a conventional distillation column. Figure by Dhole & Linnhoff [89].

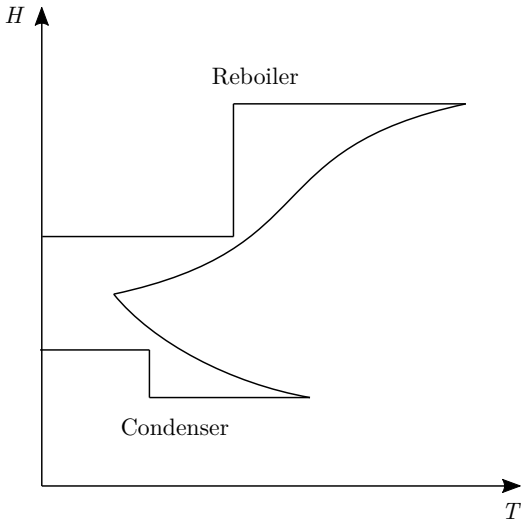

(b) An example of a grand composite curve with a side reboiler and condenser.

Figure C.2: Composite curves of conventional distillation without reboiler (C.2a) and with a reboiler (C.2b)

The area between the curve and the T-axis in Fig. C.2a displays how much heat must be added at the temperatures on the T-axis. This under the graph is this a measure of the exergy loss of the column. Side condensing or side reboiling can immediately increase the total exergy efficiency, as heating can be done at intermediate temperatures, as opposed to exclusively at the highest and lowest temperatures. With side heat exchangers, the curves can have significantly reduced exergy loss, as seen from Fig. C.2b.

C.3. Exergy loss and efficiency

Fitzmorris & Mah [90] show that exergy analysis is a useful tool to analyse the overall thermodynamic efficiency of distillation processes. They apply an exergy analysis (then

called availability analysis) to the SRV system as proposed by Mah, Nicholas & Wodnik [58]. Different overall process efficiencies can be defined, varying on what one views as the desired result of the column. This study considers the minimum work required to separate of a mixture, $W_{min,sep}$ as the desired result, and exergy loss in the condenser and reboiler utilities, $\Delta\mathrm{Ex}_u$, along with possible compression work W_c as the cost of this result, as specified in 7.

$$\eta_{\mathrm{Ex}} = \frac{\Delta\mathrm{Ex}_{sep}}{W_c/\eta_c + \Delta\mathrm{Ex}_u} \tag{7}$$

The exergy content of the utilities is defined as the maximum amount of work that can be done with a utility of temperature T_u when the environment has a temperature T_0:

$$\mathrm{Ex} = Q\left(1 - \frac{T_0}{T_u}\right) \tag{8}$$

The difference between the feed stream exergy and the product streams exergy could be used to determine the exergy change of separation. The feed and product streams have a different temperature. Exergy of product streams that comes from temperature is not considered to be a useful result of the operation. Using a different approach from theory, it is possible to calculate the minimum work of separation, assuming an ideal liquid mixture:

$$\Delta\mathrm{Ex}_{sep} = \frac{W_{min,sep}}{V_c} = -T_0 R \sum_{n=1}^{C} x_i \ln x_i \tag{9}$$

C.4. Exergy grand composite curve

The temperature of the grand composite curve can be replaced by the thermodynamic factor $\theta = 1 - \frac{T_0}{T}$ to be a direct measure of exergy [91, 92]. The resulting curve is the *exergy grand composite curve*. The curve will have a slightly different shape than the regular grand composite curve due to the thermodynamic factor.

In an ideal HIDiC, the rectifier is compressed and its regular composite curve will thus lay slightly lower on the θ axis than the stripper. The rectifier is compressed just enough so that its entire temperature profile lies above the stripper curve. Heat is exchanged between the two sections, much like heat exchange with a temperature glide. The two curves then lie closely together, making the enclosed area small, and so the loss of exergy is minimised. The available heat is used optimally if the coupling between stripper and rectifier is done correctly.

Logically, since the whole compressed rectifier is warmer than in a conventional column, the condenser temperature is higher too. This can be advantageous as the refrigeration section is a costly system. Reduction in the cooling duty or temperature potentially have a large influence on the total column cost. The extra cost of compression may however be larger than the total energy gained by heat pumping.

D. Model vectors

Python model variables are displayed in this appendix. The *parameters* – the constants used during the calculations – are printed in blue. *Variables* are printed in black. Indices start counting from zero, for both the number of components (0 and 1), and stages (0 to $N_s - 1$)

$$V_j = \begin{bmatrix} V_0 \\ V_1 \\ \vdots \\ V_{N_s-2} \\ V_{N_s-1} \end{bmatrix} \quad L_j = \begin{bmatrix} L_0 \\ L_1 \\ \vdots \\ L_{N_s-2} \\ L_{N_s-1} \end{bmatrix} \quad x_{ji} = \begin{bmatrix} x_{0,0} & x_{0,1} \\ x_{1,0} & x_{1,1} \\ \vdots & \vdots \\ x_{(N_s-2),0} & x_{(N_s-2),1} \\ x_{N_s-1,0} & x_{N_s-1,1} \end{bmatrix} \quad y_{ji} = \begin{bmatrix} y_{0,0} & y_{1,1} \\ y_{1,0} & y_{2,1} \\ \vdots & \vdots \\ y_{(N_s-2),0} & y_{(N_s-1),1} \\ y_{N_s-1,0} & y_{N_s,1} \end{bmatrix}$$

$$T_j^L = \begin{bmatrix} T_1^L \\ T_2^L \\ \vdots \\ T_{N_s-1}^L \\ T_{N_s}^L \end{bmatrix} \quad T_j^V = \begin{bmatrix} T_1^V \\ T_2^V \\ \vdots \\ T_{N_s-1}^V \\ T_{N_s}^V \end{bmatrix} \quad T_j^I = \begin{bmatrix} T_{j=2}^I \\ \vdots \\ T_{j=N_s-1}^I \end{bmatrix} \quad Q_j = \begin{bmatrix} Q_{cond} \\ Q_2^{\text{HIDiC}} \\ \vdots \\ Q_{(N_s-1)}^{\text{HIDiC}} \\ Q_{reb} \end{bmatrix}$$

The heat transferred in the HIDiC stages to the vapour phase comes from the liquid phase, so $Q_j^V = Q_j^L$. The side draw from all stages in this model are zero, so:

$$r_j^L = \begin{bmatrix} r_1^L \\ r_2^L \\ \vdots \\ r_{N_s-1}^L \\ r_{N_s}^L \end{bmatrix} = 0 \qquad r_j^V = \begin{bmatrix} r_1^V \\ r_2^V \\ \vdots \\ r_{N_s-1}^V \\ r_{N_s}^V \end{bmatrix} = 0$$

The pressure array is assumed constant and is therefore provided for every stage.

$$p_j = \begin{bmatrix} p_1 \\ p_2 \\ \vdots \\ p_{N_s-1} \\ p_{N_s} \end{bmatrix}$$

The feed is characterised by four parameters, which are all predetermined and required input parameters: feed molar flow rate, feed mole fractions, temperature and pressure. In this model, there is only one feed location, where $j = j_{feed}$. The rest of the feed flow rates are 0, which does not change the equations, but just eliminates some of

the terms in the mass and energy balances.

$$F_j = \begin{bmatrix} 0 \\ \vdots \\ 0 \\ F_{j_F} \\ 0 \\ \vdots \\ 0 \end{bmatrix} \qquad z_{ji} = \begin{bmatrix} z_{1,1} & z_{1,2} \\ z_{2,1} & z_{2,2} \\ \vdots & \vdots \\ z_{(N_s-1),1} & z_{(N_s-1),2} \\ z_{N_s,1} & z_{N_s,2} \end{bmatrix} \qquad T_j^F = \begin{bmatrix} T_1^F \\ T_2^F \\ \vdots \\ T_{N_s-1}^F \\ T_{N_s}^F \end{bmatrix} \qquad p_j^F = \begin{bmatrix} p_{cond}^F \\ p_2^F \\ \vdots \\ p_{N_s-1}^F \\ p_{N_s}^F \end{bmatrix}$$

The interface liquid and vapour compositions are a matrix with two columns (for two components) and N_s rows:

$$x_{ji}^I = \begin{bmatrix} x_{2,1}^I & x_{2,2}^I \\ x_{3,1}^I & x_{3,2}^I \\ \vdots & \vdots \\ x_{(N_s-2),1}^I & x_{(N_s-2),2}^I \\ x_{(N_s-1),1}^I & x_{(N_s-1),2}^I \end{bmatrix} \qquad y_{ji}^I = \begin{bmatrix} y_{2,1}^I & y_{2,2}^I \\ y_{3,1}^I & y_{3,2}^I \\ \vdots & \vdots \\ y_{(N_s-2),1}^I & y_{(N_s-2),2}^I \\ y_{(N_s-1),1}^I & y_{(N_s-1),2}^I \end{bmatrix} \qquad T_j^I = \begin{bmatrix} T_2^I \\ T_3^I \\ \vdots \\ T_{N_s-2}^I \\ T_{N_s-1}^I \end{bmatrix}$$

The last variable is the mass transfer of either species, N_{ji}:

$$N_{ji} = \begin{bmatrix} N_{2,1}^I & N_{2,2}^I \\ N_{3,1}^I & N_{3,2}^I \\ \vdots & \vdots \\ N_{(N_s-2),1}^I & N_{(N_s-2),2}^I \\ N_{(N_s-1),1}^I & N_{(N_s-1),2}^I \end{bmatrix}$$

Vectors that only exist for the non-equilibrium stages have length $N_s - 2$. Two stages for the condenser and the reboiler are excluded. Variables like temperatures, and mole fraction arrays have N_s stages since they also have a value for the condenser and reboiler.

E. CoolProp workaround for state evaluation

Code listing E.1 shows a code snippet that shows how possible exceptions in CoolProp are caught upon state creation. The result of these exceptions is that there might be multiple state.update calculations, which are all separate evaluations of the same state point. This increases the calculation time per stage considerably.

```
1  #  A CoolProp object is initialised with the two component names in a
       string.
2  state = AbstractState('HEOS', componentsstring)
3  def evaluate_state(P, T, molefractions):
4  global state
5  try:
6    molefractions = molefractions / molefractions.sum(0)  # normalise
7    state.unspecify_phase()  # Remove phase from object
8    state.set_mole_fractions(molefractions)  #
9   # CP.PQ_inputs means that the args are pressure and quality.
10   state.update(CP.PQ_INPUTS, P, 0.)  # Dew point, quality 0
11   Tdew = state.T()  # Assign temperature
12   state.update(CP.PQ_INPUTS, P, 1.)  # Bubble point, quality 1
13   Tbubble = state.T()  # Assign temperature
14   state.unspecify_phase()
15   if T < Tdew:  # Start searching in liquid phase
16     state.specify_phase(CP.iphase_liquid)
17     state.update(CP.PT_INPUTS, P, T)
18   elif T > Tbubble:  # Start searching in vapour phase
19     state.specify_phase(CP.iphase_gas)
20     state.update(CP.PT_INPUTS, P, T)
21   else:
22     try:  # Temperature between bubble and dew point
23       # Start searching in two-phase region
24       state.specify_phase(CP.iphase_twophase)
25       state.update(CP.PT_INPUTS, P, T)
26       return state
27     except ValueError:
28       try:
29       # Accept whatever state is returned
30         state.unspecify_phase()
31         state.update(CP.PT_INPUTS, P, T)
32         return state
33       except ValueError:
34         raise Exception('Error in state. Aborting.')
35       # The returned state contains the wanted information.
36   return state
37 except ValueError:
38   raise Exception('Error in state. Aborting.')
```

Listing E.1: Some Python code that is needed to catch most of the possible exceptions in CoolProp's functions.

Bibliography

1. Bruinsma, O., Krikken, T., Cot, J., Sarić, M., Tromp, S., Olujić, Ž. & Stankiewicz, A. The structured heat integrated distillation column. *Chemical Engineering Research and Design* **90,** 458–470 (2012).
2. Ministerie van Algemene Zaken. *Dutch goals within the EU - Climate change - Government.nl* Nov. 2014. `https://www.government.nl/topics/climate-change/eu-policy`.
3. European Commission. *2020 climate & energy package* Nov. 2016. `https://ec.europa.eu/clima/policies/strategies/2020_en`.
4. European Commission. *Two years a er Paris: Progress towards meeting the EU's climate commitments* tech. rep. 2 (European Commission, Brussels, Nov. 2017), 52. `https://ec.europa.eu/clima/sites/clima/files/strategies/progress/docs/swd_2017_xxx_en.pdf`.
5. Ministerie van Economische Zaken en Klimaat. *Over het Klimaatakkoord - Klimaatakkoord* Mar. 2018. `https://www.klimaatakkoord.nl/klimaatakkoord`.
6. European Commission. *2030 climate & energy framework* Nov. 2016. `https://ec.europa.eu/clima/policies/strategies/2030_en`.
7. IRENA. *Renewable Power Generation Costs in 2017* 2018th ed. ISBN: 978-92-9260-040-2. `/publications/2018/Jan/Renewable-power-generation-costs-in-2017` (Abu Dhabi, Jan. 2018).
8. European Commission. *2050 low-carbon economy* Nov. 2016. `https://ec.europa.eu/clima/policies/strategies/2050_en`.
9. TechnipFMC. *Sustainable development - TechnipFMC plc* `https://www.technipfmc.com/en/about-us/sustainable-development`.
10. Kiss, A. A. & Olujić, Ž. A review on process intensification in internally heat-integrated distillation columns. *Chemical engineering and processing: process intensification* **86,** 125–144 (2014).
11. Kiss, A. A., Flores Landaeta, S. J. & Infante Ferreira, C. A. Towards energy efficient distillation technologies – Making the right choice. *Energy. Asia-Pacific Forum on Renewable Energy 2011* **47,** 531–542. ISSN: 0360-5442 (Nov. 2012).
12. Hołyst, R. & Poniewierski, A. *Thermodynamics for Chemists, Physicists and Engineers* 1415–1423. ISBN: 9789400729988 (Springer Netherlands, 2012).
13. Tondeur, D. & Kvaalen, E. Equipartition of entropy production. An optimality criterion for transfer and separation processes. *Industrial & Engineering Chemistry Research* **26,** 50–56. ISSN: 0888-5885. `https://doi.org/10.1021/ie00061a010` (Jan. 1987).

14. Kister, H. Z. *Distillation operation* ISBN: 9780070349100 (McGraw-Hill, New York, 1990).

15. Kister, H. Z. *Distillation design* ISBN: 9780070349094 (McGraw-Hill, New York, 1992).

16. Strigle, R. F. J. *Packed tower design and applications: random and structured packings.* 2nd ed. ISBN: 9780884151791 (Gulf, Houston, 1994).

17. Seader, J. D., Henley, E. J. & Roper, D. *Separation process principles: chemical and biochemical operations* 3rd ed. ISBN: 9780470481837 (Wiley, Hoboken, N.J, 2011).

18. Onda, K., Takeuchi, H. & Okumoto, Y. Mass transfer coefficients between gas and liquid phases in packed column. *JOURNAL OF CHEMICAL ENGINEERING OF JAPAN* **1,** 56–62. ISSN: 0021-9592. https://www.jstage.jst.go.jp/article/jcej1968/1/1/1_1_56/_article/-char/ja/ (Feb. 1968).

19. Taylor, R., Krishna, R. & Kooijman, H. Real-world Modeling of Distillation. *Chemical Engineering Progress* **98,** 1. http://dare.uva.nl/search?arno.record.id=119017 (2003).

20. Subramanian, K. & Wozny, G. Analysis of Hydrodynamics of Fluid Flow on Corrugated Sheets of Packing. *International Journal of Chemical Engineering* (2012).

21. Stoter, F., Olujić, Ž. & de Graauw, J. Modelling and measurement of gas flow distribution in corrugated sheet structured packings. *The Chemical Engineering Journal and the Biochemical Engineering Journal* **53,** 55–66. ISSN: 0923-0467 (Nov. 1993).

22. Sulzer. *Mellapak™ and MellapakPlus™* 2018. https://www.sulzer.com/en/shared/products/2017/03/28/13/25/mellapak-and-mellapakplus.

23. Soave, G. Equilibrium constants from a modified Redlich-Kwong equation of state. *Chemical Engineering Science* **27,** 1197–1203. ISSN: 0009-2509 (June 1972).

24. Abdollahi-Demneh, F., Moosavian, M. A., Montazer-Rahmati, M. M., Omidkhah, M. R. & Bahmaniar, H. Comparison of the prediction power of 23 generalized equations of state: Part I. Saturated thermodynamic properties of 102 pure substances. *Fluid Phase Equilibria* **288,** 67–82. ISSN: 0378-3812 (Jan. 2010).

25. Valderrama, J. O. The state of the cubic equations of state. *Industrial & engineering chemistry research* **42,** 1603–1618 (2003).

26. Peng, D.-Y. & Robinson, D. B. A New Two-Constant Equation of State. *Industrial & Engineering Chemistry Fundamentals* **15,** 59–64. ISSN: 0196-4313. https://doi.org/10.1021/i160057a011 (Feb. 1976).

27. Bell, I. H., Wronski, J., Quoilin, S. & Lemort, V. Pure and Pseudo-pure Fluid Thermophysical Property Evaluation and the Open-Source Thermophysical Property Library CoolProp. *Industrial & Engineering Chemistry Research* **53,** 2498–2508. eprint: http://pubs.acs.org/doi/pdf/10.1021/ie4033999. http://pubs.acs.org/doi/abs/10.1021/ie4033999 (2014).

28. Taylor, R. & Krishna, R. *Multicomponent mass transfer* ISBN: 9780471574170 (Wiley, New York, 1993).

29. Bird, R. B. *Transport phenomena* OCLC: 964824. ISBN: 9780471073925 (Wiley, New York, 1960).

30. Krishna, R. & Wesselingh, J. The Maxwell-Stefan approach to mass transfer. *Chemical Engineering Science* **52,** 861–911. ISSN: 0009-2509 (Mar. 1997).

31. Erickson, D. C., Gomezplata, A. & Papar, R. A. Use of the colburn-drew equations to model mass transfer. *International Communications in Heat and Mass Transfer* **25,** 93–98. ISSN: 0735-1933 (Jan. 1998).

32. Górak, A. & Sørensen, E. *Distillation: fundamentals and principles* ISBN: 9780123865489 (2014).

33. Billet, R. & Schultes, M. Prediction of Mass Transfer Columns with Dumped and Arranged Packings: Updated Summary of the Calculation Method of Billet and Schultes. *Chemical Engineering Research and Design* **77,** 498–504. ISSN: 0263-8762 (Sept. 1999).

34. Bravo, J. L. & Fair, J. R. Generalized correlation for mass transfer in packed distillation columns. *Industrial & Engineering Chemistry Process Design and Development* **21,** 162–170. ISSN: 0196-4305. https://doi.org/10.1021/i200016a028 (Jan. 1982).

35. Fair, J. R., Seibert, A. F., Behrens, M., Saraber, P. P. & Olujic, Z. Structured Packing PerformanceExperimental Evaluation of Two Predictive Models. *Industrial & Engineering Chemistry Research* **39,** 1788–1796. ISSN: 0888-5885. https://doi.org/10.1021/ie990910t (June 2000).

36. Haidl, J., Rejl, F. J., Valenz, L., Moucha, T. & Petříček, R. General mass-transfer model for gas phase in structured packings. *Chemical Engineering Research and Design* **126,** 45–53. ISSN: 0263-8762 (Oct. 2017).

37. Olujić, Ž., Kamerbeek, A. B. & de Graauw, J. A corrugation geometry based model for efficiency of structured distillation packing. *Chemical Engineering and Processing: Process Intensification* **38,** 683–695. ISSN: 0255-2701 (Sept. 1999).

38. Rocha, J. A., Bravo, J. L. & Fair, J. R. Distillation Columns Containing Structured Packings: A Comprehensive Model for Their Performance. 2. Mass-Transfer Model. *Industrial & Engineering Chemistry Research* **35,** 1660–1667. ISSN: 0888-5885. https://doi.org/10.1021/ie940406i (Jan. 1996).

39. Sadeghifar, H. & Safe Kordi, A. A. A new and applicable method to calculate mass and heat transfer coefficients and efficiency of industrial distillation columns containing structured packings. *Energy* **36,** 1415–1423. ISSN: 0360-5442 (Mar. 2011).

40. Wang, G. Q., Yuan, X. G. & Yu, K. T. Review of Mass-Transfer Correlations for Packed Columns. *Industrial & Engineering Chemistry Research* **44,** 8715–8729. ISSN: 0888-5885. https://doi.org/10.1021/ie050017w (Nov. 2005).

41. Krikken, T. *Heat integrated distillation in a plate packing HIDiC* MA thesis (Delft University of Technology, Delft, Jan. 2011). https://repository.tudelft.nl/.

42. Chilton, T. H. & Colburn, A. P. Mass Transfer (Absorption) Coefficients Prediction from Data on Heat Transfer and Fluid Friction. *Industrial & Engineering Chemistry* **26,** 1183–1187. ISSN: 0019-7866. https://doi.org/10.1021/ie50299a012 (Nov. 1934).

43. Hanley, B. & Chen, C.-C. New mass-transfer correlations for packed towers. *AIChE Journal* **58,** 132–152. ISSN: 0001-1541 (2012).

44. Rocha, J. A., Bravo, J. L. & Fair, J. R. Distillation columns containing structured packings: a comprehensive model for their performance. 1. Hydraulic models. *Industrial & Engineering Chemistry Research* **32,** 641–651. ISSN: 0888-5885. https://doi.org/10.1021/ie00016a010 (Apr. 1993).

45. Rocha, J. A., Bravo, J. L. & Fair, J. R. Distillation Columns Containing Structured Packings: A Comprehensive Model for Their Performance. 2. Mass-Transfer Model. *Industrial & Engineering Chemistry Research* **35,** 1660–1667. ISSN: 0888-5885. https://doi.org/10.1021/ie940406i (Jan. 1996).

46. Shi, M. & Mersmann, A. Effective Interfacial Area in Packed Columns. **8,** 87–96 (Mar. 1985).

47. Olujic, Z., Jansen, H., Kaibel, B., Rietfort, T. & Zich, E. Stretching the Capacity of Structured Packings. *Industrial & Engineering Chemistry Research* **40,** 6172–6180. ISSN: 0888-5885. https://doi.org/10.1021/ie010323j (Dec. 2001).

48. Olujic, Z., Behrens, M., Colli, L. & Paglianti, A. Predicting the efficiency of corrugated sheet structured packings with large specific surface area. *Chemical and Biochemical Engineering Quarterly* **18,** 89–96. ISSN: 0352-9568 (2004).

49. VDI-Gesellschaft Verfahrenstechnik und Chemieingenieurwesen. *VDI heat atlas* 142. ISBN: 9783540778776. http://dx.doi.org/10.1007/978-3-540-77877-6 (Springer, Berlin; London, 2010).

50. Erasmus, A. B. *Mass transfer in structured packing* PhD thesis (Stellenbosch: University of Stellenbosch, 2004).

51. Billet, R. & Schultes, M. Predicting mass transfer in packed columns. *Chemical Engineering & Technology* **16,** 1–9. ISSN: 1521-4125 (1993).

52. Billet, R. & Schultes, M. Prediction of Mass Transfer Columns with Dumped and Arranged Packings: Updated Summary of the Calculation Method of Billet and Schultes. *Chemical Engineering Research and Design* **77,** 498–504. ISSN: 0263-8762 (Sept. 1999).

53. Fair, J. R., Seibert, A. F., Behrens, M., Saraber, P. P. & Olujic, Z. Structured Packing PerformanceExperimental Evaluation of Two Predictive Models. *Industrial & Engineering Chemistry Research* **39,** 1788–1796. ISSN: 0888-5885. https://doi.org/10.1021/ie990910t (June 2000).

54. Poling, B. E., Prausnitz, J. M. & O'Connell, J. P. *The properties of gases and liquids* OCLC: 44712950. ISBN: 9780070116825 (McGraw-Hill, New York, 2001).

55. Perry, R. H., Green, D. W. & Maloney, J. O. *Perry's chemical engineers' handbook* OCLC: 300451927. ISBN: 9780070498419 (McGraw-Hill, New York, 1997).

56. Fuller, E. N., Schettler, P. D. & Giddings, J. C. NEW METHOD FOR PREDICTION OF BINARY GAS-PHASE DIFFUSION COEFFICIENTS. *Industrial & Engineering Chemistry* **58,** 18–27. ISSN: 0019-7866. https://doi.org/10.1021/ie50677a007 (May 1966).

57. Takahashi, S. Preparation of a generalized chart for the diffusion coefficients of gases at high pressures. *Journal of Chemical Engineering of Japan* **7,** 417–420 (1975).

58. Mah, R. S. H., Nicholas, J. J. & Wodnik, R. B. Distillation with secondary reflux and vaporization: A comparative evaluation. *AIChE Journal* **23,** 651–658. ISSN: 1547-5905 (1977).

59. Fitzmorris, R. E. & Mah, R. S. H. Improving distillation column design using thermodynamic availability analysis. *AIChE Journal* **26,** 265–273. ISSN: 1547-5905 (1977).

60. Kiss, A. A. *Advanced distillation technologies: design, control, and applications* OCLC: 827120266. ISBN: 9781118544815 (2013).

61. Jana, A. K. Heat integrated distillation operation. *Applied Energy* **87,** 1477–1494. ISSN: 0306-2619 (May 2010).

62. Bisgaard, T. *Operation and Design of Diabatic Distillation Processes* PhD thesis (2016).

63. De Rijke, A. Development of a concentric internally heat integrated distillation column (HIDiC). `http://resolver.tudelft.nl/uuid:2517a2e2-7376-485c-b6fe-931516fc0cc0` (2007).

64. Wakabayashi, T. & Hasebe, S. Design of heat integrated distillation column by using H-xy and T-xy diagrams. *Computers & Chemical Engineering* **56,** 174–183 (2013).

65. Tung, H.-H., Davis, J. F. & Mah, R. S. H. Fractionating condensation and evaporation in plate-fin devices. *AIChE Journal* **32,** 1116–1124. ISSN: 1547-5905 (1977).

66. Hugill, J. A. & Van Dorst, E. M. *Design of a heat-integrated distillation column based on a plate-fin heat exchanger* in *Proceedings of Sustainable (Bio-) chemical Process Technology, incorporating the 6th International Conference on Process Intensification. Delft, the Netherlands* (2005), 27–29.

67. Glenchur, T. & Govind, R. Study on a Continuous Heat Integrated Distillation Column. *Separation Science and Technology* **22,** 2323–2338. ISSN: 0149-6395. `https://doi.org/10.1080/01496398708057189` (Dec. 1987).

68. Govind, R. US4615770A (1986).

69. De Graauw, J., Steenbakker, M. J., Rijke, A. d., Olujic, Z. & Jansens, P. J. US7678237B2 (2010).

70. Nakaiwa, M., Huang, K., Owa, M., Akiya, T., Nakane, T., Sato, M. & Takamatsu, T. Energy savings in heat-integrated distillation columns. *Energy* **22,** 621–625. ISSN: 0360-5442 (June 1997).

71. Naito, K., Nakaiwa, M., Huang, K., Endo, A., Aso, K., Nakanishi, T., Nakamura, T., Noda, H. & Takamatsu, T. Operation of a bench-scale ideal heat integrated distillation column (HIDiC): an experimental study. *Computers & Chemical Engineering* **24,** 495–499. ISSN: 0098-1354 (July 2000).

72. Nakaiwa, M., Wakabayashi, T. & Tamakoshi, A. US20120125761A1 (2012).

73. Olujić, Ž., Sun, L., de Rijke, A. & Jansens, P. J. Conceptual design of an internally heat integrated propylene-propane splitter. *Energy. ECOS 2004 - 17th International Conference on Efficiency, Costs, Optimization, Simulation, and Environmental Impact of Energy on Process Systems* **31,** 3083–3096. ISSN: 0360-5442 (Dec. 2006).

74. Gadalla, M., Olujic, Z., Sun, L., De Rijke, A. & Jansens, P. J. Pinch Analysis-Based Approach to Conceptual Design of Internally Heat-Integrated Distillation Columns. *Chemical Engineering Research and Design* **83,** 987–993. ISSN: 0263-8762 (Aug. 2005).

75. Iwakabe, K., Nakaiwa, M., Huang, K., Matsuda, K., Nakanishi, T., Ohmori, T., Endo, A. & Yamamoto, T. *An internally heat-integrated distillation column (HIDiC) in Japan* in *Institution of chemical engineers symposium series* **152** (2006), 900.

76. Toyo Engineering Corporation. *SUPERHIDIC®: Innovative Energy Saving Distillation System* July 2018. `http://www.toyo-eng.com/jp/en/products/environment/superhidic/`.

77. Sulzer Chemtech. *Structured Packings for Distillation, Absorption and Reactive Distillation* 2003. `https://www.sulzer.com/-/media/files/products/separation-technology/distillation-and-absorption/brochures/structured_packings.ashx`.

78. Rossum, G. *Python Reference Manual* Amsterdam, The Netherlands, The Netherlands, 1995.

79. Jones, E., Oliphant, T., Peterson, P. *et al. SciPy: Open source scientific tools for Python* 2001. `http://www.scipy.org/`.

80. Oliphant, T. E. *Guide to NumPy* 2nd. ISBN: 9781517300074 (CreateSpace Independent Publishing Platform, USA, 2015).

81. Bell, C. *thermo: Chemical properties component of Chemical Engineering Design Library (ChEDL)* 2016. `https://github.com/CalebBell/thermo`.

82. Design Institute for Physical Property Data (U.S.), American Institute of Chemical Engineers & National Institute of Standards and Technology (U.S.) *DIPPR chemical database.* (BYU DIPPR, Thermophysical Properties Laboratory, Provo, UT, 1998).

83. Bell, I. H., Wronski, J., Quoilin, S. & Lemort, V. Pure and Pseudo-pure Fluid Thermophysical Property Evaluation and the Open-Source Thermophysical Property Library CoolProp. *Industrial & Engineering Chemistry Research* **53,** 2498–2508. ISSN: 0888-5885. `https://doi.org/10.1021/ie4033999` (Feb. 2014).

84. Smith, R. *Chemical Process: Design and Integration* ISBN: 9780470011911 (John Wiley & Sons, June 2005).

85. Fenske, M. R. Fractionation of Straight-Run Pennsylvania Gasoline. *Industrial & Engineering Chemistry* **24,** 482–485. ISSN: 0019-7866. `https://doi.org/10.1021/ie50269a003` (May 1932).

86. The Scipy community. *scipy.optimize.fsolve â SciPy v0.14.0 Reference Guide* documentation. May 2014. `docs.scipy.org/doc/scipy-0.14.0/reference/generated/scipy.optimize.fsolve.html`.

87. The Scipy community. *scipy.optimize.minimize â SciPy v1.1.0 Reference Guide* May 2018. `docs.scipy.org/doc/scipy/reference/generated/scipy.optimize.minimize.html?`.

88. Moran, M. J., Shapiro, H. N., Boettner, D. D. & Bailey, M. B. *Principles of engineering thermodynamics: SI version* OCLC: 769849585. ISBN: 9780470918012 (Wiley ; John Wiley distributor, Hoboken, N.J.; Chichester, 2011).

89. Dhole, V. R. & Linnhoff, B. Distillation column targets. *Computers & Chemical Engineering. European Symposium on Computer Aided Process Engineering* **17,** 549–560. ISSN: 0098-1354 (May 1993).

90. Fitzmorris, R. E. & Mah, R. S. H. Improving distillation column design using thermodynamic availability analysis. *AIChE Journal* **26,** 265–273 (1980).

91. Linnhoff, B. & Dhole, V. R. Shaftwork targets for low-temperature process design. *Chemical Engineering Science* **47,** 2081–2091. ISSN: 0009-2509 (June 1992).

92. Goff, P. L., Cachot, T. & Rivero, R. Exergy analysis of distillation processes. *Chemical Engineering & Technology* **19,** 478–485. ISSN: 1521-4125 (Dec. 1996).